Carbon Nanotubes: Synthesis, Characterization and Integration

Carbon Nanotubes: Synthesis, Characterization and Integration

PhD THESIS

Dottorato di Ricerca in Scienza dei Materiali - XXIII Ciclo

UNIVERSITA' DEGLI STUDI DI CATANIA

Salvatore Bagiante

Università degli studi di Catania

⟨C⟩ –IMM   Istituto di Microelettronica e Microsistemi
Consiglio Nazionale delle Ricerche

Tutor: Prof. Francesca Simone

Supervisor: Dr. Silvia Scalese

PhD Coordinator: Prof. Antonino Licciardello

Keywords: carbon nanotubes, arc-discharge, liquid nitrogen, ultra clean nanotubes, suspended nanotubes, optoelectronics.

Cover theme: Science Mosaic

Cover design: Salvatore Bagiante

Cover image: Mosaic of a Suspended carbon nanotube device (front). SEM by Gary Steele; Titanium nitride thin film after CVD growth (back). Optical image by S. Bagiante.

An electronic version of this thesis, including color figures, is available at: http://www.

Acknowledgements

"Quello che hanno scoperto con scientifica sicurezza a forza di studiare i fiumi, tutti i fiumi, hanno scoperto che non sono matti, è la loro natura di fiumi che li obbliga a quel girovagare continuo, e perfino esatto, tanto che tutti, dico tutti, alla fine, navigano per una strada tre volte più lunga del necessario, anzi, per essere esatti, tre volte virgola quattordici, giuro, il famoso pi greco, non ci volevo credere, in effetti, ma pare che sia proprio così, devi prendere la loro distanza dal mare, moltiplicarla per pi greco e hai la lunghezza della strada che effettivamente fanno, il che, ho pensato, è una gran figata, perché, ho pensato, c'è una regola per loro vuoi che non ci sia per noi, voglio dire, il meno che ti puoi aspettare è che anche per noi sia più o meno lo stesso, e che tutto questo sbandare da una parte e dall'altra, come se fossimo matti, o peggio smarriti, in realtà è il nostro modo di andare diritti, modo scientificamente esatto, e per così dire già preordinato, benché indubbiamente simile a una sequenza disordinata di errori, o ripensamenti, ma solo in apparenza perché in realtà è semplicemente il nostro modo di andare dove dobbiamo andare, il modo che è specificatamente nostro, la nostra natura, per così dire, cosa volevo dire?, quella storia dei fiumi, sì, è una storia che se ci pensi è rassicurante, io la trovo molto rassicurante, che ci sia una regola oggettiva dietro a tutte le nostre stupidate, è una cosa rassicurante, tanto che ho deciso di crederci...."

Alessandro Baricco, da "City"

Contents

List of Figures

List of Tables

Chapter 1

Introduction

1.1   Motivations and state of the art

Since the 1950s, the semiconductor industry has been able to improve the performance of electronic systems for more than four decades by making ever-smaller devices. However, this approach will soon encounter both scientific and technical limits, which is why the industry is exploring a number of alternative device technologies. In this context, particular emphasis has been placed on research of carbon materials. Carbon nanotubes (CNTs) [1] and graphene [2] have been among the most promising candidate for the next generation electronics. CNTs materials display outstanding electrical, mechanical and thermal properties, such as long mean free paths, high mechanical strength, flexibility and excellent thermal conductivity [3]. Because of these properties, CNTs are perceived as promising materials for future electronics. Their 1D nature, however, implies that the detailed physics of the devices operation is quite different compared to conventional 3D electronics such as the silicon MOS-FET. Much of the recent progress in nanotube research is due to improvements on the quality of CNTs. This means that CNTs are now a much more reliable system than they were before and there is a lot of fun physics to be explored with them. However, purification processes (sonication and annealing) induce disordering of the CNT walls [4, 5, 6, 7, 8] which would suppress their current density. Thus, we require an advanced CNT-growth method, which can provide high-purity/defect-free CNTs without any purification processes. One may ask why carbon nanotubes? The atomic and electronic structure of a CNT provide a number of unique advantages for making

a FET channel. First, its small diameter (1-2nm) allows optimum coupling between the gate and the channel. Second, because the surface of CNTs is atomically smooth and all carbon bonds are satisfied (i.e no dangling bonds), scattering by surface states or roughness that plague conventional FETs are absent in CNT-FETs. Last, the reduced phase-space for scattering along with the energy and momentum conservation requirements imply that the CNT channel is an exceptional medium for carrier transport. There exist enormous potentials applications for nanotubes. Nanotubes can be used individually or as an ensemble to build functional device prototypes, as demonstrated by many research groups. Ensembles of nanotubes have been used for field emission based flat-panel display [9, 10], composite materials with improved mechanical properties [11], and electromechanical actuators. It has also been suggested that bulk quantities of nanotubes may be useful as high-capacity hydrogen storage media [12, 13, 14]. Individual nanotubes have been used for field emission sources, tips for scanning probe microscopy [15], and nano-tweezers [16]. Nanotubes also have significant potential as the central elements of nano-electronic devices including field-effect transistors [17, 18], single-electron transistors [19, 20] and rectifying diodes [21]. Individual semiconducting nanotubes have also been demonstrated to function as gas sensors [22] with great sensitivity.

1.2 Aim of this work

Today many different techniques are used for CNT synthesis, and the main issues concern the production yield/cost ratio and the determination and control of the produced material and its properties. Moreover, still a lot of improvement on the CNT synthesis remains to be achieved in order to have CNT grown on selected areas, with a given diameter and chirality, thereby enabling the production of well defined devices.

The main aim of this work is the study of CNT synthesis by one of the techniques that allows high yield/cost ratio: arc discharge in liquid nitrogen. This method still needs to be fully understood in order to achieve a good control of the produced nanomaterials and their properties by the use of suitable experimental parameters. This thesis work gives a contribution towards the comprehension of the arcing process for CNT production. The second aspect that has been considered in this work is the use of CNTs for the fabrication of new and innovative devices. The unconventional approach considered here is the use of ultra-clean nanotubes, grown by chemical vapor deposition (CVD) in the very last fabrication step, after all the device structure has already been completed.

In summary, the outline of the thesis is the following: after an introductive chapter on the basic properties of CNTs, with a discussion of theoretical concepts as well as fundamental experimental results (chapter 2), the next chapter (chapter 3) is devoted to the study of MWCNTs produced by arc-discharge in liquid nitrogen (LN2). In this

technique, liquid nitrogen substitutes both vacuum and cooled systems. A morphological and structural characterization of the C nanostructures obtained as the experimental parameters are varied, has been performed, by electron microscopy techniques (SEM, TEM) and Raman spectroscopy. MWCNTs produced by this technique, have a high-quality, small innermost tube diameter and, for particular synthesis conditions, hybrid system, formed by linear C chains inserted in MWCNT (LCC@MWCNTs), can be produced. LCCs have attracted considerable fundamental and practical interest in material science and astrophysics. Two different kinds of linear carbon chains exist: polyyne, with alternate single-triple bonds on the chain, and cumulene, with double bonds only. Polyynes, in particular, can be considered as precursors for carbon materials such as carbine, fullerenes and nanotubes; they are candidates for molecular wires, molecular devices for electron transport through π bonds or electronic communication, and the interpretation of some IR bands from the interstellar powder could be related to the presence of sp-coordinated carbon. In the last chapter (chapter 4), we present the fabrication steps of a device based on ultra-clean suspended nanotubes and preliminary results obtained by electrical and optical measurements. The use of ultra-clean carbon nanotubes gives many advantages such as: (i) nanotube not exposed to electron beam, (ii) in the optical measurement the brightness is 10-100 times higher of the conventional device, (iii) using suspended nanotubes we remove all possible interaction with the substrate, and (iv) in the electrical measurement the signal/noise ratio is very high. The resistance of different conductive materials (metals or alloys) during the CVD growth of CNTs (T=900ºC with Ar, H2 and CH4 gasses) has been evaluated, in order to choose the most suitable ones to create the contacts with the nanotube. Moreover, we have demonstrated that not only it is possible to have electrostatic doping of a CNT by using different gates, but even that it is possible to have an extremely precise control of the spatial electrostatic doping and therefore the p-n junction position along the CNT, by changing the voltage applied to each gate.

References

[1] Iijima, S. Helical Microtubules of Graphitic Carbon. Nature 354, 56-58 (1991).

[2] K. S. Novoselov, A. K. Geim, S. V. Morozov, D. Jiang, Y. Zhang, S. V. Dubonos, I. V. Grigorieva, and A. A. Firsov, Science 306, 666 (2004).

[3] A. Jorio, M. Dresselhaus, G. Dresselhaus (springer New York 2008).

[4] S. C. Tsang, P. J. F. Harris, and M. L. H. Green, Nature 362, 520 (1993).

[5] P. M. Ajayan, T. W. Ebbesen, T. Ichihashi, S. Iijima, K. Tanigaki, and M. Hiura, Nature 362, 522 (1993).

[6] S. C. Tsang, Y. K. Chen, P. J. F. Harris, and M. L. H. Green, Nature 372, 159 (1994).

[7] K. L. Lu, R. M. Lago, Y. K. Chen, M. L. H. Green, P. J. F. Harris, and S.C. Tsang, Carbon 34, 814 (1996).

[8] J. Liu, A. G. Rinzler, H. Dai, J. H. Hafner, R. K. Bradley, P. J. Boul, A. Lu,T. Iverson, K. Shelimov, C. B. Huffman, F. Rodriguex-Macia, D. T. Colbert, and R. E. Smalley, Science 280, 1253 (1998).

[9] Saito, Y., et al., Ultramicroscopy, 1998. 73: p. N1-4:1-6.

[10] Wang, Q., et al., Appl. Phys. Lett., 1998. 72: p. 2912-2913.

[11] Ajayan, P.M., et al., Science, 1994. 265(5176): p. 1212-14.

[12] Dillon AC, J.K., Bekkedahl TA, Kiang CH, Bethune DS, Heben MJ, 1997. 386(6623): p. 377-379.

[13] Chen P, W.X., Lin J, Tan KL, Science, 1999. 285(5424): p. 91-93.

[14] Liu C, F.Y., Liu M, Cong HT, Cheng HM, Dresselhaus MS, Science, 1999. 286(5442): p. 1127-1129.

[15] Dai, H., et al., Nanotubes for Nanoprobes. Nature, 1996. 384: p. 147-150.

[16] Kim, P. and C. Lieber, Nanotube Nanotweezers. Science, 1999. 286: p. 2148-2150.

[17] Tans, S., A. Verschueren, and C. Dekker, Nature, 1998. 393: p. 49-52.

[18] Martel, R., et al., Appl. Phys. Lett., 1998. 73: p. 2447-2449.

[19] Tans, S.J., et al., Nature, 1997. 386(6624): p. 474-477.

[20] Kong, J., et al., Applied Physics Letters, 2000. 77(24): p. 3977.

[21] Kong, J. and H.J. Dai, Journal of Physical Chemistry B, 2001. 105(15): p. 2890-2893.

[22] Kong, J., et al., Science, 2000. 287: p. 622-625.

Chapter 2

Carbon nanotubes: structure and properties

Carbon nanotubes (CNTs) are thin hollow cylinders made of graphite sheets. There are many types of carbon nanotubes and carbon nanotube-like structures. The most basic ones are two: multiwall nanotubes (with diameters, d, of order ~10 nm) and single wall nanotubes (d~1 nm) (see Fig. 2.1). Multiwall carbon nanotubes were discovered by Japanese scientist Sumio Iijima in 1991 [1] and, two years later, individual single wall carbon nanotubes were re- ported [3, 2]. Immediately after their discovery, it became clear that these tiny objects would have very remarkable electronic properties [4, 5]. Only in 1997 the first electronic transport measurements on carbon nanotubes were performed[6, 7], thanks by a large part to a new growth method developed by the group of R. Smalley that enabled the production of large amounts of carbon nanotube material [8]. Since then, the number of groups working on the electronic properties of carbon nanotubes has increased hugely.
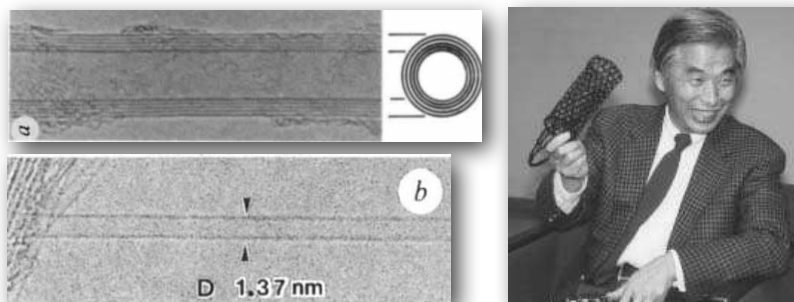
Figure 2.1: Discovery of carbon nanotubes. Left: Transmission electron microscope pictures of a multiwall nanotube (top) and an individual single wall nanotube (bottom) (from refs. [1, 3]). Right: Sumio Iijima, discoverer of carbon nanotubes.

2.1 Carbon allotropes

Carbon is an important element in chemistry. It is the sixth most abundant element in the universe and it has been known since ancient times. There are about sixteen million compounds of carbon, more than for any other element. Carbon is most commonly obtained from coal deposits, although it usually must be processed into a form suitable for commercial use. Allotropes are different physical forms of the same element, differing in the way in which the atoms bond to each other and arrange themselves into a structure. Because of their different structures, allotropes have different physical and chemical properties. Carbon has six electrons, four of which are in the outer shell. The s-orbital and p-orbitals of carbon's outer electronic shell have similar energies. As a result, carbon can adapt to form chemical bonds with different geometries. The most common allotropes of carbon are diamond, graphite and amorphous carbon (examples of amorphous carbon include charcoal, soot and the coal-derived fuel called coke). The density of diamond is about 3.5 g/cm^3, graphite range from 1.9 to 2.3 g/cm^3 and amorphous carbon range from 1.8 to 2.1 g/cm^3. Diamond is one of the hardest known materials, while graphite is one of the softest. These differences depend on the differences in bonding between the carbon atoms. Carbon atoms in the elemental substances (e.g., diamond, graphite, etc...) bond to each other covalently, by the sharing of electron pairs. The covalent bonds have directional properties. This in turn gives carbon the ability to adapt into various molecular and crystalline structures. The nature of these bonds underlies the varied chemical and physical properties of the carbon allotropes. At normal pressures carbon takes the form of graphite in which the atoms form planar, or flat layers. Each layer is made up of rings containing six carbon atoms, just like those in aromatic

Salvatore Bagiante, PhD Thesis in Material Science, University of Catania, 2010.

hydrocarbons. The rings are linked to each other in a structure that resembles the hexagonal mesh of a honeycomb. Each atom has three σ bonds and belongs to three neighboring rings. The fourth electron of each atom becomes part of an extensive π bond system. Graphite conducts electricity because the electrons in π bond system can move around and throughout in the graphite. Bonds between atoms within a layer of graphite are strong, but the forces between the layers are weak (van der Waals force). Because the layers can slip past each other, graphite is soft and can be used as a lubricant. The two known forms of graphite, alpha (hexagonal) and beta (rhombohedral), have identical physical properties, except for their crystal structure. Graphite that naturally occur have been found to contain up to 30% of the beta form, whereas the synthetically-produced one contains only the alpha form. The alpha form can be converted to the beta form through mechanical treatment and the beta form reverts back to the alpha form when it is heated above 1000°C. Diamond makers can transform graphite into diamond by applying extremely high pressure (about 100000 atm) and temperature (about 3000°C). High temperatures break the strong bonds in graphite so that the atoms can rearrange themselves into a diamond lattice. In diamond each C atom bonds tetrahedrally to four other carbon atoms to form a three-dimensional lattice. The shared electron pairs are held tightly in sigma bonds between adjacent atoms. Pure diamond is an electrical insulator: it does not conduct current. It is colourless and, due to its hardness, it is used in industrial cutting tools. The transition to graphite at room temperature is so slow as to be unnoticeable. Under some conditions, carbon crystallizes as lonsdaleite, a form similar to diamond but with hexagonal structure. In its amorphous form carbon is essentially graphite but not held in a crystalline macrostructure. It is actually made up of tiny crystal-like bits of graphite with varying amount of other elements, which are considered impurities. It is rather present as a powder which is the main constituent of substances as charcoal, lamp black (soot) and activated carbon. It can also be pressed into shapes and it used to form the cores of most dry cell batteries. Several exotic allotropes have also been synthesized or discovered, including fullerenes, carbon nanotubes, lonsdaleite and aggregated diamond nanorods. In particular fullerenes have a graphite-like structures, but instead of pure hexagonal packing, they contain pentagons (or possibly heptagons) of carbon atoms, which bend the sheet into spheres, ellipse or cylinders. The properties of fullerenes (also called buckyballs) have not yet been fully analyzed.

A summary of the most known carbon allotropes is given below:

- Diamond: the hardest known natural mineral. Each atom is bonded tetrahedrally to four others, making a 3-dimensional network of six-member rings of atoms.

- Graphite: one of the softest substances. Each atom is bonded trigonally to three other atoms, making a 2-dimensional network of flat six-member rings; the flat sheets are loosely bonded.
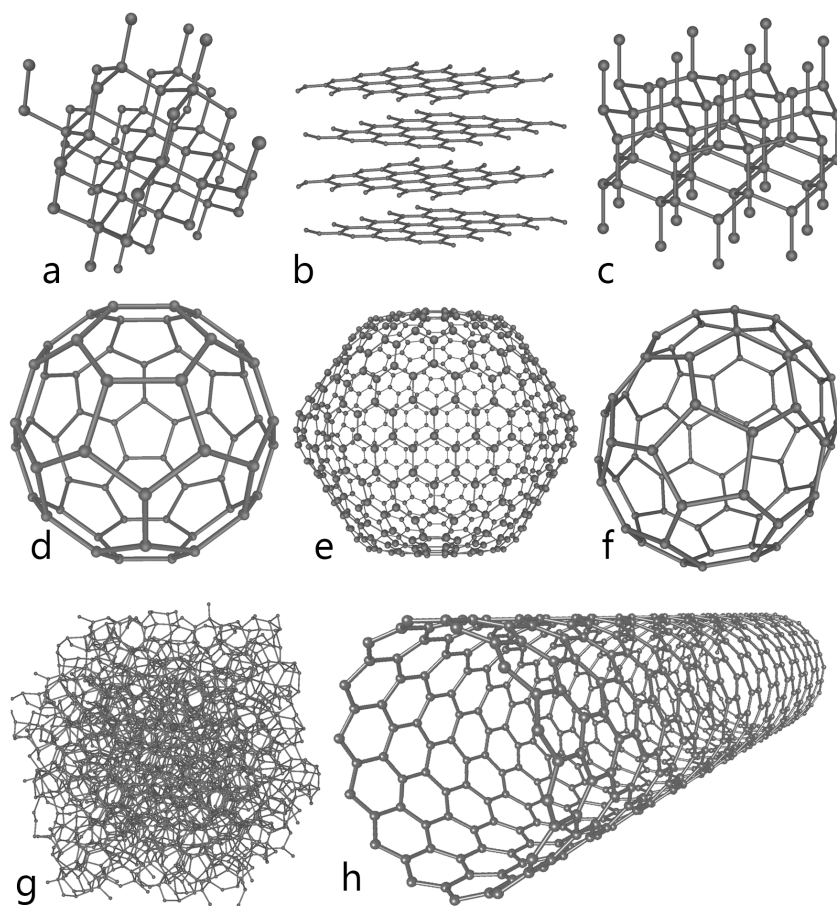
Figure 2.2: a) Diamond, b) Graphite, c) Lonsdaleite, d) C60 (Buckminsterfullerene), e) C540 (see Fullerene), f) C70 (see Fullerene)g) Amorphous carbon, h) single-walled carbon nanotube.

Salvatore Bagiante, PhD Thesis in Material Science, University of Catania, 2010.

- Fullerenes: Large molecules formed completely of carbon bonded trigonally, forming spheroids (of which the best known and simplest is the C60 or buckyball, having soccerball-shaped structure).

- Chaoite: A mineral believed to be formed in meteorite impacts.

- Lonsdaleite: It is similar to diamond, but forming a hexagonal crystal lattice.

- Amorphous carbon: a glassy substance. An absorption of carbon atoms in a non-crystalline, irregular, glassy state.

- Carbon nanofoam (discovered in 1997): an extremely light magnetic web. A low-density web of graphite-like clusters, in which the atoms are bonded trigonally in six- and seven- member rings.

- Carbon nanotubes: Each atom is bonded trigonally in a curved sheet that forms a hollow cylinder.

- Nanobud: A hybrid carbon nanotube/fullerene material discovered in 2007 which combines the properties of both in a single structures in which fullerenes are covalently bonded to the outer wall of a nanotube.

- Aggregated diamond nanorods (synthesised in 2005)

- Lampblack: Consists of small graphitic areas. These areas are randomly distributed, so the whole structure is isotropic.

- Glassy carbon: An isotropic substance that contains a high proportion of closed porosity. Unlike normal graphite, the graphite layer are not stacked like pages in a book, but have a more random arrangement.

- White carbon: was produced in 1969. It is a transparent material that can split a single beam of light into two beams, a property known as birefringence. Very little is known about this form of carbon [9].

In the following paragraphs we will focus on carbon nanotubes properties.

2.2   Constructing a carbon nanotube

Carbon nanotubes have cylindrical structure and can be thought off as a rolled graphene sheet (graphene, a single sheet of graphite, is a honey-comb lattice of covalently bonded carbon atoms, see Fig. 2.3). There are many ways to roll a graphene sheet to form a CNT, so there are, in principle, an infinite amount of CNTs (if you allow the diameter to be as large as you want). One of the most interesting properties of CNTs is that the orientation of a carbon nanotube axis with respect to the
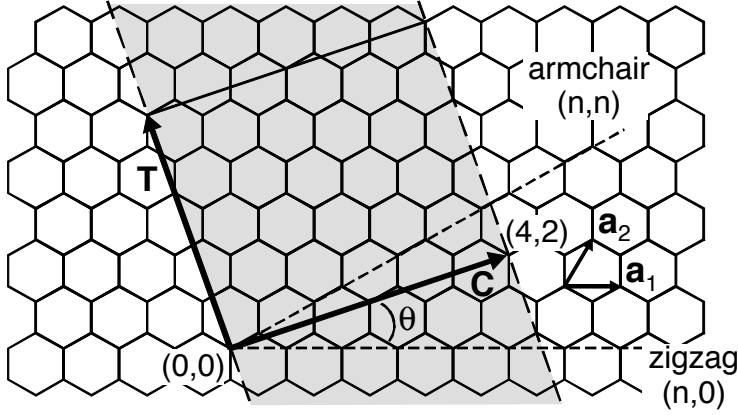
Figure 2.3: Construction of a carbon nanotube from a graphene sheet. By wrapping C onto itself, a CNT is generated with axis parallel to T. The grey area becomes the CNT. Any CNT, characterized by indexes (n, m), can be constructed in a similar way. In this case, it is a (4,2) NT. a_1 and a_2 are the unit vectors of the graphene lattice. Nanotubes constructed along the zigzag and armchair dashed lines are non-chiral.

graphene crystal axes influences its electronic behavior very strongly. In particular, as we will see, CNTs can behave as semiconductors or as metals. The geometry of a CNT is described by a wrapping vector. The wrapping vector encircles the waist of a CNT so that the tip of the vector meets its own tail. One possible chiral vector, C, is shown in Figure2.3. In this example, the shaded area of graphene will be rolled into the NT. The chiral vector can be any C= na_1+ma_2, where n and m are integers and a_1 and a_2 are the unit vectors of the graphene lattice. The angle between the chiral vector and the lattice vector a1 is called the chiral angle of a NT. The pair of indexes (n, m) identifies the nanotube and each (n, m) pair corresponds to a specific chiral angle, ϑ, and diameter d:

$$\theta = \arctan\left[\sqrt{3m/\left(m+2n\right)}\right] \tag{2.1}$$

$$d = \frac{C}{\pi} = \frac{a}{\pi}\sqrt{n^2 + m^2 + nm} \tag{2.2}$$

where a = $|a_i|$ ($\sim$ 0.25 nm) is the lattice constant. A nanotube whose (n,m) indices are (12,6), for example, will have then a diameter d = 1.24 nm and a chiral angle of 19.1. Vector T is perpendicular to C and it points from (0,0) to the first lattice site through which the dashed line passes exactly.
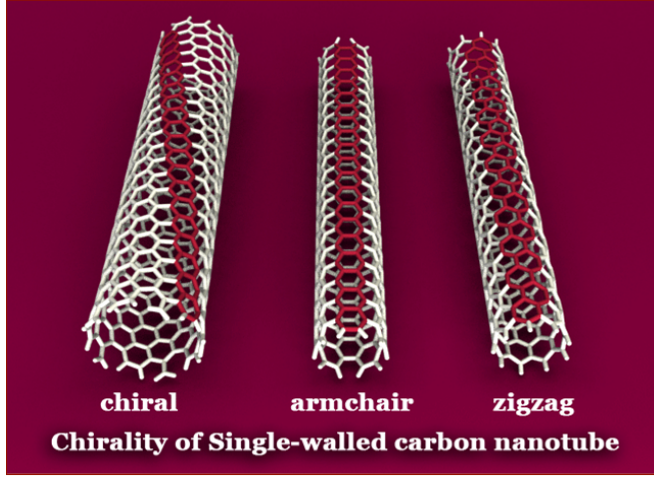
Figure 2.4: Examples of carbon nanotube geometries. From left to right: chiral, armchair and zigzag nanotube.

There are two special directions in the graphene lattice that generate non- chiral tubes. These correspond to the (n, 0) and (n, n) lines in Fig. 2.3 and are called zigzag and armchair directions, respectively. They differ by a chiral angle of $30^{\underline{o}}$. Figure 2.4 shows examples of an armchair, a zigzag and a chiral nanotube[10].

2.3 Graphene band structure

The electronic structure of carbon nanotubes can be derived from the band structure of graphene, which we describe here. A graphene sheet consists of a two-dimensional array of carbon atoms arranged in an hexagonal lattice. Each carbon atom in graphene is covalently bonded to other three atoms, with which it shares one electron forming sp^2 'σ-bonds'. The fourth valence electron of carbon occupies a p^z orbital. The p^z states mix to gather ('π-bonds') forming delocalized electron states with a range of energies that includes the Fermi energy. These states are responsible for the electrical conductivity of graphene. The real space geometry of graphene (a triangular Bravais lattice with a two-atom basis) is shown in Fig. 2.5a. There are two inequivalent sites in the hexagonal carbon lattice, labelled A and B. All other lattice sites can be mapped onto these two by a suitable translation using vectors a_1 and a_2.

The real space unit cell contains the two carbon atoms at A and B. Figure 2.5b shows the reciprocal space lattice, with the corresponding reciprocal space vectors and first Brillouin zone. P. R. Wallace calculated the band structure of graphene
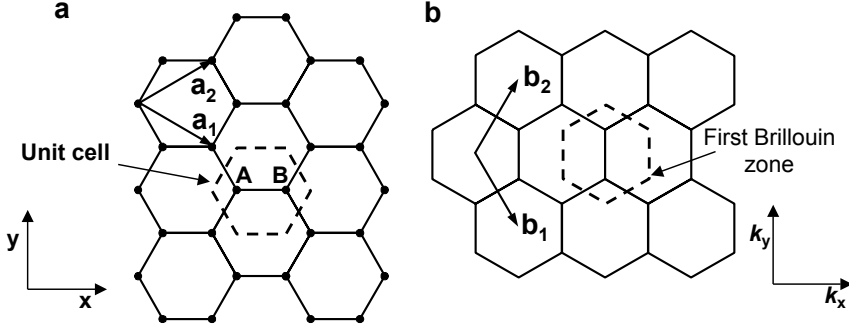
Figure 2.5: a) Real space atomic lattice of graphene. b) Reciprocal space lattice. In both cases the dashed lines denote the unit cells. The unit vectors satisfy $a_i \cdot b_j = 2\pi\delta i,j$.

within a tight- binding approximation in 1947 [11]. Rather than giving here the explicit formula for the graphene band structure, and derive mathematically from it the band structure of carbon nanotubes (see, e.g., [12]), we will simply try to 'visually' understand the basic electronic properties of CNTs from the band structure of graphene. The energy dispersion relation for graphene, $E(k_x, k_y)$, is plotted in Fig. 2.6a. Valence and conduction bands 'touch' each other at six points, which coincide with the corners of the hexagonal Brillouin zone. The Fermi surface reduces thus just to these six points. Because of this, graphene is called a semimetal, or zero band gap semiconductor. These special points, where conduction and valence bands meet, are called 'K points'. The dispersion relation near these points is conical. Figure 2.6b shows a contour plot of the energy of the valence band states.

The circular contours around the K points reflects the conical shape of the dispersion relation around them. Only two of the six K-points are inequivalent (resulting from the two inequivalent atom sites of the graphene lattice), labelled K_1 and $K_2 = -K_1$. In Fig. 2.6b, the lower two K-points on the hexagon sides can be reached from K_1 by a suitable reciprocal lattice vector translation, so they are equivalent to K_1. Similarly, the two upper K-points are equivalent to K_2. The electronic properties of a conductor are determined by the electrons near the Fermi energy. Therefore the shape and position of the dispersion cones near the K points is of fundamental importance in understanding electronic trans- port in graphene, and therefore in nanotubes. The two K points, K_1 and K_2 in Fig. 2.3b have coordinates $(k_x, k_y) = (0, \pm 4\pi/3a)$. The slope of the cones is , where $\gamma o \sim 2.7$ eV is the energy overlap integral between nearest[10].
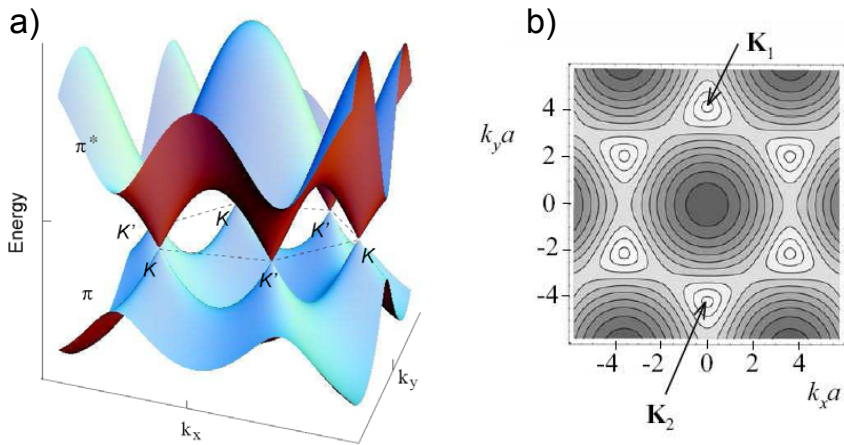
Figure 2.6: Graphene band structure. a) Energy dispersion relation for graphene. The valence band (which is of π-character) and conduction band (which is of π*-character) meet at six points at the Fermi energy, E_F. b) Contour-plot of the valence band states energies in a (darker indicates lower energy). The hexagon formed by the six K points (white contour points) defines the first Brillouin zone of the graphene band structure. Outside this unit cell, the band structure repeats itself. The two inequivalent points, K_1 and K_2 are indicated by arrows [12].
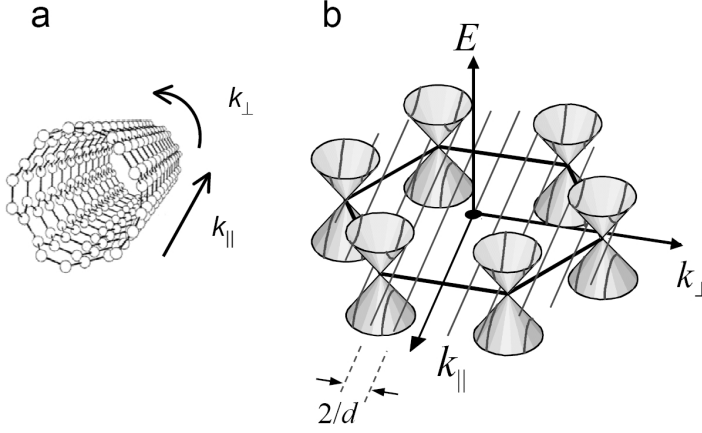
Figure 2.7: Quantized one-dimensional (1D) subbands. a) CNT and direction of k-axis. b) Low-energy band structure of graphene (near EF), showing the one-dimensional subbands of CNTs obtained by imposing periodic boundary conditions along the NT circumference (adapted from [13]).

2.4   Band structure of carbon nanotubes

The band structure of carbon nanotubes can be derived from that of graphene by imposing appropriate boundary conditions along the nanotube circumference. Typically, the diameters of carbon nanotubes ($\tilde{\ }$ few nm) are much smaller than their lengths (anywhere from hundreds of nm to several cm). This implies that there is a very large difference in the spacing between the quantized values of the wavevectors in the directions perpendicular, $k_\perp$, and parallel, $k_{||}$, to the tube axis. In this section, we will regard $k_{||}$ to be effectively continuous (infinitely long NTs) and consider only the quantization effects due to the small diameter of NTs.

By imposing periodic boundary conditions around the NT circumference we obtain the allowed values of $k_\perp$:

$$C \cdot k = \pi d k_\perp = 2\pi j \tag{2.3}$$

where d is the NT diameter and j is an integer number. The small diameter of CNTs makes the spacing in $k_\perp$ to be rather large ($\Delta k_\perp = 2/d$), resulting in strong observable effects even at room temperature. The quantization of $k_\perp$ leads to a set of 1-dimensional subbands in the longitudinal direction (intersection of vertical planes parallel to $k_{||}$ with the band structure of graphene). These are shown in Fig. 2.7b. The electronic states closest to the Fermi energy lie in the subbands closest to the K points. One of the most remarkable properties of CNTs becomes apparent now: if a
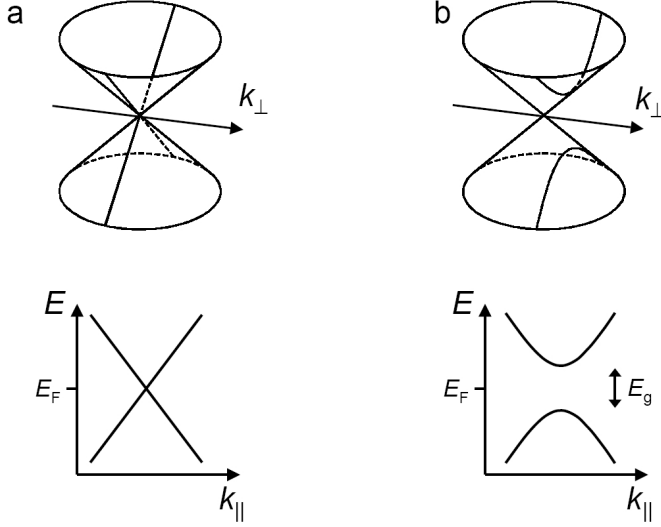
Figure 2.8: Low energy band diagrams for carbon nanotubes around the K_1 point. a) For p = 0, there is an allowed value of k⊥ whose subband passes through K_1, resulting in a metallic nanotube and band structure. b) For p = 1, the closest subband to K_1 misses it by $\Delta k\perp = 2/3d$, resulting in a semiconducting nanotube with band gap Eg. In both figures, E_F refers to the value of the Fermi energy in graphene.

subband passes exactly through the middle of a dispersion cone, then the nanotube will be metallic.

If not, then there will be an energy gap between valence and conduction bands and the nanotube will be a semiconductor. To first approximation, all nanotubes fall into one of these categories: either they are metallic or semiconductors. In fact, for a given (n, m) nanotube, we can calculate n − m = 3q + p, where q is an integer and p is -1, 0 or +1 [14]. If p = 0, then there is an allowed value of k\perp that intercepts the K points, and the nanotube is metallic. The slope of the dispersion cones gives the Fermi velocity in metallic nanotubes: with $v_F \sim 8 \cdot 10^5$ m/s[15]. For p = ±1, there is no allowed value of k\perp intercepting the K points, resulting then in a semiconducting nanotube (see Fig. 2.8). The closest k⊥ to the K points misses them by

$\Delta k\perp = \pm 2/3d$, for p = ±1, respectively. This means that the value of the band gap is: $Eg = 2(dE/dk)\Delta k\perp = 2\gamma_0 a/(\sqrt{3d})$ ~ 0.8 eV/d[nm], independent of chiral angle. Of all carbon nanotubes, approximately 1/3 are metallic and 2/3 are semiconducting (see Fig. 2.9).
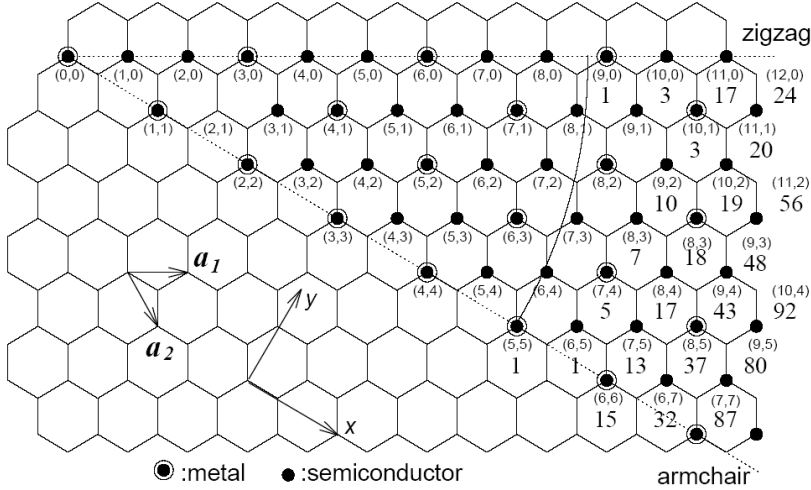
Figure 2.9: Possible nanotube wrapping vectors, characterized by (n, m), with n > m. Black dots indicate semiconducting nanotubes and circled dots indicate metallic nanotubes (from ref. [14]).

It is quite remarkable that carbon nanotubes can be metallic or semiconducting depending on chirality and diameter, despite the fact that there is no difference in the local chemical bonding between the carbon atoms in the different tubes. This fact results from an elegant combination of quantum mechanics and the peculiar band structure of graphene[10].

2.5 Electrical properties

Theoretical studies have predicted that electrons in metallic armchair SWCNTs can propagate ballistically over several micrometers, even in the presence of moderate disorder such as substitutional impurities or local bending [16, 17]. A similar conclusion has been obtained for metallic zig-zag and chiral type SWCNTs [18, 19]. For a defect-free ideally contacted armchair SWCNT, a value of $2G_0$ for the low bias conductance is predicted by the Landauer theory, where $G_0=2e^2/h$ is the conductance quantum. This conductance value is explained by the presence of two linear dispersing bands crossing at the Fermi level. Later, room temperature conductances between $1/2G_0$ and G_0 were reached with the aid of Ti/Au electrodes evaporated on top of the tubes [20, 21], or via placing the tubes over flat electrodes in order to avoid mechanical tube deformation which would introduce local transport barriers [22]. Scanned probe stud-

Salvatore Bagiante, PhD Thesis in Material Science, University of Catania, 2010.

ies on such SWCNTs revealed that the applied potential predominantly drops close to the metal contacts, supporting the existence of near-ballistic electron motion [23]. The first experimental observation of two units of quantum conductance ($2G_0 = 4e^2/h$) in metallic tubes has then been achieved with pure noble metal (Au/Pd) top contacts for a ~150nm long tube section [24]. Subsequent studies have further consolidated the existence of ballistic transport in metallic SWCNTs by demonstrating waveguide behaviour over tube lengths of several hundreds of nanometers[25, 26]. The presence of defects in the tube structure cause resonant electron scattering at Fermi energies corresponding to the defect levels. In this scenario, the carriers are able to freely propagate between the defects, while elastic backscattering occurs at the defect sites. Theoretical studies suggest that the resonance states could be originated from topological defects such as substitutional atoms or Stone-Waals (pentagon- heptagon pair) defects [27, 28]. Compared to metallic SWCNTs, the electric behaviour of semiconducting tubes is more complicated due to their pronounced sensitivity against adsorbates or background charges on the substrate. Semiconducting nanotubes, unless further processed, in general show p-type behaviour, i.e. their conductance increases as the gate voltage is decreased [29]. The conductance of semiconducting SWCNTs can be modulated by more than six orders of magnitude through the action of a gate potential [30]. There is ample experimental and theoretical evidence that the nature of the contact between semiconducting SWCNTs and metals depends on the metal work function. High-work function metals such as gold or palladium make ohmic contacts to p-type tubes [31, 32]. The operation mechanism of such transistor devices within the p-type regime follows closely a classical mechanism as in conventional silicon devices. In contrast, the operation of carbon nanotube field-effect transistors with low-work function metal contacts like chromium or titanium is dominated by gate-induced modulation of the Schottky barrier transmissivity [33, 34, 35, 36]. Due to the sharp metal-nanotube contact and the quasi-1D channel of the tube, the Schottky barriers (typical barrier height 0.3-0.4 eV) can be thinned sufficiently by an applied gate voltage to allow thermally assisted tunnelling of charge carriers [37]. The higher sensitivity of semiconducting SWCNTs against long-range disorder, as compared to metallic nanotubes, has been attributed to the massive character of the nearest subbands in the former type of tubes, whereas the two linear dispersing bands that cross at the Fermi energy in metallic tubes are massless[38]. The carrier mobility could be significantly enhanced owing to recent improvements in the structural quality of the SWCNTs. Ballistic transport has recently been achieved with high-quality semiconducting CVD-Grown SWCNTs contacted by the high-work function metal palladium [39]. To measure electrical transport in SWCNTs, the tubes are usually dispersed on a patterned substrate. The substrate is a silicon wafer, used as a back gate, with a 100-1000nm thick SiO2 layer. On this layer a large array of metal electrodes is prepared by electron-beam lithography. After depositing the tubes, the sample is scanned with an atomic force microscope to find the tubes that, by coincidence, cross two or more

electrodes. With the procedure described, many interesting physical phenomena were investigated, and it was also demonstrated that carbon nanotubes can be built into transistors and logical elements [40, 16, 41]. However, it is obvious that this approach is not suitable for application in technology. One of the biggest problem is that it is not possible to separate metallic and semiconducting nanotubes before deposition them. A solution to the separation problem was suggested by Krupka et al. [45]. When the conductance is independent of the gate voltage, it is attributed to metallic nanotubes. The crossing of the valence and conduction band in the metallic tubes provides conducting electrons independently of the gate voltage. The conductance in semiconducting nanotube, in contrast, changes by order of magnitude when changing the gate voltage. Recently, another approach is been used by F. Bussolotti and al. [46]. They showed in situ manipulation and electrical transport characterization of individual MWCNTs grown on a Ni tip by using a piezoelectric nanomanipulators system operating in a scanning electron microscope chamber. By nanomanipulators it is possible to contact carbon nanotubes and applying a voltage to measure the electrical current. Independently of the different technique used, there are two problems to get rid: the difficult to manipulate structures with nanometric size and the contact effects on CNTs. The presence of a high energy barrier at the metal/nanotubes contacts has been clearly brought to light [42, 43], which leads to an overall resistance value significantly higher with respect to the theoretically predicted quantum ballistic limit ($h/2e^2 = 13k\Omega$ form metallic MWCNTs[42]) and which, in general, masks the intrinsic electrical conduction properties of the individual CNTs. The reported contact resistance ranges from 104 to 109Ω [44, 42, 47, 48].

2.6 Elastic properties

The results of various studies over the years have shown a large variation in the value reported for the Young's modulus (elastic modulus) and tensile strength. In 1996, researchers at NEC in Princeton and the University of Illinois measured the average modulus to be 1.8 TPa [37]. This was measured by first allowing a tube to stand freely and then taking a microscopic image of its tip. The modulus is calculated from the amount of blur seen in the photograph at different temperatures. In 1997, G. Gao et al. [49] presented a talk at the Fifth Foresight Conference on Molecular Nanotechnology where they reported three variations on the Young's modulus to five decimal places that were dependent on the chiral vector. These values were calculated from the second derivatives of potential. Using these two different methods, a discrepancy arises. In 1998, Dujardin et al. [50] reported an elastic modulus of 1.25TPa. Using an AFM, they pushed the unanchored end of a freestanding nanotube out of its equilibrium position and recorded the force that the nanotube exerted back onto the tip. In 1999, E. Hernàndez and A. Rubio [62] showed, using tight-binding calculation, the Young's modulus was dependent on the size and chirality of SWCNT. The previous

Salvatore Bagiante, PhD Thesis in Material Science, University of Catania, 2010.

evidence would lead us to assume that the diameter and shape of the nanotube was the determining factor for its elastic modulus. Working with different CNTs, Forrò et al [56] noted that the Young's modulus measurements by AFM depend on the diameter of the SWCNTs. In particular, an individual tube had a modulus of about 1TPa while bundles (or ropes) of 15 to 20 nm in diameter had a modulus of about 100GPa. Instead, for MWCNTs they argued that the modulus did not depend on the diameter, but it is strongly correlated to the amount of disorder in the nanotube walls. Dynamic simulations on large nanotubes (3nm, 480 atoms) [54] show the deformation of carbon nanotubes under tensile strain conditions, with the relative defects formation, their evolution and influence on CNTs modulus. The general relationship between a macroscopic stress σ applied to a material and the resulting microscopic deformation ε is usually described with the elastic-constant tensor C[52]: σ_{ij}=Cijklεkl. The symmetry of a crystal restricts the number of non-zero and linearly independent constants C_{ijkl}. For example, in nanotube C_{xxxx}=C_{yyyy}, since the tubes are isotropic in the plane perpendicular to the z-axis. The elastic constants can be measured by a variety of techniques like ultrasound experiments or direct measurements of the lattice constants under stress. Despite the large interest in the mechanical properties of carbon nanotubes, in particular as reinforcement material [55], successful measurements of the elasticity constants have not yet been reported. Young's modulus was investigated several times both theoretically and experimentally; it was generally found to be on the order of the value of graphite [57, 58, 59, 60, 61, 63]. For some selected tubes elastic constants were calculated with an empirical force-constants model by Lu [68]. Ru [69] included in his model for multiwall nanotubes the van der Waals interaction between neigh borough layers. Some authors proposed a continuum model [66] to study the elastic response of nanotubes under pressure. In this model the nanotube is looked at as a hollow cylinder with closed ends and a finite wall thickness made of graphene. This approximation, in addition to yielding the deformation of a nanotube under pressure, provides an insight into the question whether the differences in elastic properties of graphite and carbon nanotubes follow plainly from their different topologies or from additional physical effects, e.g., rehybridization. It has been suggested that the controversy into the value of the modulus is due to the author's interpretation of the thickness of the walls of the nanotube. If the tube is considered to be a solid cylinder, then it would have a lower Young's Modulus. If the tube is considered to be hollow, the modulus is higher, and the thinner we treat the walls of the nanotube, the higher the modulus will become [67].

2.7 Optical properties

The optical absorption spectra in the UV-vis-NIR range reflect the singularities in the joint density of states (JDOS) of the tubes. The JDOS function can be expressed by[71]:

$$JDOS(E) = \sum_j \int \frac{\Gamma}{2\pi \left[E - 2E^c(j,k)\right]^2 + \Gamma^2} dk \qquad (2.4)$$

where the summation index J is the angular momentum quantum belonging to the different sub-bands, Γ a phenomenological level broadening parameter, end E^C the conduction band dispersion. Optical selection rules predict that for parallel orientation of the electric field vector and the tube axis, $\Delta J=0$ is required, which corresponds to interband transitions between mirror-like van Hove singularities. In case of perpendicular orientation between electric field vector and tube axis, allowed excitations are restricted to those that satisfy $\Delta J=\pm 1$. However, such transitions between van Hove singularities located non-symmetrically with respect to the Fermi level contribute only weakly to the optical absorption due to a depolarisation field induced along the tube circumference, which opposes the applied external field (antenna effect)[72]. Studying the optical properties one is often hampered by the bundling of the tubes. The luminescence efficiency is greatly reduced due to rapid transfer processes from semiconducting to metallic tubes, where non-radiative recombination occurs. This is why reports of luminescence have appeared only long after the discovery of nanotubes. O' Connell et al. [73] reported the preparation of isolated nanotubes in which they were able to prevent rebuilding. They prepared such isolated tubes by first ultrasonicating raw nanotube products [74] and dispersing them in an aqueous sodium dodecyl sulphate (SDS) surfactant. The isolated nanotubes had richly structured absorption spectra and showed strong luminescence. Figure 2.10 shows the optical spectra in the near-infrared for tubes with a diameter of 0.7 to 1.1 nm.

The isolated tubes show narrow absorption lines and photoluminescence with no shift between absorption and emission. The photoluminescence was excited with an energy $\hbar\omega$ of 2.3 eV, which is much higher than the first excited state. The absorption is thus into the second or higher band of the nanotube, and the carriers relax quickly to the lowest excited state before recombining. There are several reasons why the emitted light does not originate from the coating of the tubes. For one, the detected emission energy matches quite well the expected nanotube band gap. Secondly, the emission was also observed in unprocessed nanotubes from free-standing isolated tubes grown on small pillars by chemical vapour deposition [75]. The problem with absorption and emission measurements on bulk samples is that usually a huge number of different nanotubes with varying diameter and chiral angle is present. These measurements alone do not allow to identify the absorption peaks with two transitions of the same tube. To overcome this problem, O'Connell et al.[73] measured the photoluminescence as a function of the energy of the exciting light, a so called photoluminescence excitation spectrum (PLE): the photoluminescence of a particular tube, which is selected by a fixed detection energy is high when the absorption is strong for an excitation energy. Such a spectrum thus resembles the absorption of a single tube and allows the determination of the higher-lying van Hove singularities.
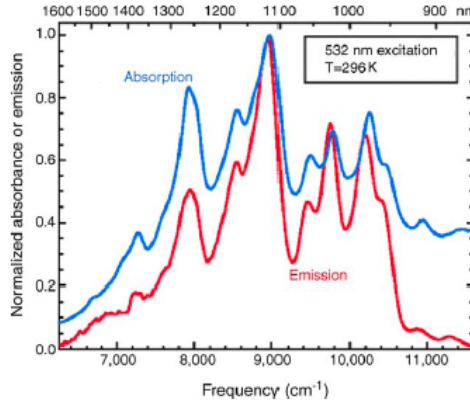
Figure 2.10: Photoluminescence spectrum (red) of individual SWCNT, and optical absorption spectrum (blue) of the same sample in the region of first van Hove band gap transitions, at room temperature [73].

We can then try to use these energies for an assignment of the chiral indices (m, n) [76].

2.8   Synthesis methods

In this section different techniques for nanotube synthesis are explained. The CNT properties depend on the technique used for their synthesis and, therefore, the study of the material produced allows to identify pros and cons of each growth method. The main techniques used for carbon nanotubes production are: arc discharge, laser ablation and chemical vapour deposition. Normally the presence of a catalyst is necessary for the synthesis [77]. In the case of CNT growth on a substrate, clusters of the catalytic elements usually are deposited on the surface before the growth takes place. It has been shown that the structural properties of the growing nanotubes are influenced by the cluster properties (chemical element, size, etc.)[79, 80]. Recently, some papers have demonstrated [81, 78] that radio-frequency (RF) magnetron sputtering can be used for CNT growth on a silicon substrate. Arc discharge methods produce large quantities of carbon nanotubes, but the produced material is impure. Laser ablation produces purer CNTs but with a smaller yield with respect to arc discharge. The CVD method is the most favourable commercial technique for the growth of carbon nanotubes well aligned on a substrate.
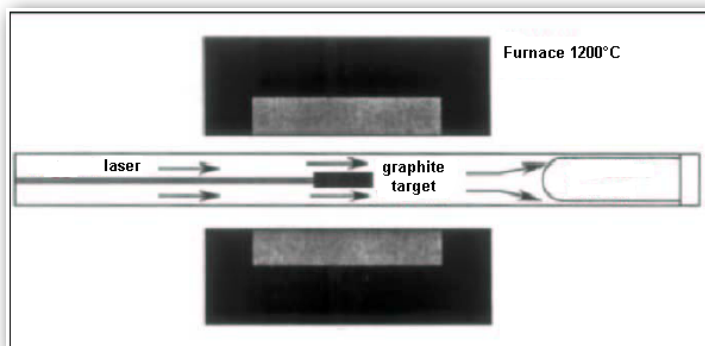
Figure 2.11: Schematic of laser ablation system.

2.8.1 Laser ablation

In 1995 the synthesis of carbon nanotubes by laser vaporisation was reported [121]. A pulsed [84, 85] or continuous laser [86, 87] is used to vaporise a graphite target in furnace at 1200°C (fig. 2.11).

The furnace is filled with helium or argon gas in order to keep the pressure at 500 Torr. A very hot vapour plume forms, that expands and cools rapidly. In the case of pure graphite target MWCNTs would be synthesised; if a mixture of graphite with Co, Ni, Fe or Y is used SWCNTs could be synthesised. As the vaporised species cool, small carbon molecules and atoms quickly condense to form larger clusters. Also the catalyst begin to condense but more slowly and attach to carbon clusters preventing their closing into cage structures. From these initial clusters tubular structures grow into single-wall carbon nanotubes, until the catalyst particles become too large or until the cooling down stops the carbon diffusion through or over the surface of the catalyst particles. The SWCNTs formed are bundled together by Van der Waals forces [88]. Laser ablation is quite similar to arc discharge, so the optimum background gas and catalyst mix is the same as in the arc discharge process. The carbon nanotubes obtained by this technique are contaminated with carbon nanoparticles. The diameter of the SWCNTs range between 0.7-2 nm.

2.8.2 Arc discharge

The arc discharge method in the beginning was used to produce C60 fullerenes, but today is the most common and easiest way to produce carbon nanotubes. However, the material produced with this technique consists of several kinds of C structures: nanotubes, amorphous carbon, fullerenes, etc., shown in fig.2.12.
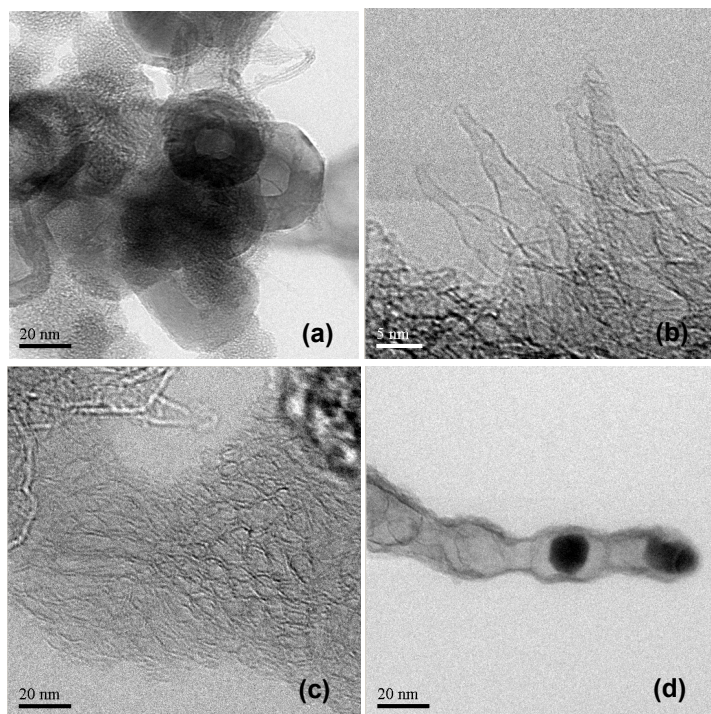
Figure 2.12: Different carbon nanostructures produced by arc discharge; in particular (a) carbon nanonions, (b) carbon nanohorns, (c) skein of SWCNTs and (d) MWCNT with catalytic cluster present inside.
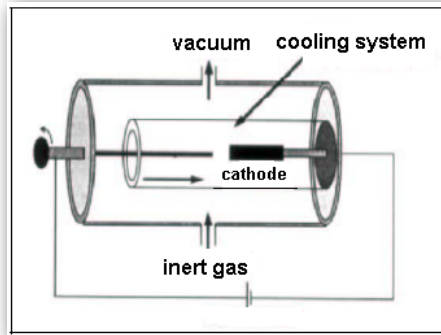
Figure 2.13: Schematic of arc discharge system.

In fig.2.13 a schematics of an arc discharge system is reported.

Two carbon rods are placed end to end, and separated approximately by 1mm inside a chamber with inert gas (helium, argon) at low pressure (between 50 and 700 mbar). Between the two electrodes a voltage in the range of 20V is applied and a discharge takes place, with a current value that is normally kept in the range 50-100 A. The discharge vaporises one of the carbon rods and a deposit is created on the other rod. Producing nanotubes in high yield depends on the uniformity of the plasma arc and the temperature reached by the plasma during the discharge [89], that is about 4000°C. The different diameter distributions of the nanotubes so obtained have been found to depend on the mixture of helium and argon, temperature, carbon density and metal catalyst. In order to synthesize SWCNT the anode must be doped with metal catalyst, such as Fe, Co, Ni, Y or their mixtures. The quantity and quality of the nanotubes obtained depend on the type of metal, its concentration, inert gas pressure, kind of gas, voltage, current and system geometry [90, 91, 92]. The most common problems with SWCNT obtained with this technique are that the products contain a lot of metal catalyst, and purification is hard to perform. Generally the diameter is in the range of 1.2 to 1.4 nm. Typically MWCNTs have an innermost diameter of 1-3 nm and an outermost diameter of approximately 10 to 30nm. In this process no catalyst is involved, so purification step with acids is not necessary. For this reason MWCNTs can be obtained with a low amount of defects. Recently it was shown that it is possible to obtain nanotubes by the arc method in liquid nitrogen and deionised water [93, 94, 95]. For this option low pressures and expensive inert gasses are not needed.
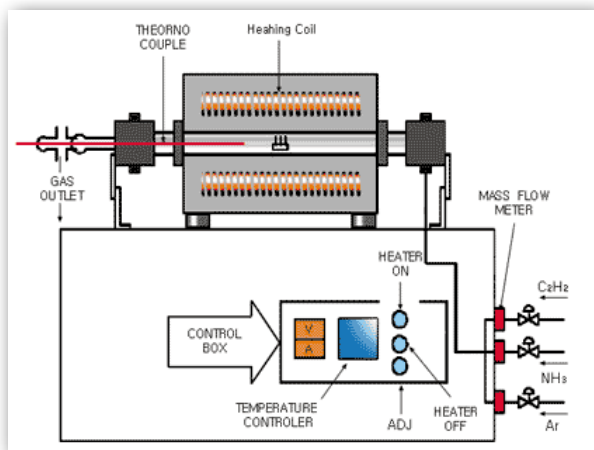
Figure 2.14: Schematic of chemical vapour deposition system.

2.8.3 Chemical vapour deposition

In chemical vapour deposition (CVD) synthesis (fig. 2.14) a carbon source in the gas phase is used with an energy source, such as a plasma or a resistively heated coil, necessary to transfer energy to a gaseous carbon molecule.

Generally gaseous carbon sources include methane, carbon monoxide and acetylene. The energy source is used to break the gas molecule into reactive atomic carbon. Then the carbon diffuses towards the substrate, that is heated and coated with a catalyst (usually Ni, Fe or Co) where it will bind and start to form the nanotube structure. Excellent alignment and control of the diameter can be obtained by CVD technique [97, 98]. The catalyst is generally prepared by sputtering onto a substrate and then using chemical etching or thermal annealing to induce catalyst particles nucleation. Thermal annealing produces clusters formation on the substrate, from which the nanotubes will grow. The temperatures for the synthesis of nanotubes by CVD are generally between 650-900°C [99, 100]. SWCNTs and MWCNTs synthesised depending on the catalyst size present on the substrate surface. In the last years different kinds of CVD techniques have been developed for the carbon nanotubes synthesis, such as: plasma enhanced CVD[101], thermal chemical CVD[102], alcohol catalytic CVD[103], aereo gel-supported CVD [104, 105]and laser assisted CVD [105].

2.9 Purification of CNTs

In spite of the high CNT yield obtained by large scale synthesis techniques, like arc discharge, a big issue must be faced up: the presence of impurities. The main impurities in the soot are graphite sheets, amorphous carbon, metal catalyst particles and fullerenes. These impurities can interfere with most of the properties of the CNT. Different techniques exist and generally they are divided into two groups: structure selective and size selective separations. The first separates the CNT from the impurities; the second gives a more homogeneous diameter or size distribution. The most common techniques are: oxidation, acid treatment, thermal process, ultrasonication, micro filtration, ferromagnetic separation, cutting, functionalization and chromatography techniques. Generally not only one technique but a combination of them is used to purify the CNTs [106]. Oxidative treatment of the CNTs is a good way to remove carbonaceous impurities [107, 108, 109, 110, 111], even though also the CNTs can be oxidized. However the damage induced on the impurities is bigger than on the CNTs, since the impurities have more defects and open structures. The efficiency of the process depend on a lot of factors, such as metal content, oxidation time, environment, oxidation agent and temperature [112, 113, 114]. In general the acid treatment removes the metal catalyst. The metal catalyst is exposed to acid solutions or solvent. For a treatment in HNO3 only the metal catalyst is etched, and no effects on CNTs and carbon particles are observed. If HCl is used, produces also a little damage on the CNTs and other carbon particles [115]. High temperatures (873-1873 K) annealing processes allow a rearrangement of the nanotubes and defects can be consumed[116]. The metal can be melted and can be removed using high temperature vacuum treatment. In ultrasonication the particles are separated by ultrasonic vibrations. Agglomerated of different particles are forced to vibrate and in this way they can be dispersed. The separation of the particles depend on the surfactant, solvent and reagent used [117, 118]. The solvent influences the stability of the dispersed CNTs. When an acid is used like solvent, the purity of the CNTs depend on the treatment time. For a short exposure time only the metal solvates, for a longer exposure time the CNTs can be chemically cut. In magnetic purification ferromagnetic particles are mechanically removed. The CNTs are mixed with inorganic nanoparticles (ZrO2 or CaCO3) and put in an ultrasonic bath to remove the ferromagnetic particles. Then the particles are trapped with permanent magnetic poles [119]. Micro filtration is based on size and particles separation. CNTs and a small quantity of carbon nanoparticles are trapped in a filter, the other nanoparticles (catalyst metal, fullerenes and carbon nanoparticles) pass through the filter. A way to separate fullerene from the CNTs by micro filtration is to soak the as-produced CNTs in a CS2 solution: the purified CNTs are trapped in a filter, and the fullerenes solved in the CS2 pass through the filter [120]. Cutting of the CNTs can be induced chemically, mechanically or by a combination of both. CNTs can be chemically cut by partially functionalizing the tubes, for example with fluorine [121]. Then the flu-

orated carbon will be driven off in the form of CF4 or COF2. This leaves behind the chemically cut nanotubes. Mechanical cutting of the CNTs can be induced by ball-milling [122]. Here the bonds are broken to the high friction between the nanoparticles and the nanotubes. Ultrasonical technique is a combination between mechanical and chemical cutting. The ultrasonic vibration provides to the nanotubes sufficient energy to leave the catalyst surface. Finally, the technique of functionalization is based on making CNTs more soluble than the impurities by attaching other groups to the tubes. In this way it becomes easy to separate them from insoluble impurities (metal) with filtration [123, 124].

2.10 Characterization of CNTs by Raman spectroscopy

Carbon nanotubes have proven to be a unique system for the application of Raman spectroscopy, and at the same time Raman spectroscopy has provided an exceedingly powerful tool useful in the study of the vibrational properties and electronic structures of CNTs. Raman spectroscopy has been successfully applied for studying SWCNTs and MWCNTs. The large van der Waals interactions between the CNTs lead to an agglomeration of the tubes in the form of bundles or ropes. This problem can be solved by wrapping the tubes in a surfactant or functionalizing the CNTs by attaching appropriate chemical moieties to the sidewalls of the tube. Functionalization causes a local change in the hybridization from sp^2 to sp^3 of the side-wall carbon atoms, and Raman spectroscopy can be used to determine this change. In addition information on length, diameter, electronic type (metallic or semiconducting), and whether nanotubes are separated or in bundle can be obtained by the use of Raman spectroscopy. Recent progress in understanding the Raman spectra of single walled carbon nanotubes have stimulated Raman studies of more complicated multi-wall carbon nanotubes. Raman spectroscopy is a single resonance process, i.e., the signals are greatly enhanced if either the incoming laser energy (E_{laser}) or the scattered radiation matches an allowed electronic transition in the sample. For this process to occur, the phonon modes are assumed to occur at the center of the Brillouin zone (q = 0). Owing to their one dimensional nature, the Π-electronic density of states of a perfect, infinite, SWNTs form sharp singularities which are known as van Hove singularities (vHs), which are energetically symmetrical with respect to Fermi level (E_f) of the individual SWNTs. The allowed optical transitions occur between matching vHs of the valence and conduction band of the SWNTs, i.e., from first valence band vHs to the first conduction band vHs (E_{11}) or from the second vHs of the valence band to the second vHs of the conduction band (E_{22}). Since the quantum state of an electron (k) remains the same during the transition, it is referred to as k-selection rule. The electronic properties, and therefore the individual transition energies in SWNTs are given by their structure, i.e., by their chiral vector that determines the way SWNT is rolled up to form a cylinder [see section2.2]. Raman spectroscopy of
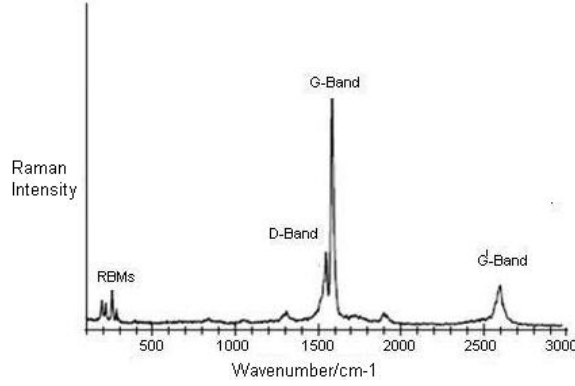
Figure 2.15: Raman spectrum of HiPco SWNTs using a laser of wavelength of λexc = 633 nm[126].

an ensemble of many SWNTs having different chiral vectors is sensitive to the subset of tubes where the condition of allowed transition is fulfilled. A 'Kataura-Plot' [125] gives the allowed electronic transition energies of individual SWNTs as a function of diameter d, hence information on which tubes are resonant for a given excitation wavelength can be inferred. Since electronic transition energies vary roughly as $1/d$, the question whether a given laser energy probes predominantly semiconducting or metallic tubes depends on the mean diameter and diameter distribution in the SWNT ensemble. However, the transition energies that apply to an isolated SWNT do not necessarily hold for an ensemble of interacting SWNTs owing to the mutual Van der Waals interactions. Figure 2.15 shows a typical Raman spectrum from 100 to 3000 cm^{-1} taken of SWNTs produced by catalytic decomposition of carbon monoxide (HiPco-process). The three dominant Raman features are the radial breathing mode (RBM) at low frequencies, tangential (G-band) multi feature at higher frequencies and the disorder induced D-band. Another weak features, the G' band (an overtone mode) is also shown.

The RBM Raman features appear between 100 cm^{-1} $< \omega_{RBM} <$ 500 cm^{-1} from the elastically scattered laser line. It corresponds to the vibration of the C atoms in the radial direction, as if the tube is breathing (Figure2.16). An important point about these modes is the fact that the energy (or wavenumber) of these vibrational modes depends on the diameter (d) of the tube, and not on the way the SWNT or MWCNT is rolled up to form a cylinder, i.e., they do not depend on the ϑ of the tube.

These features are very useful for characterizing nanotube diameters through the relation:
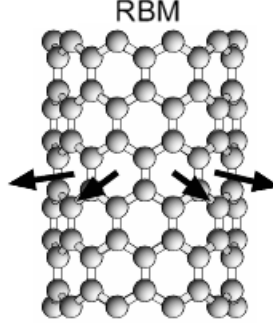
Figure 2.16: Schematic picture showing vibration for RBM [127].

$$\omega_{RBM} = A/d + B \qquad (2.5)$$

where A and B are constants and their variations are often attributed to environmental effects, i.e., whether the SWNTs are present as individual tubes wrapped in a surfactant, isolated on a substrate surface, or in the form of bundles. However, for d less than 1 nm, nanotube lattice distortions lead to chirality dependence of ω_{RBM} [128]and for large diameters tubes when, d is more than 2 nm the intensity of RBM feature is weak and is hardly observable. The tangential modes are the most intensive high-energy modes of SWNTs and form the so-called G-band, which is typically observed at around 1582 cm^{-1}. Unlike graphite, the tangential G mode in SWNTs gives rise to a multi-peak feature, also named the G band, where up to six Raman peaks can be observed in a first-order Raman process. However, a simple analysis can be carried out considering the two most intense peaks, that basically originate from the symmetry breaking of the tangential vibration when the graphene sheet is rolled to make a cylindrically shaped tube (see figure 2.17a). The two most intense G peaks are labelled G^{+}, for atomic displacements along the tube axis, and G^{-}, for modes with atomic displacement along the circumferential direction (see figures 2.17a and 2.17b), and the lowering of the frequency for the G^{-} mode is caused by the curvature of the nanotube which softens the tangential vibration in the circumferential direction.

Spectra in the frequency between 1450-1650 cm^{-1} can be used for SWNT characterization, independent of the RBM observation. This multi-peak feature is useful in distinguishing semiconducting from metallic SWNTs. The D-band is observed at 1300-1400 cm^{-1}. The appearance of D-peak can be interpreted due to the breakdown of the k-selection rule. This behavior is interpreted as a double resonance effect, where not only one of the direct, k-conserving electronic transitions, but also the emission of phonon is a resonant process. In contrast to single resonant Raman scattering, where only phonons around the center of the Brillouin zone (q = 0) are excited, the phonons
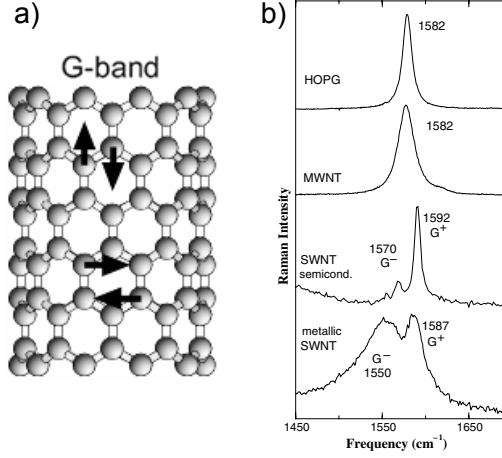
Figure 2.17: a) Schematic picture showing the atomic vibrations for the G-band. b) G band for highly ordered pyrolytic graphite (HOPG), MWNT bundles, one isolated semiconducting SWNT and one isolated metallic SWNT[128].

that provoke the D-band exhibit a non-negligible q vector. This explains the double resonance theory for D-band in Raman spectroscopy. In few cases, the overtone of the D-band known as the G'-band (or D*-band) is observed at 2600-2800 cm^{-1}, and it does not require defect scattering as the two phonons with q and -q are excited. This mode is therefore observed independent of the defect concentration. The presence of D-band peak usually indicates the presence of various defects (such as hetero-atoms, vacancies, heptagon-pentagon pairs, kinks, or even the presence of impurities, etc) [129].

References

[1] Iijima, S. Helical Microtubules of Graphitic Carbon. Nature 354, 56-58 (1991).

[2] Iijima, S. & Ichihashi, T. Single-Shell Carbon Nanotubes of 1-Nm Diameter. Nature 363, 603-605 (1993).

[3] Bethune, D. S. et al. Cobalt-Catalyzed Growth of Carbon Nanotubes with Single-Atomic-Layerwalls. Nature 363, 605-607 (1993).

[4] Hamada, N., Sawada, S. & Oshiyama, A. New One-Dimensional Conductors Graphitic Microtubules. Phys. Rev. Lett. 68, 1579-1581 (1992).

[5] Saito, R., Fujita, M., Dresselhaus, G. & Dresselhaus, M. S. Electronic- Structure of Chiral Graphene Tubules. Appl. Phys. Lett. 60, 2204-2206 (1992).

[6] Tans, S. J. et al. Individual single-wall nanotubes as quantum wires. Nature 386, 474-477 (1997).

[7] Bockrath, M. et al. Single-electron transport in ropes of carbon nanotubes. Science 275, 1922-1925 (1997).

[8] Thess, A. et al. Crystalline ropes of metallic carbon nanotubes. Science 273, 483-487 (1996).

[9] en.wikipedia.org/wiki/Carbon_nanotube

[10] P. D. Jarillo-Herrero "Quantum transport in carbon nanotubes", PhD Thesis, Technology University of Delft, 2005.

[11] Wallace, P. R. The Band Theory of Graphite. Phys. Rev. 71, 622-634 (1947).

[12] M. Dresselhaus, S. Dresselhaus, G. & Eklund, P. C. Science of Fullerenes and Carbon Nanotubes (Academic Press, San Diego, 1996).

[13] Minot, E. D. Tuning the band structure of carbon nanotubes. Ph.D. Thesis (2004).

[14] White, C. T. & Mintmire, J. W. Density of states reflects diameter in nanotubes. Nature 394, 29-30 (1998).

[15] Dresselhaus, M. S., Dresselhaus, G. & Avouris, Ph. Carbon Nanotubes: Synthesis, Structure, Properties, and Applications (Springer, New York, 2001).

[16] P.L. McEuen, M. Brockrath, D.H. Cobden, Y.G. Yoon, S.G. Louie, Phys. Rev. Lett. 83, (1999), 5098-5101

[17] C.T. White, T.N. Todorov, Nature 393, (1998), 240-242

[18] M. Hjort, S. Stafstrom, Phys. Rev. B, 63, (2001)

[19] J. Jiang, M.J. Dong, H.T. Yang, D.Y. Xing, Phys. Rev. B, 64, (2001)

[20] J. Kong, C. Zhou, A. Morpurgo, H.T. Soh, C.F. Quate, C. Marcus, H. Dai, Appl. Phys. A: Mater. Sci. Process. 69, (1999), 305-308

[21] J. Nygard, H.D. Cobden, P.E. Lindelof, Nature, 408, (2000), 342-346

[22] H.T. Soh, C.F. Quate, A.F. Morpurgo, C.M. Marcus, J. Kong, D.J. Dai, Appl. Phys. Lett. 75, (1999), 627-629

[23] Z. Yao, C.L. Kane, C. Dekker, Phys. Rev. Lett. 84, (2000), 2941-2944

[24] A. Bachtold, M.S. Fuhrer, S. Plyasunov, M. Forero, E.H. Anderson, A. Zettl, P.L. McEuen, Phys. Rev. Lett. 84, (2000), 6082-6085

[25] V. Krstic, S. Roth, M. Burghard, Phys. Rev. B 62, (2000), R16353-R16355

[26] J. Kong, E. Yenilmez, T.W. Tombler, W. Kim, H.J. Dai, R.B. Laughlin, L. Liu, C.S. Jayanthi, S.Y. Wu, Phys. Rev. Lett. 87, (2001)

[27] W.J. Liang, M. Bockrath, D. Bozovic, J.H. Hafner, M. Tinkham, H. P[33]ark, Nature 411, (2001), 665-669

[28] H.J. Choi, J. Ihm, S.G. Louie, M.L. Cohen, Phys. Rev. Lett. 84, (2000), 2917-2920

[29] C.C. Kaun, B. Larade, H. Mehrez, J. Taylor, H. Guo, Phys. Rev. B 65, (2002)

[30] X.R. Wang, Y.P. Wang, Z.Z. Sun, Phys. Rev. B, 65, (2002)

[31] L.F. Yang, J.W. Chen, H.T. Yang, J.M. Dong, Phys. Rev. B, 69, (2004)

[32] V. Derycke, R. Martel, J. Appenzeller, P. Avouris, Appl. Phys. Lett. 80, (2002), 2773-2775

[33] P. Avouris, R. Martel, V. Derycke, J. Appenzeller, Physica B: Condens. Matter 323, (2002), 6-14

[34] A. Maiti, A. Ricca, Chem. Phys. Lett. 395, (2004), 7-11

[35] Y. Yaish, J.Y. Park, S. Rosenblatt, V. Sazonova, M. Brink, P.L. McEuen, Phys. Rev. Lett. 92, (2004)

[36] J. Appenzeller, J. Knoch, V. Derycke, R. Martel, S. Wind, P. Avouris, Phys. Rev. Lett. 89, (2002)

[37] S. Heinze, J. Tersoff, R. Martel, V. Derycke, J. Appenzeller, P. Avouris, Phys. Rev. Lett. 89, (2002)

[38] R. Martel, V. Derycke, C. Lavoie, J. Appenzeller, K.K. Chan, J. Tersoff, P. Avouris, Phys. Rev. Lett. 87, (2001)

[39] S.J. Wind, J. Appenzeller, P. Avouris, Phys. Rev. Lett. 91, (2003)

[40] J. Appenzeller, M. Radosavljevic, J. Knoch, P. Avouris, Phys. Rev. Lett. 92, (2004)

[41] S. Reich, C. Thomsen, J. Maultzsch, Carbon Nanotubes, WILEY-VCH (2004)

[42] A. Javey, J. Guo, Q. Wang, M. Lundstrom, H.J. Dai, Nature, 424, (2003), 654-657

[43] S.J. Tans, A. Verschueren, C. Dekker, Nature, 393, (1998), 6680

[44] A. Bachtold, P. Hadley, T. Nakanishi, C. Dekker, Science, 294, (2001), 1317

[45] R. Krupka, F. Hennrich, H. v.Löhneysen, M.M. Kappes, Science 301, (2003), 344

[46] F. Bussolotti, L. D'Ortenzi, V. Grossi, L. Lozzi, S. Santucci, M. Passacantando, Phys.Rev.B 76, 125415 (2007)

[47] M.P. Anatram, F. Leonard, Rep. Prog. Phys. 69, 507 (2006)

[48] A. Rocherfort, P. Avouris, F. Lesage, D.R. Salahub, Phys. Rev. B 60, 13824 (1999)

[49] Z. Chen, J. Appenzeller, J. Knoch, Y. Lin, P. Avouris, Nano Lett. 5, 1497 (2005)

[50] I. Deretzis, A. La Magna, Nanotech. 17, 5063 (2006)

[51] Q. Ngo, D. Petranovic, S. Krishnan, A. Cassell, Qi Ye, Jun Li, M. Meyyappan, C. Yang, Aust. Math. Soc. Gaz. 3, 311 (2004)

[52] http://www.aip.org/enews/physnews/1996/split/pnu279-2.htm

[53] http://www.wag.caltech.edu/foresight/foresight_2.htm

[54] E. Dujardin, T.W. Ebbesen, A. Krishnan, P.N. Yanilos, M.M.J. Treacy, Physical Review B, 58, (20), (1998), 14013-14019

[55] http:// www.fam.cie.uva.es/~arubio/psi_k/node5.htm

[56] L. Forrò, J.P. Salvetat, J.M. Bonart, R. Basca, N.H. Thomson, S. Garaj, L. Thien-Nga, R. Gaàl, A. Kulik, B. Ruzicka, L. Degiorgi, A. Backtold, C. Schönenberger, S. Pekker, K. Hernadi, Science and Application of Nanotubes, Edit by D. Tomànek, R.J. Enbody, Kluwer Academic/ Plenum Publishers, New York, 2000

[57] J. Bernholc, C. Brabec, M. Buongiorno Nardelli, A. Maiti, C. Roland, B.I. Yakobson, Appl. Phys. A 67 (1998) 39

[58] J.F. Ney, Physical Properties of Crystals, Oxford, Oxford, London, 1979

[59] V.G. Handjiev, M.N. Iliev, S. Arepalli, P. Nikolaev, B.S. Files, Appl. Phys. Lett. 78, (2001), 3193

[60] M.M.J. Treacy, T.W. Ebbesen, J.M. Gibson, Nature (London), 381, (1996), 678

[61] D. Sánchez-Portal, E. Artacho, J.M. Soler, A. Rubio, P.Ordejón, Phys. Rev. B, 59, (1999), 12678

[62] E. Hernández, C. Goze, P. Bernier, A. Rubio, Phys. Rev. Lett. 80, (1998), 4502

[63] A. Charlier, E. McRae, M.F. Charlier, A. Spire, S. Forster, Phys. Rev. B, 57, (1998), 6689

[64] B.I. Yakobson, C.J. Brabec, J. Bernholc, Phys. Rev. Lett. 76, (1996), 2511

[65] Z. Xin, Z. Jianijun, O. Zhong-can, Phys. Rev. B, 62, (2000), 13692

[66] V.N. Popov, V.E.V. Doren, M. Balkanski, Phys. Rev. B 61, (2000), 3078

[67] Y. Xia, M. Zhao, Y. Ma, M. Ying, X. Liu, P. Liu, L. Mei, Phys. Rev. B, 65, (2002), 155415

[68] J. Lu, Phys. Rev. Lett. 79, (1997), 1297; J.P. Lu, J. Phys. Chem. Solids 58, (1997), 1649.

[69] C.Q. Ru, Phys. Rev. B, 62, (2000), 16962

[70] http://www.pa.msu.edu/~tomanek/tomanek.htm

[71] M.F. Lin, Phys. Rev. B, 62 (2000), 13153-13159

[72] C.L. Kane, E.J. Mele, Phys. Rev. Lett. 78, (1997), 1932-1935

[73] M.J. O'Connell, S.M. Bachilo, C.B. Huffman, V.C. Moore, M.S. Strano, et al., Science, 297, (2002), 593

[74] M.J. Bronikowski, P.A. Willis, D.T. Colbert, K.A. Smith, R.E. Smalley, J. Vac. Sci. Technol. A 19, (2001), 1800-1805

[75] J. Lefebreve, Y. Homma, P. Finnie, Phys. Rev. Lett. 90, (2003), 217401

[76] S.M. Bachilo, M.S. Strano, C. Kittrell, R.H. Hauge, R.E. Smalley, R.B. Weisman, Science, 298, (2002), 2361

[77] A. Huczko, Appl. Phys. A 74 (2002) 463

[78] S. Scalese, Physica E-Low-Dimen. Syst. & Nanostruc. 40 (2008) 4

[79] S. Pannala, R.F. Wood, J. Nanosci. Nanotechnol. 4 (4) (2004) 463

[80] Y.M. Scin, S.Y. Jeong, S.J. Eum, C.W. Yang, C.Y. Park, Y.H. Lee, J. Crystal Growth 271 (2004) 81.

[81] K.-Y. Lee, T. Ikuno, K. Tsuji, S. Ohkura, S. Honda, M. Katayama, K. Oura, T. Hirao, J. Vac. Sci. Technol. B 21 (4) (2003) 1437

[82] N. Hayashi, S.-I Honda, K. Tsuji, K.-Y. Lee, T. Ikuno, K. Fujimoto, S. Ohkura, M. Katajama, K. Oura, T. Hirao, Appl. Surf. Sci. 212 (2003) 393

[83] T. Guo, P. Nikolaev, A. Thess, D.T. Colbert, R.E. Smalley, Chemical Physics Letters, 243, 1-2, (1995)

[84] M. Yudasaka, R. Yamada, N. Sensui, T. Wilkins, T. Ichihashi, S. Iijima, Journal of Physical Chemistry B, 103, 30, (1999)

[85] P.C. Eklund, B.K. Pradhan, U.J. Kim, Q. Xiong, J.E. Fischer, A.D. Friedman, B.C. Holloway, K. Jordan, M.W. Smith, Nano Letters, 2, 6, (2002)

[86] W.K. Maser, E. Munoz, A.M. Benito, M.T. Martinez, G.F. de la Fuente, Y. Maniette, E. Anglaret, J.L. Sauvajol, Chemical Physics Letters, 292, 4-6, (1998)

[87] A.P. Bolshakov, S.A. Uglov, A.V. Saveliev, V.I. Konov, A.A. Gorbunov, W. Pompe, A. Graff, Diamond and Related Materials, 11, 3-6, (2002)

[88] C.D. Scott, S. Arepalli, P. Nikolaev, R.E. Smalley, Applied Physics A: Materials Science & Processing, 72, 5, (2001)

[89] T.W. Ebbesen, P.M. Ajayan, Nature, 358, (1992), 220-222

[90] S. Farhat, M.L. La Chapelle, A. Loiseau, C.D. Scott, S. Lefrant, C. Journet, P. Bernier, Journal of Chemical Physics, 115, 14, (2001), 6752-6759

[91] S. Farhat, I. Hinkov, D.I. Chapelle, S.S. Fan, G.H. Li, C.D. Scott, NASA Conference Publication, (2001)

[92] C. Journet, P. Bernier, Applied Physics A-Materials Science & Processing, 67, 1, (1998), 1-9

[93] H. Takikawa, Y. Tao, Y. Hibi, R. Miyano, T. Sakakibara, Y. Ando, S. Ito, K. Hirahara, S. Iijima, AIP Conference Proceedings, 590, (Nanonetwork Materials), (2001)

[94] H. Takikawa, M. Ikeda, K. Hirahara, Y. Hibi, Y. Tao, P.A. Ruiz, T. Sakakibara, S. Itoh, S. Iijima, Physica B: Condensed Matter, 323, 1-4, (2002)

[95] S.H. Jung, M.R. Kim, S.H. Jeong, S.U. Kim, O.J. Lee, K.H. Lee, J.H. Suh, C.K. Park, Applied Physics A-Materials Science & Processing, 76, 2, (2003), 285-286

[96] Z.F. Ren, Z.P. Huang, J.W. Xu, J.H. Wang, P. Bush, M.P. Siegel, P.N. Provencio, Science, 282, 5391, (1998)

[97] Z.F. Ren, Z.P. Huang, D.Z. Wang, J.G. Wen, J.W. Xu, J.H. Wang, L.E. Calvet, J. Chen, J.F. Klemic, M.A. Reed, Applied Physics Letters, 75, 8, (1999)

[98] M. Yudasaka, R. Kikuchi, T. Matsui, Y. Ohki, S. Yoshimura, E. Ota, Applied Physics Letters, 67, 17, (1995)

[99] M. Yudasaka, R. Kikuchi, Y. Ohki,, E. Ota, S. Yoshimura, Applied Physics Letters, 70, 14, (1997)

[100] M. Chen, C.M. Chen, C.F. Chen, Journal of Materials Science, 37, 17, (2002), 3561-3567

[101] J.B. Park, G.S. Choi, Y.S. Cho, S.Y. Hong, D. Kim, S.Y. Choi, J.H. Lee, K.I. Cho, Journal of Crystal Growth, 224, 2, (2002), 211-217

[102] S. Maruyama, S. Chiashi, Y. Miyauch, Thermal Engineering Joint Conference, 6, (2003)

[103] M. Su, B. Zheng, J. Liu, Chemical Physics Letters, 322, 5, (2000)

Salvatore Bagiante, PhD Thesis in Material Science, University of Catania, 2010.

[104] B. Zheng, Y. Li, J. Liu, Applied Physics A: Materials Science & Processing, 74, 3, (2002)

[105] R. Alexandreascu, A. Crunteanu, R.E. Morjan, I. Morjan, F. Rohmund, L.K.L. Falk, G. Ledoux, F. Huisken, Infrared Physics & Technology, 44, 1, (2003)

[106] A.G. Rinzler, J. Liu, H. Dai, P. Nikolaev, C.B. Huffman, F.J. Rodriguez-Macias, P.J. Boul, A.H. Lu, D. Heymann, D.T. Colbert, R.S. Lee, J.E. Fischer, A.M. Rao, P.C. Eklund, R.E. Smalley. Appl. Phys. A 67 (1998) 29-37

[107] E. Borowiak-Palen, T. Pichler, X. Liu, M. Knupfer, A. Graff, O, Jost, W. Pompe, R.J. Kalenczuk, J. Fink, Chemical Physics Letters, 363, 5-6, (2002), 567-572

[108] S.M. Huang, L.M. Dai, Journal of Physical Chemistry B, 106, 14, (2002), 3543-3545

[109] I.W. Chiang, B.E. Brinson, R.E. Smalley, J.L. Margrave, R.H. Hauge, Journal of Physical Chemistry B, 105, 6, (2001), 1157-1161

[110] A.R. Harutyunyan, B.K. Pradhan, J.P. Chang, G.G. Chen, P.C. Eklund, Journal of Physical Chemistry B, 106, 34, (2002), 8671-8675

[111] E. Farkas, M.E. Anderson, Z.H. Chen, A.G. Rinzler, Chemical Physics Letters, 363, 1-2, (2002)

[112] P.X. Hou, C. Liu, Y. Tong, M. Liu, H.M. Cheng, Journal of Materials Research, 16, 9, (2001), 2526-2529; 57

[113] H. Kajiura, S. Tsutsui, H.J. Huang, Y. Murakami, Chemical Physics Letters, 364, 5-6, (2002), 586-592

[114] J.M. Moon, K.H. An, Y.H. Lee, Y.S. Park, D.J. Bea, G.S. Park, Journal of Physical Chemistry B, 105, 24, (2001), 5677-5681

[115] I.W. Chiang, B.E. Brinson, A.Y. Huang, P.A. Willis, M.J. Bronikowski, J.L. Margrave, R.E. Smalley, R.H. Hauge, Journal of Physical Chemistry B, 105, 35, (2001), 8257-8301.

[116] V. Georgakilas, D. Voulgaris, E. Vazquez, M. Prato, D.M. Dirk, A. Kukovecz, H. Kuzmany, Journal of the American Chemical Society, 124, 48, (2002).

[117] S. Bandow, A.M. Rao, K.A. Williams, A. Thess, R.E. Smalley, P.C. Eklund, Journal of Physical Chemistry B, 101, 44, (1997).

[118] K.B. Shelimov, R.O. Esenaliev, A.G. Rinzler, C.B. Huffman, R.E. Smalley, Chem. Phys. Lett., 282, 429-434, (1998).

[119] L. Thien-Nga, K. Hernadi, E. Ljubovic, S. Garaj, L. Forro, Nano Letters, 2, 12, (2002), 1349-1352.

[120] S. Bandow, A. Asaka, X. Zhao, Y. Ando. Appl. Phys. A 67 (1998) 23-27.

[121] Z. Gu, H. Peng, R.H. Hauge, R.E. Smalley, J.L. Margrave, Nano Letters, 2, 9, (2002), 1009-1013.

[122] B. Gao, C. Bower, J.D. Lorentzen, L. Fleming, A. Kleinhammes, X.P, Tang, L.E. Mcneil, Y. Wu, O. Zhou, Chemical Physics Letters, 327, 1-2, (2000), 69-75.

[123] S. Niyogi, H.Hu, M.A. Hamon, P. Bhowmik, B. Zhao, S.M. Rozenzhak, J. Chen, M.E. Itkis, M.S. Meier, R.C. Haddon, Journal of the American Chemical Society, 123, 4, (2001), 733-734 .

[124] B. Zhao, H. Hu, S. Niyogi, M.E. Itkis, M.A. Hamon, P. Bhowmik, M.S. Meier, R.C. Haddon, Journal of the American Chemical Society, 123, 47, (2001), 11673-11677.

[125] Kataura H, Kumazawa Y, Maniwa Y, Uemezu I, Suzuki S, Ohtsuka Y and Achiba Y 1999 Synth. Met. 103 2555

[126] R. Graupner, J. Raman Spectrosc., 2007, 38, 673.

[127] http://cnx.org/content/m22925/1.2/

[128] A Jorio, M A Pimenta, A G Souza Filho2 R Saito3 G Dresselhaus and M S Dresselhaus, New Journal of Physics 5 (2003) 139.1–139.17.

[129] Ferrari A C and Robertson J 2000 Phys. Rev. B 61 14095.

Chapter 3

Synthesis of carbon nanotubes by arc discharge in liquid nitrogen

"Cos'era? Non lo so. Quando non sai cos'è, allora è Jazz"

(A. Baricco, Novecento).

Arc discharge is a very common technique for the synthesis of carbon nanotubes (CNTs), due to its high yield and easiness of the process. Although many experimental studies have been reported in the literature [1, 3, 4], the complete understanding of the process is still far to be reached and not so much is known about the influence of the experimental parameters on the products of arc discharge. In the last few years in parallel with arc discharge in the gaseous phase, arc discharge in liquids has been developed as a low-cost (no vacuum systems are needed), effective method to produce several carbon nano-materials, such as multi-walled and single-walled CNTs (MWCNTs and SWCNTs). In particular, arc discharge in liquid nitrogen allows to cool the electrodes and keep them in a clean environment during arcing. In this chapter, we describe the experimental apparatus used and discuss the role of the arc discharge parameters in the synthesis of carbon nanotubes (CNTs) in liquid nitrogen. We report a morphological study of the C-deposit produced and study the effect of the size of electrodes, applied voltage and discharge current on the formation of MWCNTs and hybrid structure (linear carbon chains (LCC) and CNTs).
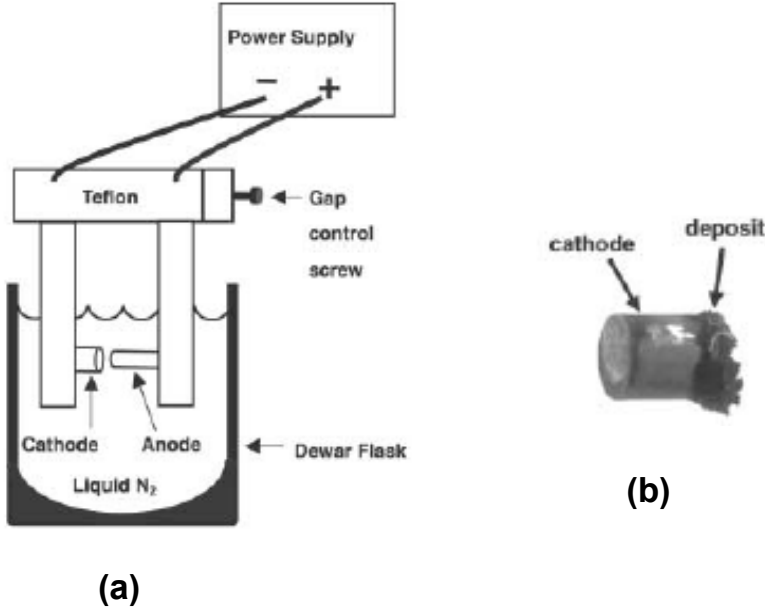
Figure 3.1: (a) Schematic drawing of the arc discharge apparatus. (b) Image of the CNTs-rich material deposited on the cathode[2].

3.1 Experimental apparatus

As discussed before (section2.8), there are several synthesis methods for the production of CNTs and each of them produces CNTs with different peculiarities. Electric arc discharge is advantageous for obtaining highly crystalline CNTs. The conventional arc discharge method, however, requires a complicated vacuum apparatus with an efficient cooling system. Ishigami et al. [1] proposed a modified method for the synthesis of CNTs, in which liquid nitrogen was filled into the arc discharge chamber. Liquid nitrogen prevents the electrodes from contamination with unwanted gases and effectively lowers the temperature of the electrodes. Moreover, CNTs do not stick to the wall of the chamber, so that a clean sample of CNTs can be obtained. In 2003 Jung et al [2] reported the MWCNTs synthesis, with high purity, by arc discharge in which vacuum is replaced with liquid nitrogen. Figure3.1 shows a schematic drawing of the arc discharge apparatus and in Figure3.2 we report our system.

Anode and cathode are two high purity (99.99%) graphite rods, submerged in LN2 and connected to a DC power supply. The distance between the two electrodes is adjusted (about 1mm) until arc discharge takes place. Carbon is evaporated from
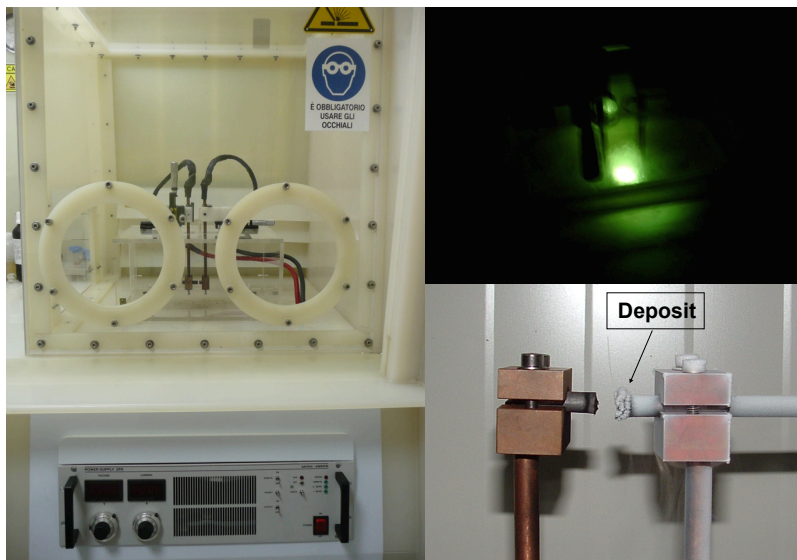
Figure 3.2: (a) equipment used to synthesize CNTs by arc discharge in liquid nitrogen; (b) arc discharge between the two electrodes; (c) electrodes after discharge.

the anode and deposited on the cathode (fig. 3.1b).

The distance between the two electrodes is adjusted (about 1mm) until arc discharge takes place. Carbon is evaporated from the anode to the cathode. The applied voltage to start the electric arc ranges between 15V and 45V and the discharge current values are in the range of 15-80A. The structural characterization of the samples was performed by scanning electron microscopy (SEM), using a ZEISS SUPRA 35 FE-SEM system equipped with field emission electron gun, and by transmission electron microscopy (TEM), using a JEM 2010F JEOL microscope operating with acceleration voltage of 200 kV. Furthermore, Raman spectroscopy was used in order to get information on the local vibrational properties and, consequently, on the chemical bonds among the atoms contained in the samples. Raman scattering has been performed by three different laser systems: a 325 nm radiation from He-Cd laser, 514.5 nm radiation coming from an Ar ion laser and 632.8nm radiation coming from an He-Ne laser. For the source at 325 nm, a micro Raman spectra were taken in backscattering geometry with a HORIBA Jobin-Yvon system, equipped with Olympus BX40 microscope and a spectrometer with 2400 lines/mm grating has been used. For the 514.5 nm radiation, a backscattering configuration has been used in order to collect the scattered light which has been analyzed by a single 460 mm monochromator (Jobin–Yvon HR460), equipped with a notch filter and a liquid nitrogen cooled charge-coupled device detec-

tor with an overall spectra resolution of 4 cm^{-1}. For the sources at 632.8 nm , a micro Raman spectra were taken in backscattering geometry with a HORIBA Jobin-Yvon system, equipped with Olympus BX41 microscope has been used. The laser power on the sample was about 6 mW and a spectrometer with 600 or 2400 lines/mm grating was used.

3.2 Morphological study of C-deposit

We have analyzed C deposit samples in cross section, after cleaving them perpendicularly to the surface, in order to observe the morphology of the deposit and to identify the spatial distribution of CNTs in the deposit, that could be useful to explain the formation kinetics of nanotubes during the discharge. The difficulties in the cross section analyses are due to the fact that the sample cannot be cut, as this procedure might alter the morphology, but it has to be cleaved in two parts just pressing the deposit on the edge. Changes in the morphology of the C deposit have been observed by varying the voltage between 15 and 45 V and keeping the maximum current value at 80 A; alternatively, the voltage has been fixed at 25 V and the current has been varied between 30 and 80 A (see section 3.3.1). In figure 3.3a we report the SEM image in cross section of the C deposit produced at 25 V, with a current value of 80 A. It appears to be formed by two different parts: a kind of bowl, consisting of C structures with long-range disorder, and the core, containing straight pillars well aligned along the growth direction of the deposit, i.e. along the electrode axis, as schematized in figure 3.3b. The disordered carbon columns and the pillars are shown more in detail in figure 3.3c,d respectively.

The pillars reported in Figure 3.3d are shown at higher magnification in Fig. 3.4 a and b. These images reveal that the pillars are formed by carbon nanotubes randomly oriented. In figure 3.4c we report a TEM image of a typical CNT obtained in these experimental conditions, with the innermost tube diameter smaller than 1 nm.

Similar observations have been made for the morphology of C deposits produced by arc discharge in gaseous environments [5, 6]. In order to observe the influence of the electric field on the C deposit morphology, we have produced other samples at lower and higher voltage, using the same current (80 A).

When the voltage is varied, the main differences we observe consist of: (1) the spatial distribution of CNT pillars in the deposit; (2) the sharpness of the pillar contours. If we define α as the angle formed between the pillar axis direction and the
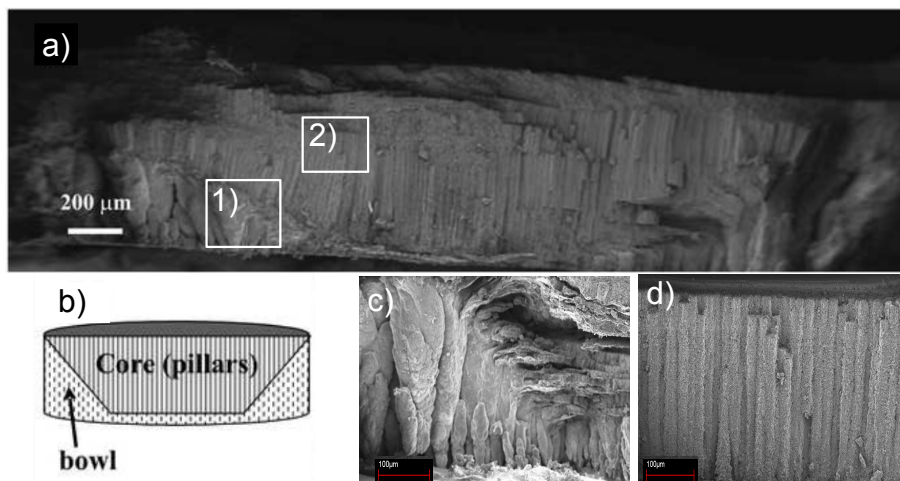
Figure 3.3: SEM images at different magnifications of the C deposit produced at 25 V, 80 A, for a 30 s arc discharge; (b) schematics of C deposit in cross-view; in (c) and (d) higher magnification SEM images of the C structures and CNTs present in the regions marked respectively by the boxes b and c are shown.
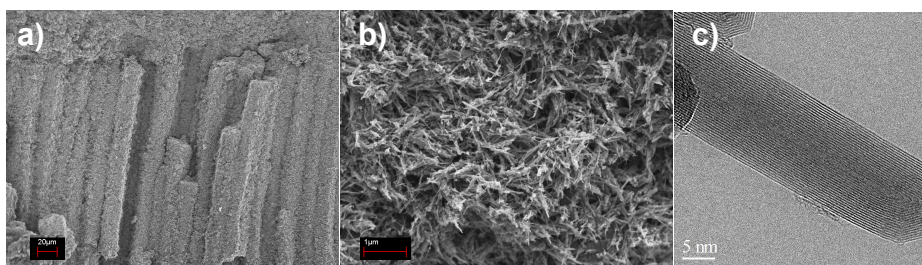
Figure 3.4: a) CNT pillars; b) a detail of a pillar containing randomly oriented CNTs; c) TEM image of a CNT contained in a pillar.
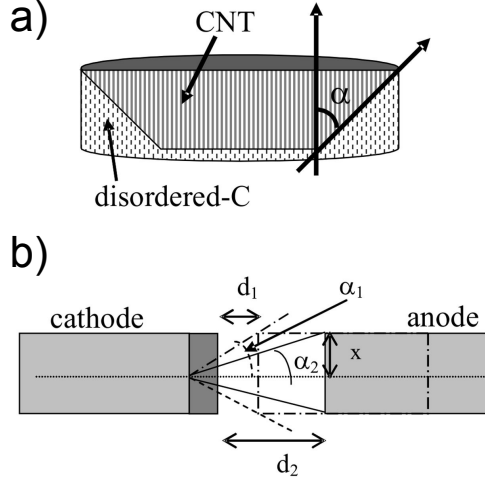
Figure 3.5: a) schematics of the C deposit forming on the cathode surface; b) graphite electrodes and geometric parameters for different voltages $V_1 < V_2$ ($d_1 < d_2$; $\alpha_1 > \alpha_2$)

border between the bowl and the pillar region (as shown in fig. 3.5a), we observe that α increases as the voltage decreases, changing from 55° for 45 V to 65° for 25V, up to about 85° for 15 V samples. The α values versus applied voltage are reported in table I, and they can be used in order to estimate the distance between the electrodes during the arc discharge, as reported in the drawing of figure 3.5b. For three voltages, we get three different α values, and by simple geometric considerations we can estimate the corresponding inter-electrode distances, for an anode radius of 5 mm: for V_1=15V, α_1=85° and d_1=0.4 mm; for V_2=25V, α_2=65° and d_2=2.3 mm; for V_3=45V, α_3=55° and d_3=3.5 mm.

In table 3.1 we also report the width W of the pillars. Excluding the sample produced at 15 V, where the CNT pillars are not well defined, in all the other samples they are about 20 μm large. We have also analyzed the behavior of the C structures by keeping fixed the voltage at 25 V and making the current change between 30 A and 80 A. The SEM images of some of them (30A, 50 A and 70 A) are reported in figure3.6a, b and c, respectively. In these cases, α is 65° and does not change with the current; the contours of the pillars in the 30 A sample are blurred (Fig.3.6a) and it is hard to evaluate the pillar width, whilst they become sharper at higher current values and a width of about 20 μm is found for all the discharge current values from 50 A to 80 A. Raman analysis has been performed on the cross section of the samples, to identify the C structures present in the different regions and their

V (I=80 A)	W	α
15 V	-	80°-90°
20 V	≈20 µm	75°-80°
25 V	≈20 µm	60°-65°
30 V	≈20 µm	60°-65°
40 V	≈20 µm	45°-55°
45 V	20 - 25 µm	45°-55°

Table 3.1: Width of the CNT pillars and α values obtained for different applied voltages.

ordered or disordered morphology.

In figure 3.7(a) we report the cross-section SEM image of a C deposit produced at 45V, 80A, and in figure3.7(b) a Raman map of the I_D/I_G ratio obtained from all Raman spectra acquired on the same cross section. The color-scale of the Raman map indicate the order degree of the carbon structures contained in the deposit: black regions (low I_D/I_G value) means ordered structures; yellow regions (high I_D/I_G value) indicate disordered carbon. In Fig. 3.7(c), (d), (e) we report the Raman spectra acquired on the sample in three different positions, indicated respectively by three crosses 1, 2, 3 in the map of figure 3.7(b).

In particular, in the spectrum relative to point 1, the high I_D/I_G ratio indicate a disorder in the C structures, but reveal that they are not amorphous [7, 9]. Furthermore, the presence of a second peak in the G band has to be noticed, known as D'. We have observed here that the structural quality of CNTs does not improve with increasing the current if 10 mm wide electrodes are used, as will discuss in section 3.3. An improvement of the CNT quality, instead, is observed as the voltage is increased from 15 V up to 20V, but then it remains nearly constant, as indicated by the calculation of the I_D/I_G ratio in the Raman spectra, reported in figure 3.8.

In order to explain the above described results we have to take into account the arcing process and the related parameters. By changing the applied voltage, arcing takes place at different distance values between the electrodes: the lower is the voltage, the shorter is the inter-electrode distance necessary to start the electric arc, as already discussed above and schematically shown in Fig. 3.5 For two voltage values V_1 and V_2, with $V_1 < V_2$, the inter-electrode distance for starting the electric arc d_1, is lower than d_2, and the angle α_1 is larger than α_2, as confirmed by our experimental observations. The distance between the electrodes influences the temperature
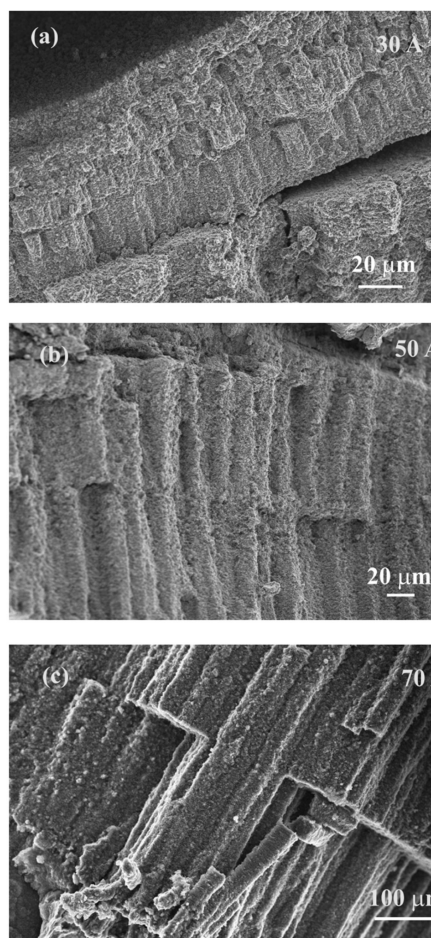
Figure 3.6: Cross-view SEM images of C deposits, showing the CNTs, produced at 25 V with a current of a)30 A; b) 50 A; c) 70 A.
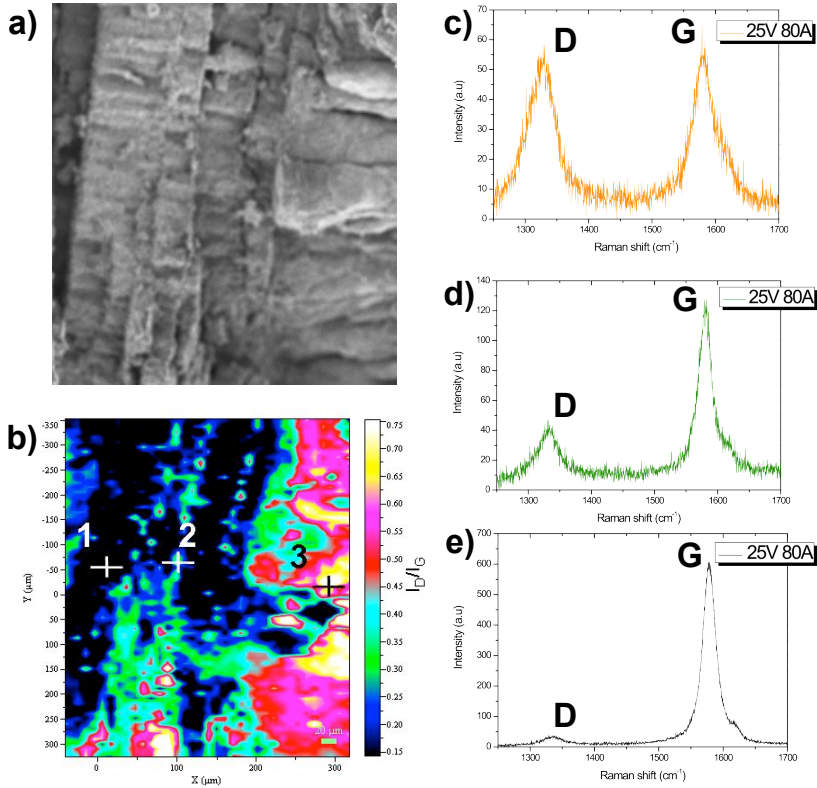
Figure 3.7: a) Cross-section SEM image of a C deposit and b) the correspondent Raman map showing the I_D/I_G ratio values. The spectra corresponding to the point 1, 2, 3 indicated in the map are reported in c), d) and e), respectively. Using a laser of wavelength of $\lambda_{exc} = 632.8$ nm.
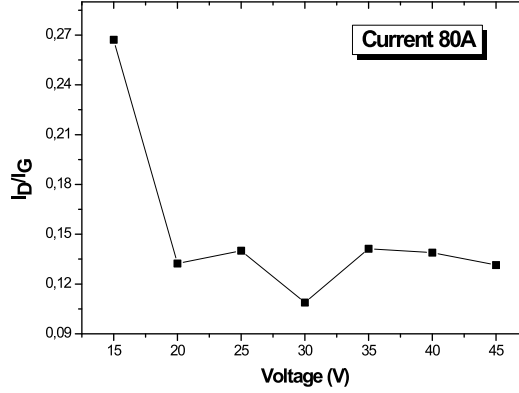
Figure 3.8: Plot of I_D/I_G ratio calculated in Raman spectra acquired on CNT samples produced at different voltages. Using a laser of wavelength of λexc = 632.8 nm.

distribution and the density of carbon species in the inter-electrode region and, in particular, on the cathode surface along the radial direction [8]. Even though optical emission spectroscopy (OES) measurements [10] reveal that the average plasma temperature is about the same (2200-2300 K) for all the arc processes performed at different voltages in the voltage range here considered, the spatial distribution of C structures is not the same for the different deposits. Their spatial distribution mimics the spatial distribution of the temperature that changes as the inter-electrode distance is varied, in agreement with the mathematical model by Bilodeau et al. [8], that reports the case of arc discharge in gaseous environment. They found that at larger distances (4 mm) the highest temperature is obtained in the proximity of the center of the cathode surface, and considerably reduces by moving along the radial direction towards the border. For smaller inter-electrode distance (1 mm) the highest temperature is found in the middle of the inter-electrode space and the temperature gradient is small in the radial direction in the proximity of the cathode surface. These findings can explain the differences observed in the deposit shape depending on the applied voltage. The inter-electrode distances reported in the theoretical model are comparable with the ones estimated in our experiments, ranging between 0.4 mm (for 15 V) and 3.5 mm (for 45 V), as reported above. In general, for any applied voltage: in the central part of the cathode the temperature is higher, as well as the density of carbon ions, and here CNTs are formed; in the radially outer region of the deposit, cooling, due to the presence of liquid nitrogen around the cathode, is more efficient and the vapor density is lower. Here, disordered columns and the stacked (nearly

graphitic) planes are formed. Changing the applied voltage produces relevant effects on the spatial distribution of the C structures (CNTs and disordered carbon) in the deposit: we have identified a new parameter, α, related to the voltage (and, therefore, to distance) between the electrodes during arcing. This parameter is definitely related to the temperature distribution and, probably, to the vapor density in the inter-electrode space and in the proximity of the deposit surface. An effect of the low density of C species on the cathode surface could be the low definition and sharpness of CNT pillars obtained for arc discharge at low voltage (15 V) or at low current (30 A). Indeed, in these cases, low voltage means small inter-electrode distance and, according to the same model described above, low density of C species current; low current (even at inter-electrode distance large enough) determines low density of C species current on the cathode surface too. All these observations should be taken into account when arc discharge is used for CNT production, in order to improve the CNT yield and quality, for example by modifying the arc discharge system geometry. Furthermore, a selection of the regions containing CNTs can be done, allowing to remove most of the large disordered structures in advance and to minimize the purification procedures.

3.3 Role of the growth parameters on the CNT structure

3.3.1 Role of the discharge current and electrode diameter

We have produced several samples changing the electrode diameter (5, 6 and 10 mm) and, for each case, the current has been varied between 15 and 80 A, keeping the voltage at 25 V. The arc duration is usually about 60s. In the Figure 3.9 we report the SEM images of samples produced at different currents using electrodes with diameters of 5-6mm, 6-6mm and 10-10mm as anode-cathode couples: it is evident that the use of larger electrodes leads to the formation of nanotubes with smaller diameters and lower amount of amorphous carbon.

In particular Raman spectra show a progressive decrease of the I_D/I_G intensity ratio, as reported in figures 3.10, 3.11 and 3.12 as the electrodes diameter increases. It is generally agreed in the literature that this decrease is related to an improvement in the structural order of the nanotubes and in general of graphite-like materials [11].

In all the spectra, the D-band at ~1358 cm^{-1}, the G-band at ~1593cm^{-1}, and G'-band at ~2730 cm^{-1}, are visible. The D-band is indicative of defects in the CNTs, like carbonaceous impurities with sp^3 bonds or broken sp^2 bonds on the walls. The G-band indicates the graphitic nature of the sample. The intensity ratio between the D- and G-bands (I_D/I_G) gives information on the graphitic order of the C material synthesized: the lower is I_D/I_G, the better is the structural order.

For the configuration with two rods of 6mm (Fig. 3.11), we observed a noteworthy
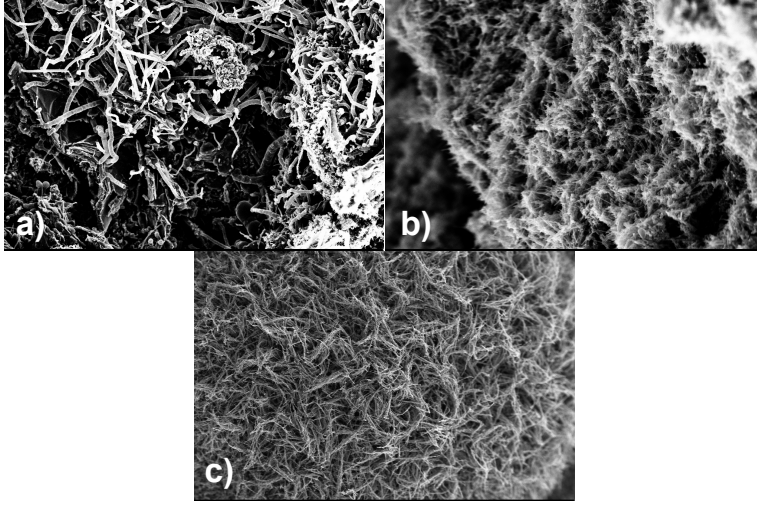
Figure 3.9: SEM image for the samples produced at 25V 50A. SEM image for samples produced by a couple of electrodes 5 mm -6 mm (a), 6 mm - 6 mm (b), 10 mm -10 mm (c).

discharge instability during the synthesis of samples produced with a current of 70 and 80 A. This instability, consisting of frequent current fluctuations below the maximum current value set and/or interruptions, is probably due to a faster erosion of the anode for such high current values, determining rapid changes of the electrode shape and distance between the two electrodes, that has to be frequently readjusted in order to keep on arcing. The result is a large variability of the measured I_D/I_G ratio, depending on the analyzed region of the sample. In these particular conditions another band centered at about 1850 cm^{-1} is clearly visible, that cannot be associated to CNTs or to any other sp^2 or sp^3 hybridized carbon form. We will explain what this band is due to, in section 3.4.

Particularly interesting is the analysis of the nanotubes obtained by using 10mm electrodes (Fig. 3.12). In this case, it is possible to observe a series of RBMs for all current values, in the low frequency region (100–500cm^{-1}). These are due to MWCNTs having very thin innermost diameters, reported up to now in the literature only in the case SWCNTs and purified MWCNTs [12]. The three low frequency signals, observed at 273, 320 and 390 cm^{-1} , as reported in Figure 3.12b, can be associated to 0.82, 0.7 and 0.57 nm innermost tube diameters, respectively, using the relation found for SWCNTs [15], as above mentioned. An up-shift of 5–10% in the RBM frequency due to interlayer interaction is generally reported in the literature for MWCNT [16] and SWCNT bundles [17]. In this case the values of the innermost diameter, for a
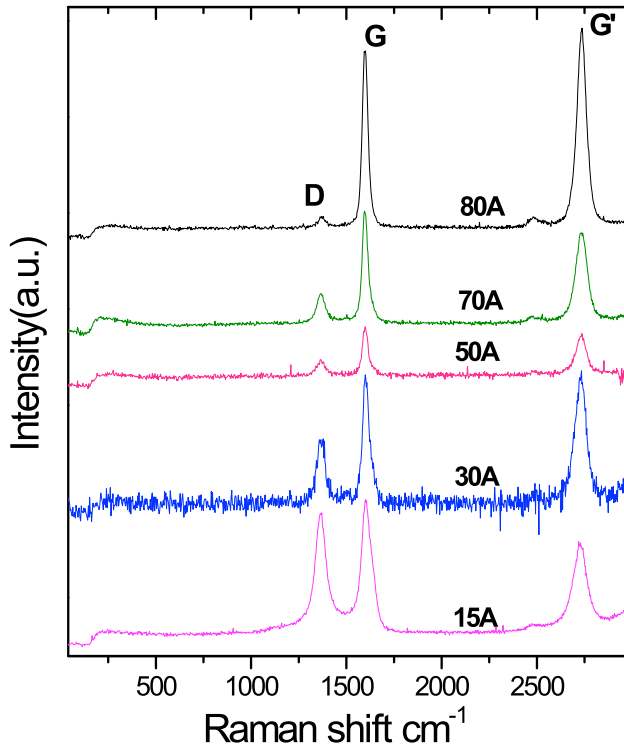
Figure 3.10: Raman spectra of CNTs produced at different current values for 5 mm-6 mm electrodes, using a of laser wavelength $\lambda_{\mathrm{exc}} = 514$ nm.
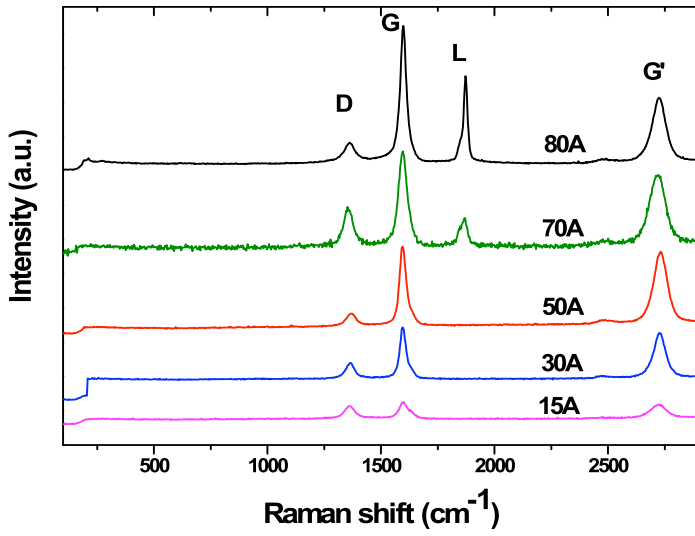
Figure 3.11: Raman spectra of CNTs produced at different current values for 6 mm-6 mm electrodes, using a laser of wavelength $\lambda_{exc} = 514$ nm.
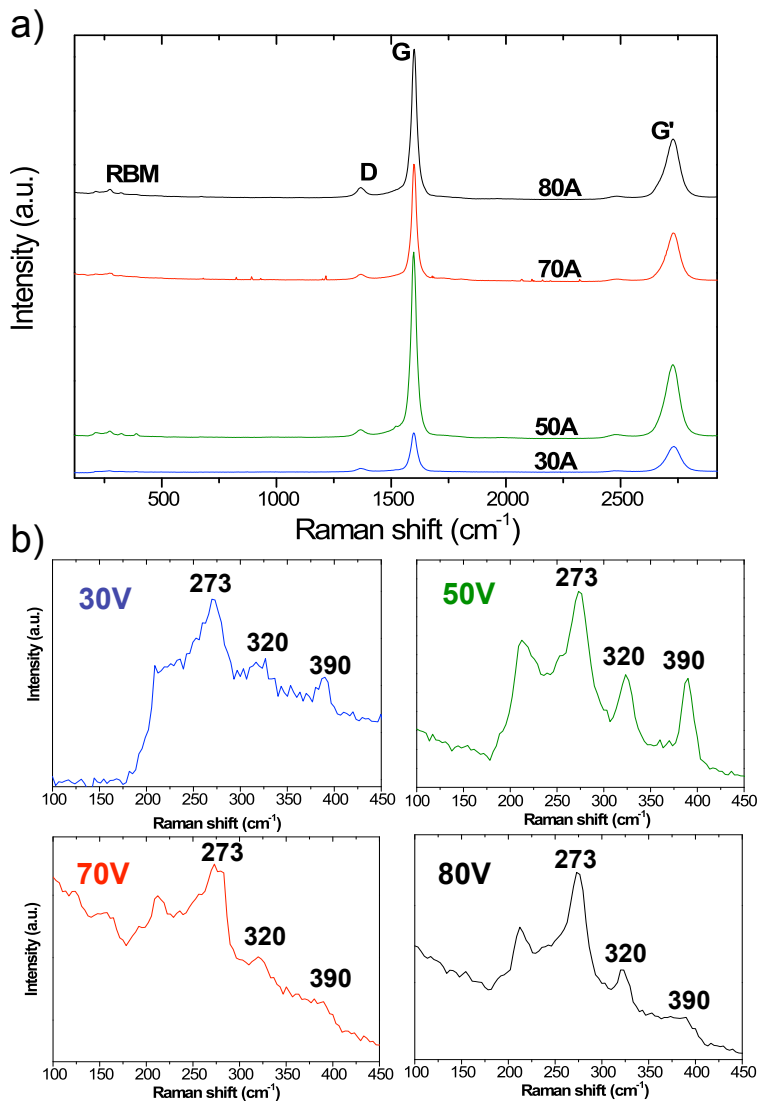
Figure 3.12: (a) Raman spectra of CNTs produced at different current values for 10-10 mm electrodes. (b) Detail of the RBM features for each current. (λ_{exc} = 514 nm).
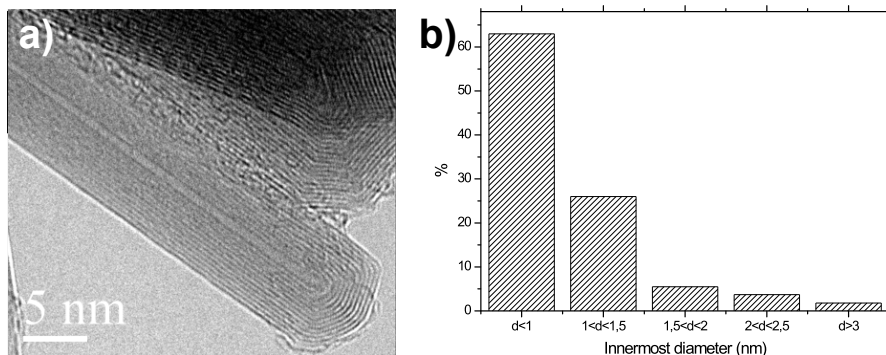
Figure 3.13: a) An MWCNT with the innermost diameter d = 0.8 nm, b) statistical analysis of the innermost tube diameter size by TEM.

5% frequency up-shift, become: 0.86, 0.73 and 0.60 nm. These experimental Raman results are confirmed by a statistical analysis performed by TEM. In Figure 3.13 we report (a) a TEM image of an MWCNT with an innermost tube diameter of 0.82 and (b) a histogram of the innermost tube diameters measured in many TEM micrographs of MWCNTs. Here 63% of our MWCNTs have an innermost diameter thinner than 1nm, while 37% show a diameter larger than 1 nm. Nanotubes with the innermost diameter of 0.7 nm have been found to be suitable to host carbon linear chains, that can therefore be stabilized [12]. The presence such kinds of CNTs is not sufficient for the formation of CNT-C linear chain hybrid systems and a more complex interaction among different factors (electrode size, discharge current, etc.) during the arcing has to be considered for the entrapment of C chains inside the CNTs.

We can summarize the results achieved by Raman spectroscopy for the different electrode couples and discharge current values in the graph reported in Figure 3.14.

We found that an increase in the electrode size and/or in the discharge current determines a better quality of the nanotubes as shown by the reduction of theI_D/I_G ratio in the Raman spectra [18]. A clear picture of the nanotube growth during an arc discharge experiment has been given by Gamaly. This picture nicely fits with the data reported up to now. In particular, the CNT formation in an electric discharge depends on the balance between two velocity distributions (anisotropic and isotropic or Maxwellian) of the carbon species as proposed by Gamaly et al. [19]. The anisotropic velocity distribution is due to the strong potential drop, from the cathode surface, which accelerates the C^+, ions towards the cathode itself. On the other hand the isotropic (or Maxwellian) velocity distribution is related to the carbons expelled from the cathode surface due to thermal effect. The anisotropic velocity carbons are responsible for building a nanotube in length, while the Maxwellian velocity carbons
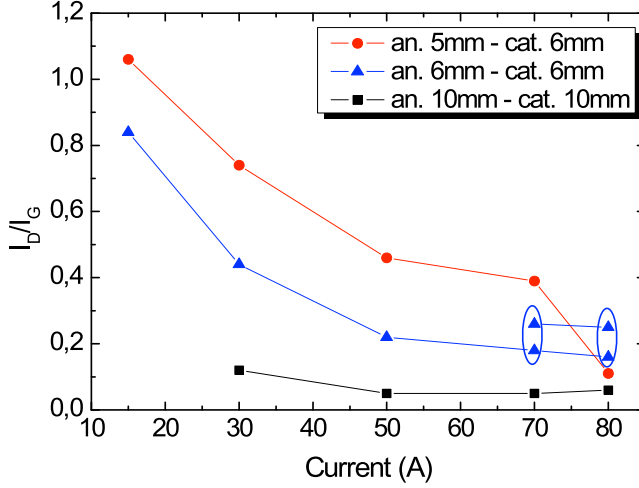
Figure 3.14: Trend of I_D/I_G ratio versus the discharge current values, for different electrode couples. The circles around indicate I_D/I_G values relative at two instability points.

determine the CNT growth in width. On the other hand, by increasing the current value, the isotropic effect decreases, leading to longer and more ordered nanotubes, in agreement with the trend reported in Fig. 3.14 . As concerns the electrode size effect, since the CNT formation process occurs near the cathode surface, the cathode shape is a very crucial factor. If we consider two electrodes with flat parallel surfaces, there is a clear axial symmetry and the nanotube formation is favored. On the other hand, in the case of a needle-like cathode, the anisotropic-velocity ions have a high tangential component along the cathode surface. This produces turbulence in the plasma flow near the cathode surface and, consequently, a homogeneous mixture without any axis of symmetry. In these conditions, very short CNTs and nanospheres are formed. We can therefore conclude that, by increasing the cathode surface area, the turbulence is reduced and we obtain a higher contribution of the C-ions with anisotropic velocity distribution with respect to the isotropic one and, as a consequence, longer nanotubes with a lower amount of other smaller structures. This is responsible for the decrease in the I_D/I_G ratio observed in the Raman spectra.

3.3.2 Role of the voltage

In the previous section we have reported the dependence of the CNT growth on the current and the size rods. Another important aspect that we have studied is the influence of the voltage on the CNTs growth. In Fig.3.15 we report SEM images of the CNTs obtained using both anode and cathode with 10mm diameter (configuration 10-10), by changing the applied voltage between 15 and 45 V for a current value of 80A. In particular, increasing the applied voltage (≥ 25V) a reduction of amorphous C and C nano-particles, on the surface of the deposit, is visible. These results have been confirmed by Raman spectroscopy.
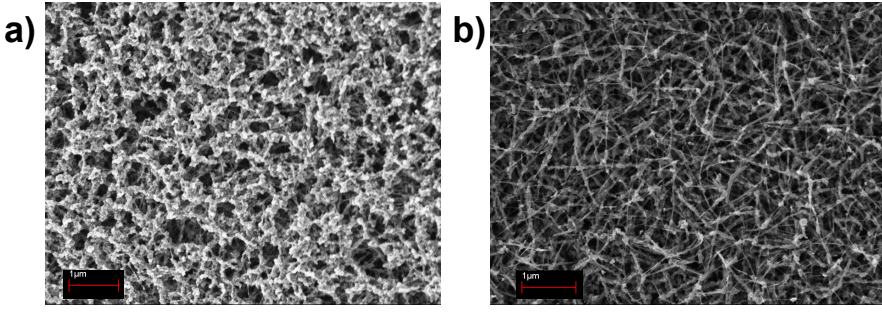
Figure 3.15: SEM images of the C deposit produced for a current value of 80A, applying a voltage of a) 20V and b) 25V.

Raman spectra for the samples produced at 15, 20, 25, 30, 40 and 45V are reported in Figure 3.16. An improvement of the CNT quality, instead, is observed as the voltage is increased: in particular, I_D/I_G value decreases from 0.27, for the sample produced at 15V, to a mean value of about 0.13 for samples obtained up to 20V, as reported in Figure 3.8- section 3.2.

In addition to the characteristic D, G and G´ bands, radial breathing mode (RBM) features can be observed in the low frequency region (100-450 cm^{-1}). In Figure 3.17 a magnification of RBM region is reported. We observed that as the applied voltage is increased, RBM modes at higher frequencies appear. In particular, for applied voltage of 20V, different peaks are present at frequencies lower than 170cm^{-1}, that indicates the presence of MWCNTs with an innermost tube diameter greater than 1.3nm. For a voltage of 25V, we observe a considerable reduction of these modes (lower than 170cm^{-1}) and the appearance of a small peak at 328cm^{-1}, related to CNTs with an innermost tube diameter of 0.72nm [see eq. 2.5]. For samples produced at 25V only peaks at frequencies higher than 170cm^{-1} are present. The intensity ratio between the RBM peaks and G bands (I_{RBM}/I_G) gives information on the relative amount of MWCNTs with a particular diameter present in the different samples. In particular
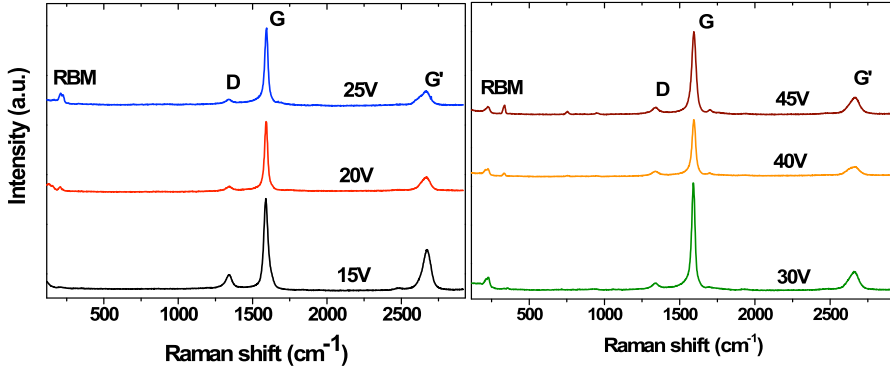
Figure 3.16: Raman spectra of CNTs samples produced at different voltages, exciting the samples by 632.8 nm radiation.

the I_{RBM}/I_G ratio, shows that the amount of MWCNTs with smaller innermost tube diameter increases when the voltage increase.

In fact, as reported in Table3.2, the higher value of I_{RBM}/I_G ratio for the voltage of 20V corresponds to the CNTs with diameter d>1.3nm (ω<170cm^{-1}), for 25V corresponds to diameters between 1.09<d<1.18nm (218<ω<200cm^{-1}) and for the voltage 45V corresponds to the diameters, d~0.72nm (ω~328cm^{-1}) and d~1.08nm (ω~222cm^{-1}) .

In order to explain this trend of the RBM modes we have used TEM analysis to get the statistical distribution of the diameter size in the produced CNTs, for different applied voltages. This is shown in Figure 3.18, where the amount of CNTs is reported in percentage, for innermost and outermost tube diameter, measured by TEM in the center and right column respectively. On the left column we report the amount of CNTs with innermost diameter d<1nm, 1nm≤d<1.5nm and d≥1.5nm, as calculated from table 3.2. Tube diameters larger than about 2nm cannot be observed by Raman spectroscopy due to truncation problems in the spectra acquisition of our experimental apparatus for the Raman shift values smaller than 100 cm^{-1}. For the voltage of 20V, the CNTs with innermost tube diameter d_{in}>2.5nm and with outermost tube diameter 10nm<d_{out}<15nm is ~55%. As the voltage is increased at 25V, the quantity of CNTs with innermost tube diameter d_{in}<1nm rises to 63%.

For the outermost tube diameter instead, we observe that increasing the voltage the amount of CNTs with a outermost tube diameter between 10nm<d_{out}<15nm decreases from 55% for the voltage of 20V to 35% for the voltage of 45V. The amount of CNTs having outermost tube diameter between 5nm<d_{out}<10nm,
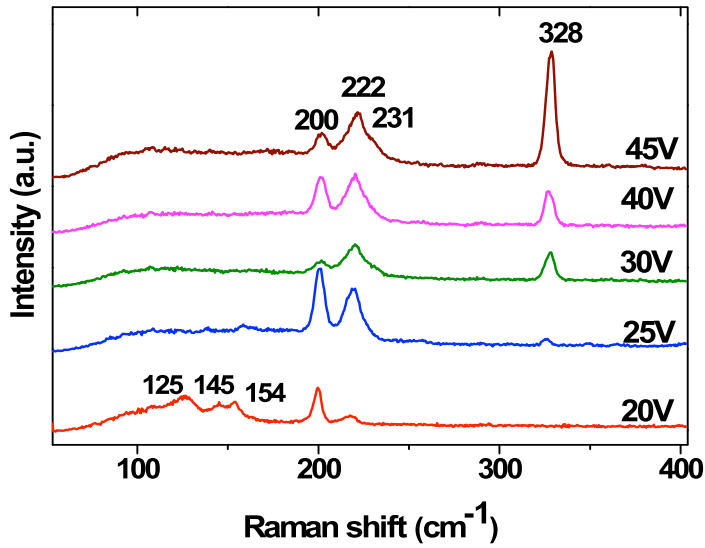
Figure 3.17: RBM region of CNTs samples produced at different voltages (λ_{exc} = 632.8 nm).

Salvatore Bagiante, PhD Thesis in Material Science, University of Catania, 2010.

Frequency [cm^{-1}] (diameter)	I$_{RBM}$/I$_G$		
Voltage [volt]	20	25	45
125 (1.88nm)	0.0204	//	//
138 (1.70nm)	//	0.0015	//
145 (1.62nm)	0.006	//	//
154 (1.53nm)	0.01	//	//
158 (1.49nm)	//	0.0035	//
200 (1.175nm)	0.017	0.038	0.0068
215 (1.09nm)	0.002	//	//
218 (1.09nm)	0.0024	0.039	//
222 (1.08nm)	//	0.0031	0.0292
231 (1.02nm)	//	//	0.0025
328 (0.72nm)	//	0.0033	0.0353
348 (0.68nm)	//	0.0011	//
364 (0.65nm)	//	0.001	//

Table 3.2: Ratio between I$_{RBM}$/I$_G$ ratio for different RBM frequencies, for the samples produced at 20V, 25V and 45V.

increases from 31.5% for a voltage of 20V, to 56%, applying a voltage of 45V. These observation imply that as the voltage is increased up to 45V, CNTs with a lower number of walls are created, as shown in Figure 3.19.

If we compare the I$_{RBM}$/I$_G$ ratio and the TEM statistics (Fig. 3.18) we find a correspondence for the 20V and 45V samples. Nevertheless, for the sample produced at 25V, the I$_{RBM}$/I$_G$ ratio and the TEM statistic show a big difference.

In order to explain the discrepancies observed between Raman spectroscopy and TEM analysis, and to rule out the possibility that Raman results are affected by unhomogeneities in the analyzed samples, we have performed Raman spectroscopy using different laser energies and acquiring several spectra in different regions of each sample. In figure 3.20 we report Raman spectra obtained for CNT samples produced at 20, 25 and 45V, using lasers with three different wavelengths: 325nm, 514nm and 632.8nm. In particular, for the sample obtained at 25V-80A, we observe: (Fig. 3.20f) six peaks at 138, 158, 200, 218, 222 and 328 cm^{-1} with the 632.8nm (1.96 eV) laser, corresponding, respectively, to different diameter values: 1.70nm, 1.49 nm, 1.17 nm, 1.09 nm, 1.08 nm and 0.72 nm; three peaks at 274, 323 and 390 cm^{-1} with the 514.5nm (2.41 eV) laser, corresponding, respectively, to the diameter values 0.86 nm, 0.73 nm, 0.60 nm(Fig. 3.20e); and one peak at 321cm^{-1} with the 325nm (3.80 eV) laser, corresponding to 0.73 nm (Fig. 3.20d). Several Raman spectra were acquired on different regions of the sample for each laser energy, showing that the observation of
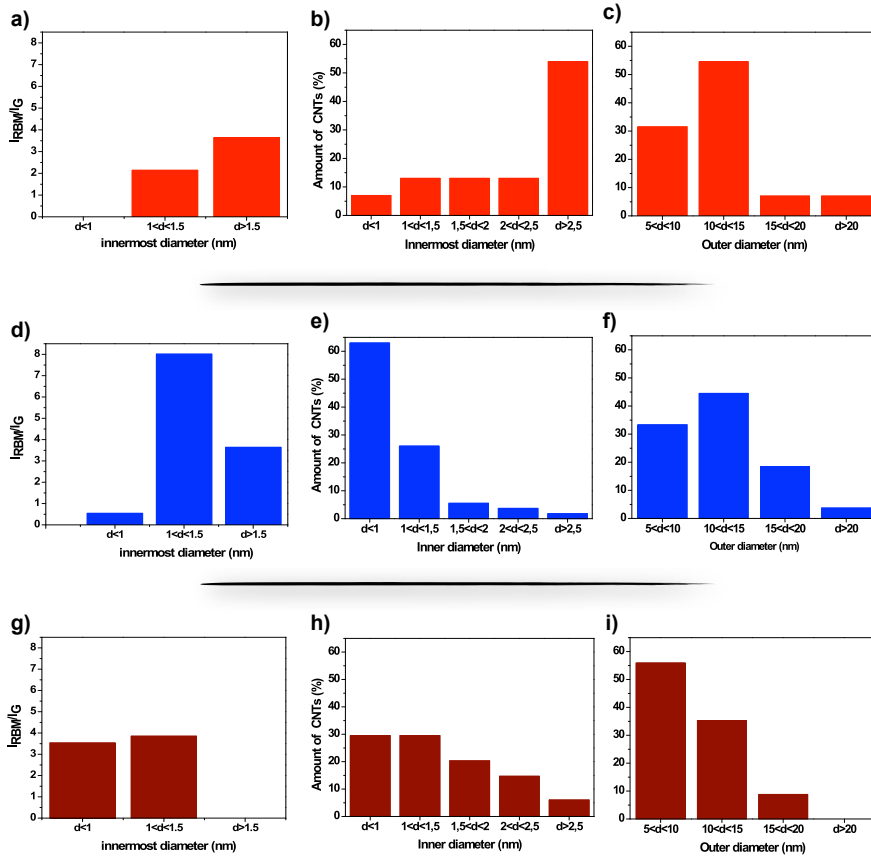
Figure 3.18: I_{RBM}/I_G ratio (left column) and statistical distribution by TEM analysis of innermost (center column) and outermost (right column) tube diameter of the CNTs produced for three different voltage (a-c) 20V, (d-f) 25V and (g-i) 45V.
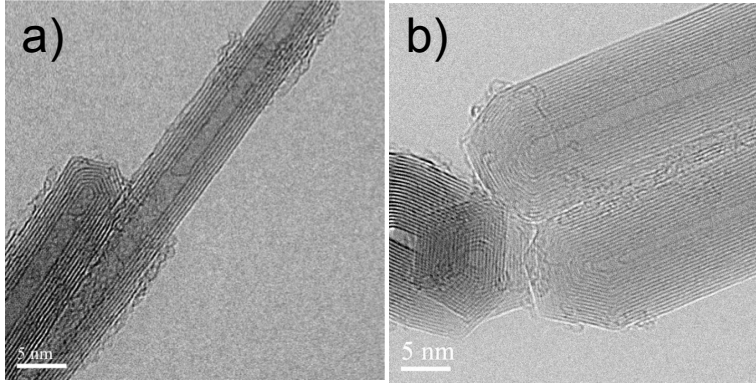
Figure 3.19: TEM image of CNTs produced applying a voltage of a)45V and b)25V. Is possible notice as CNTs obtained at 45V have fewer walls (~7walls), than CNTs obtained at 25V (~20 walls).

different peak positions is related only to a laser energy change and not to a different sampling area.

We argue that the observation of RBM modes depends on the laser-energy in MWCNTs as in SWCNTs. Atomistic electronic structure calculations of MWCNT systems have been performed in order to interpret the obtained Raman activity and, in particular, the selective response of the spectra according to the different laser energies. Optically, SWCNTs are characterized by allowed electronic transitions between resonant peaks of the Density of States (DOS) spectrum known as Van Hove Singularities (VHS). Correspondent, Raman scattering is enhanced for these energies, giving rise to characteristic spectra on the basis of CNT diameter and conductivity [13]. Such a consideration is not directly applicable also to the case of MWCNTs with decades of internal walls, where the form of the DOS distribution is expected to change radically from discrete (well-separated VHS) to continuous (VHS with very near resonances). It is therefore important to investigate the electronic configurations of MWCNTs on the basis of a theoretical formalism that accounts for the effects of the spatial distribution and topological localization of the DOS spectrum. We have hence calculated [14] the electronic structure of various MWCNT systems with interwall distances of ~0.34 nm. The electronic Hamiltonian is written according to the Extended Hückel theory using a basis set of double-ζ Slater-type orbitals that decay exponentially with the distance and do not suffer cutoff truncations [21, 22]. This feature remains fundamental within the theoretical formalism since it allows for the proper evaluation of localization effects in the electronic distribution. Hamiltonian elements have been suitably parameterized from first-principles calculations [13]. Fig-
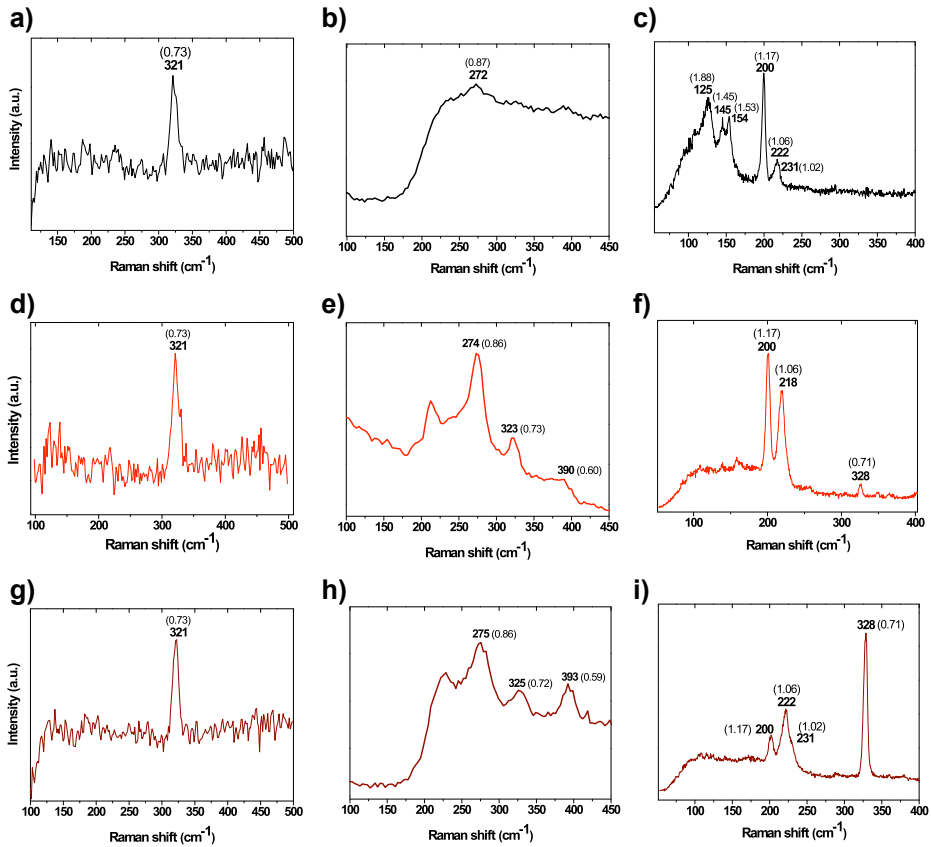
Figure 3.20: RBM features of CNTs samples produced at (a-c)20V, (d-f)25V and (g-i)45V, exciting the samples by different radiations: 325nm, 514.5nm and 632.8nm (from left to right).

64
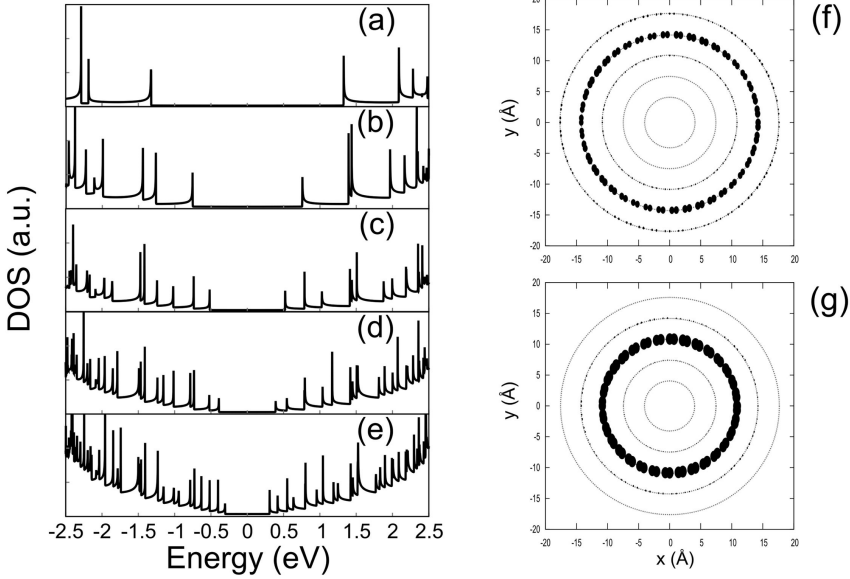
Figure 3.21: DOS as a function of energy for (a) a single-wall (6,6) CNT, (b) a double-wall (6,6)-(11,11) CNT, (c) a three-wall (6,6)-(11,11)-(16,16) CNT, (d) a four-wall (6,6)-(11,11)-(16,16)-(21,21) CNT, and (d) a five-wall (6,6)-(11,11)-(16,16)-(21,21)-(26,26) CNT. Schematic representation of the projected density of states on the atom positions for the (6,6)-(11,11)-(16,16)-(21,21)-(26,26) MWCNT, for energies that correspond to the second VHS below the charge neutrality level (f), and the third VHS below the charge neutrality level (g).

ure 3.21(a)-(e) shows, as an example, DOS spectra of a 5-wall armchair CNT starting from an internal (6,6) tube and adding the respective external ones that maintain the typical graphitic 0.34 nm interlayer distance (i.e (11,11), (16,16), (21,21), (26,26) respectively).

The main phenomenon that accompanies the addition of the external walls is an increase of the VHS throughout the spectrum that gradually transforms the discrete characteristics of the spectrum towards a continuous distribution. Therefore, one would expect that a MWCNT system should always be excited by incident laser beams of different frequencies; correspondingly, the Raman spectra should be similar for all laser lines. Such eventuality is not confirmed by the results of the experiment. The key issue for understanding laser selectivity effects experimentally observed in MWCNT systems stands on the strong localization aspects that are present in the electronic configuration of these systems. A careful analysis of the projected den-

sity of states on the atomic positions of the simulated system reveals that the DOS spectrum at a specific energy maintains a spatially localized character and does not expand throughout the entire system, as schematically shown in Fig.3.21(f)-(g) for two different energies (E=-0.4 eV and E=-0.52 eV). This is due to electrons being strongly bound at their CNT wall of origin, independent of the number of walls in the system. According to this picture, the various walls of a MWCNT system are only electronically coupled with few neighboring walls, whereas decoupled with respect to the rest of the system. On the basis of this assumption, if the interest of the vibrational spectrum is restricted to the RBMs of the internal wall, first order electronic interactions and therefore allowed optical transitions should be restricted to the innermost double or triple wall system. In this sense, the RBM features observed in the Raman spectra derive not only from a direct excitation of the innermost tube, as in SWCNTs, but also from eventual optical transitions between neighboring walls, that determine a loosening of the strict selection rules valid for resonant Raman spectroscopy of SWCNTs. These consideration explain the different results obtained by Raman spectroscopy and TEM analysis on the diameter population of MWCNTs. Indeed, by Raman spectroscopy we detect only those CNT owning an innermost tube diameter in resonance condition with the laser energy used and by TEM analysis we detect all kinds of CNTs present in the sample. On the basis of our experimental results, we observe that a variation of the applied voltage leads to the formation of different kinds of CNTs. In order to get statistical information on tube diameters Raman spectroscopy is not very useful due to resonance effects, but it confirms itself to be a good method to identify the presence of particular CNT structures. By TEM we observe also a dependence of the outermost tube diameter size distribution on the applied voltage, in particular an increase of the amount of CNTs with smaller outermost tube diameter (between 5-10nm) for higher applied voltage. If we compare samples produced at 25V and 45V, we observe that CNTs produced at 45V have, on average, larger innermost tube diameter and smaller outermost tube diameter, that means fewer walls than in the case of CNTs produced at 25V, as already shown in Fig. 3.19. Following the model by Gamaly and Ebbesen [19] the formation of thicker nanotubes (i.e with a larger number of walls), depend on the presence of C atoms that having a Maxwellian distribution and attaching to the elongated structure, already formed, from parallel directions to the cathode surface. If this holds true in our case, in a carbon plasma produced at 45V the amount of C species having isotropic distribution is lower than in the case of 25V. In other words, at 45V the formation of thinner MWCNTs is favoured, due to a higher amount of directional (along the electrode axis) C species, respect to the isotropic carbons.
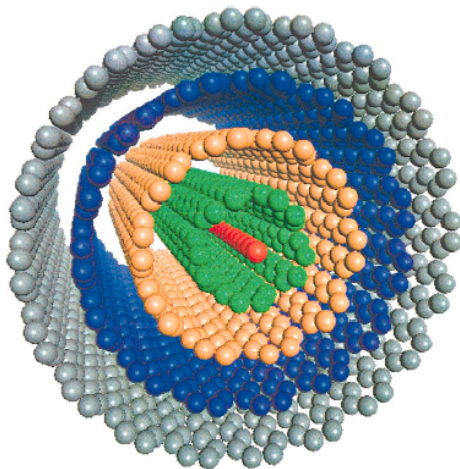
Figure 3.22: Linear chain inside MWCNT [29].

3.4 Synthesis of multi-wall CNT/ Linear carbon chain hybrid system

Linear carbon chains (LCCs) have attracted a lot of academic and practical inter-est, since they can be considered as precursors of fullerenes and nanotubes, and as candidates for molecular wires to be used in molecular devices for electron transport. Their instability, due to cross-linking and oxidation phenomena, can be overcome if they are end-capped by bulky or special groups [23, 24], or if they are inserted in carbon nanotubes [25, 26], forming carbon nanowires (CNWs). Such linear C chains show remarkable stretching modes in the region between 1900 and 2200cm^{-1}, in ac-cordance with the chain length and bonding structure (polyynes or polycumulenes) [27, 28]. Actually there are two theories explaining the origin of the L-band measured in CNTs. Zhao et al. [29] observed an intense band around 1825 and 1850 cm^{-1} in the Raman spectrum of MWCNTs, and ascribed that band to long linear carbon chains, containing more than 100 atoms, and inserted inside a MWCNT, as shown in figure 3.22.

Jinno et al.[31] observed similar Raman peaks in MWCNTs and DWCNTs, as-cribing these modes to linear carbon chains inside inner carbon nanotubes with small diameter, about 0.6nm. The necessity to have a very small inner diameter depends on the possibility to stabilize linear carbon chains inside the CNTs, preventing the linear carbon chains to reorganize in a different structure. Recently Fantini et al. [33] pro-posed another approach to explain the origin of the L-band. From their simulations,

atomic carbon threads appear during nanotube coalescence. Besides the formation of carbon threads on the outer nanotube shell, simulations also show carbon chains containing 3, 4, and 5 atoms linking the inner and outer tubes covalently to the hexagonal network. Today, the theory of Zhao better explains the experimental evidences; nevertheless, some aspects about the nature of this hybrid material have still to be clarified. The frequency down-shift observed in LCC contained in CNTs respect to "free" LCC, has been explained as a weakening of C–C bond in the chain when the chain is confined in the tube [24]. Furthermore, it has been shown to depend on the number of C atoms in the chain [26]. Different kinds of linear C chains have been reported in the literature, in particular, besides hydrogen-terminated polyynes, the formation of dicyanopolyynes was observed during arc discharge between two graphite electrodes in liquid nitrogen, due to the incorporation of nitrogen in the chain end capping [32]. Whilst this discrimination between polyynes and cyanopolyynes is possible in the case of ''free'' C chains dispersed in a solution, it is quite hard to discriminate between these two kinds of structures when C chains are contained in a nanotube. From previous considerations and findings we argue that the geometry of the discharge system and, in particular, the electrode size and shape play a crucial role. As reported in section 3.3.1 for the configuration with anode and cathode of 6mm at high current (70A and 80A), we observed in the Raman spectra the L-band at about 1850 cm^{-1} (see figure3.11, section 3.3.1), due to the presence of LCCs inside CNTs. As discussed in section 3.3.1, MWCNTs with very small innermost diameter (0.5-0.82nm) can be produced by arc discharge in liquid nitrogen and, in particular conditions of rod diameter, current and voltage, hybrid systems formed by LCCs inserted in CNTs can be obtained, by arc discharge in liquid nitrogen, as shown in the following paragraph.

3.4.1 LCC@MWCNT Hybrid system

The presence of LCC in CNTs has been observed in the samples produced at 25V 70A and 80A using the rods configuration 6mm-6mm, as reported in the Raman spectra in Fig. 3.11. For electrode configuration 5mm - 5mm and 10mm - 10mm the L-band in the Raman spectra is not present, even though for the configuration 10-10mm, the MWCNTs have a innermost diameter that would be compatible with the stabilization of linear chain[29]. In order to find the best condition for the formation of Cn@MWCNT, we have investigated other intermediate configurations, with a 6 mm anode and a 10 mm cathode (configuration 6–10), and a 10 mm anode and a 6 mm cathode (configuration 10–6), respectively. For both cases the current value varied between 30 and 80 A. In the samples produced with the configuration 6–10, we do not observe well-defined RBM features, and the hybrid systems, identified by the presence of the L-band, are obtained only for a current value of 50 A, lower than in the configuration 6–6. The corresponding Raman spectrum is reported in figure 3.23a. When using configuration 10–6, instead, the hybrid systems were obtained at
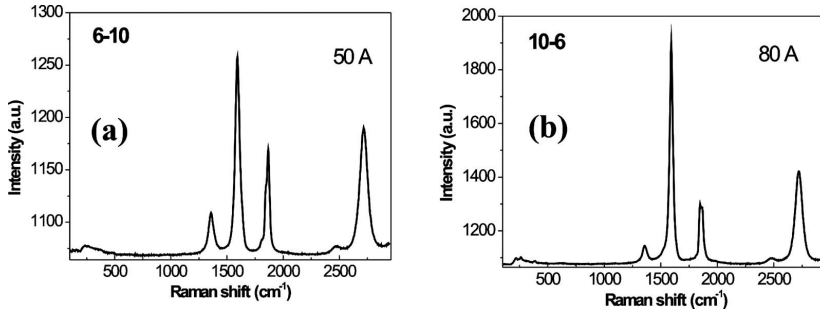
Figure 3.23: Raman spectra relative to CNTs obtained at a) 50 A, with 6 mm anode and 10 mm cathode and b) 80 A, with 10 mm anode and 6 mm cathode. Using a laser of wavelength of λexc = 514 nm.

80A (Fig. 3.23b), as in the configuration 6–6.

In both configurations (6–10 and 10–6), no instability in the discharge was observed for all the investigated current values. This can be explained only if we assume that the electrode geometry changes more rapidly for the configuration 6–6 than for the other ones, due to faster anode erosion. In fact, a smaller anode is eroded more rapidly than a larger one [34] and, at the same time, a smaller cathode submerged in liquid nitrogen is cooled more easily than a larger one and emits more electrons, so increasing the erosion rate of the anode. The cathode erosion cannot be easily evaluated, due to the presence of C deposit on it. The rapid modifications of the electrode geometry (shape and distance between electrodes) cause more frequent current fluctuations and, therefore, more frequent distance rearrangements have to be performed to keep on arcing at the set current value and to avoid interruptions. The main findings observed by changing the experimental setup are the following: (1) a big amount of spherical and shorter nanostructures are obtained in the presence of unstable current condition (small cathode and high current), (2) good quality CNTs, with innermost tubes thinner than 1 nm are clearly observed for large rod diameters, in particular, when the anode is 10 mm, and (3) the presence of hybrid systems depends on the particular combination of experimental parameters, such as discharge current and rod diameters. In order to understand these differences we have to make some considerations, taking into account the existing models. The growth mechanism of CNTs by arc discharge is still a subject of controversy, and more than one mechanism might be operative during their formation. In the model proposed by Gamaly and Ebbesen[19] the CNT formation in an electric discharge depends on the competition between two velocity distributions of the C species: (1) carbon atoms evaporated from the cathode surface, with a Maxwellian (or isotropic) velocity distribution and (2) carbon ions coming from the anode and accelerated in the gap between the positive space charge

69
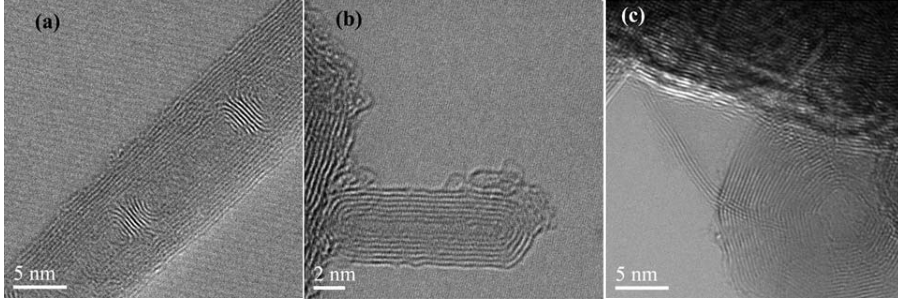
Figure 3.24: TEM images showing different nanostructures obtained using 6 mm electrodes at 80 A: a) C nanostructures enclosed in CNT, b) C beans, and c) C onions.

and the cathode, with anisotropic velocity distribution. The first group is responsible for the formation of all three-dimensional (3D) structures and for the growth of CNTs in width; the second group is responsible for the growth of nanotubes in length. Therefore, if a sudden current interruption takes place, the anisotropic component immediately disappears or reduces and the isotropic velocity distribution dominates the formation process, capping the ends of the tubes and forming other nanoparticles with radial symmetry. This explains the reason why a fluctuating arc, like in the case of 6 mm electrodes at high current values, leads to the formation of shorter and spherical nanostructures, such as carbon beans and nanospheres, shown in figure 3.24. Stable discharge conditions, as in the case of larger electrodes, lead to the formation of better quality CNTs, as confirmed by the I_D/I_G ratios calculated from Raman spectra.

According to the same model, since the CNT formation process occurs near the cathode surface, the cathode shape is a very crucial factor. In the case of a needle-like cathode, the anisotropic velocity ions have a high tangential component along the cathode surface. This produces a turbulence in the plasma flow close to the cathode surface and, consequently, a homogeneous mixture without any axis of symmetry. In these conditions, very short CNTs and nanospheres are formed. As the cathode surface area increases, the turbulence reduces and the contribution of carbon ions with anisotropic velocity prevails, getting, as a consequence, more ordered and longer structures, in agreement with the model. The model proposed by Zhao et al. [29] suggests the necessity to have CNTs with innermost diameter of 0.7 nm, in order to have a spacing between C chain and innermost tube wall equal to the distance between two graphite planes. This would allow one to stabilize the linear carbon chains, preventing the rearrangement in a different structure. The presence of CNTs with 0.7 nm innermost diameter is not a sufficient condition to obtain a hybrid system. In fact, as reported in section 3.3.1, using two electrodes with 10 mm diameter, we obtain CNTs with an innermost diameter appropriated to stabilize linear C chains, as confirmed by

Raman spectra (Fig. 3.12, section3.3.1) but we do not observe the presence of linear C chains inside CNTs, for any current value in the range of 30–80 A. The observation of a hybrid system only for particular sets of experimental parameters suggests that the formation and/or the entrapment of linear C chains in CNTs are favored only when some physical conditions are met. We found that by fixing the cathode diameter at 6 mm and changing the anode diameter, 6 or 10 mm, C chain/CNT hybrid systems form for the same current value of 80A. So the effect of the cathode shape and of carbon atoms with isotropic velocity emitted by the cathode itself appears to be dominant. In fact, in this way, we change only the anisotropic velocity distribution responsible of the growth of nanostructure in length but do not change the isotropic velocity distribution. On the other hand, if we fix the anode diameter (6 mm) and change the cathode size, 6 or 10 mm, we instead get the formation of linear C chains in CNTs for a current value of 80 or 50A, respectively. Different factors have to be taken into account in order to explain these results. One factor that could influence the formation of linear C chains in CNTs could be the same as the one used to explain the conditions for obtaining elongated or 3D structures: the competition between the anisotropic and isotropic velocity distributions of the carbon species. During arcing between the two electrodes, carbon ions move to the vapor layer (formed by the atoms emitted by thermal effect from the cathode) in a direction perpendicular to the cathode surface. They are responsible for the formation of the elongated structures that, at the beginning, we can suppose to be linear chains cross-linking each other afterwards to form more complex structures. Due to the collision with the vapor layer, the elongated structures begin to bend and CNTs are end-capped. In this phase, if linear chains are still present, they can be trapped inside nanotubes. As we have already described, the smaller is the cathode surface the higher is the probability to form 3D structures with respect to elongated ones. Therefore, in the case of small cathodes, in order to get a larger amount of elongated structures (CNTs and C chains) it is necessary to compensate the larger contribution of carbons with isotropic velocity by increasing the current value, i.e., the amount of C ions with anisotropic velocity. This would explain the formation of hybrid systems at higher current (80A) in the case of smaller cathode diameters (6 mm), with respect to a current of only 50 A needed in the case of larger cathodes (10 mm). Based on the current investigations, the reason why no linear C chains are formed and/or trapped in CNTs in the case of both anode and cathode with 10 mm diameter, is not clear yet. We have considered additional factors that can affect the formation of CNTs and linear C chains, as the plasma temperature during the discharge and the temperature of the electrodes. It is reported in the literature that the plasma temperature is influenced by the electrode size [34], in particular a decrease in the plasma temperature was found by using anodes with larger diameter. Actually, we feel to assert that the plasma temperature is not only influenced by the anode but also the cathode: indeed a smaller cathode submerged in liquid nitrogen is cooled more easily than a larger one and efficient cooling produces

an increase in the electron emission from the cathode itself [29]; that contributes to the increase in the plasma temperature. Therefore, a more quantitative investigation would be necessary in order to explain the results, case by case. In the configuration 10–10, both anode and cathode with large diameter would contribute to decrease the plasma temperature with respect to other configurations; here RBM modes are visible, indicating the presence of nanotubes with very thin innermost diameter, while no C chains in CNTs are observed. In the 6–6 configuration both anode and cathode with small diameter would contribute to increase the plasma temperature: here C chains are observed, and this suggests that for the formation and/or trapping of C chains in CNTs a higher plasma temperature is required. No RBM features are visible in this case, at least for the laser wavelength used (514.5 nm), and this should be verified for other wavelengths in further experiments. In the other intermediate configurations the relation between plasma temperature and electrode size is more complex, and we observe the presence of RBM features and/or L-band, indicating, respectively, nanotubes with very thin innermost tube diameter and formation of C chains in CNTs.

In the electrode configuration 10-6 we observe the simultaneous presence of RBM and L-band features.

The material produced in the 10-6 configuration, at 25V 80A has been analyzed by Raman spectroscopy. The spectra were acquired in different regions of the cathode deposit (center and border). The results are shown in figure3.25: in (a) we report a spectrum acquired from the border of the sample, showing the D-band at 1361 cm-1, the G-band at 1591 cm-1. The low frequency region (between 100 and 500 cm^{-1}) of the spectrum is reported in (b) and shows the features due to the radial breathing modes at 267, 317 and 384cm^{-1} (see eq. 2.5sec. 2.10). In our case, the innermost diameter calculated values corresponding to the observed frequencies are: 0.84, 0.71 and 0.58 nm, respectively, and become 0.80, 0.68 and 0.55 nm if a 5% frequency up-shift is considered. The low value of I_D/I_G ratio (~0.08), confirms the good quality of our nanotubes, having a high degree of graphitization. In figure 3.25c, we report the spectrum obtained in the center of the sample, showing another band (L-band) formed by two peaks at about 1863 and 1844 cm^{-1}, as evidenced in the inset, usually associated to the presence of linear C chains with different structures [29]. A comparison between this spectrum and the one reported in figure 3.25a shows a change in the low frequency region, as reported in detail in figure 3.25d: the RBM at 315 cm^{-1}, corresponding to the 0.71 nm diameter, is suppressed. Such a suppression can be correlated to a radial breathing freeze for the innermost tube containing the C chain and having a diameter twice the distance between two graphitic planes. The observation of both the L-band and the RBM loss indeed is a direct proof of the presence of C chains inside nanotubes produced by arc discharge in liquid nitrogen and allows us to reject the hypothesis formulated by Fantini et al. [33], according to which the 1865 cm^{-1} feature would be due to the presence of short linear C chains
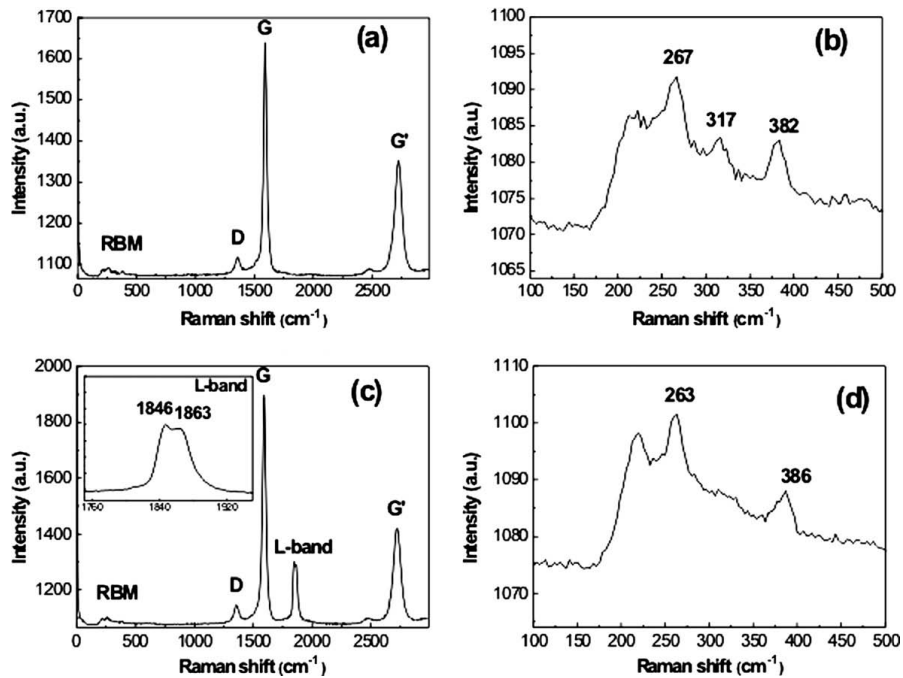
Figure 3.25: Raman spectra of a) CNTs and c) CNTs containing polyynes; in b) and d) we report RBM features corresponding to spectra a) and c), respectively. Using a laser of wavelength of λexc = 514 nm.
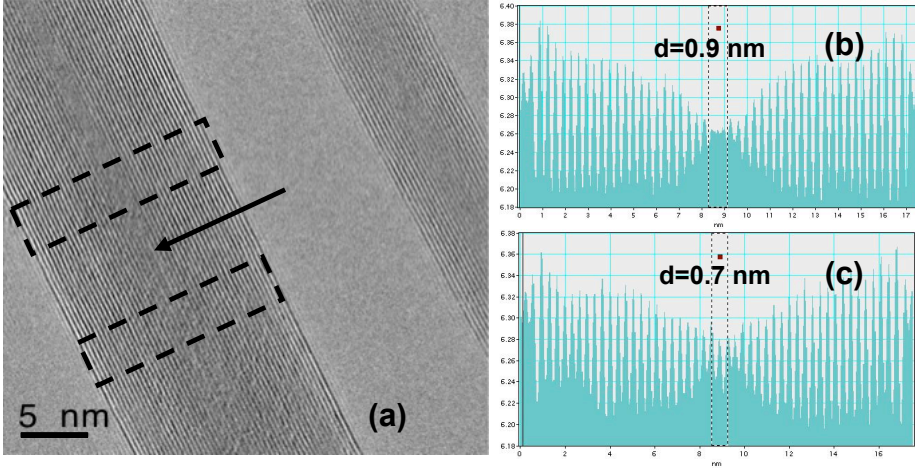
Figure 3.26: TEM analysis of two CNTs, containing a C chain. The arrow indicates the ending point of the chain. In b) and c) the integrated intensity profiles obtained in the boxes 1 and 2 drawn in a) are reported.

formed during the coalescence process between two double-wall CNTs. The presence of C chains inside MWCNTs is clearly confirmed by TEM analysis.

In figure 3.26, we report two CNTs with different number of walls, both containing a C chain; in the larger one it is possible to see that the C chain is shorter than the entire nanotube length and an arrow indicates the point where the chain ends. The innermost diameter size in the two regions, where the innermost tube is empty and where it is filled with the C chain, can be measured: the image intensity signal is integrated in two rectangular boxes drawn in (a), and two intensity profiles perpendicular to the CNT axis can be extracted, as reported in (b) and (c). The diameter of the innermost tube, where the tube is empty, is given by the distance between the inner peaks and results to be 0.9 nm. In the region where the C chain is inserted the distance between the innermost peak and the nearest ones is 0.35 nm that is the innermost tube diameter reduces from 0.9 to 0.7 nm, in agreement with the findings of Zhao et al. [29].

We have used TEM analysis in order to get the statistical distribution of the innermost tube diameter size in the produced CNTs. This is shown in figure 3.27, where the amount (%) of CNTs with the innermost diameter $d < 1$ nm or $d > 1$ nm is 82.2% and 17.8%, respectively. The column $d < 1$ nm contains both the nanotubes with C chains (64.3%) and the empty ones (17.9%). We observed that CNTs containing the linear chains have the outer diameter ranging between 8 and 16 nm. It has to be noticed that the number of nanotubes, with d<1, containing a C
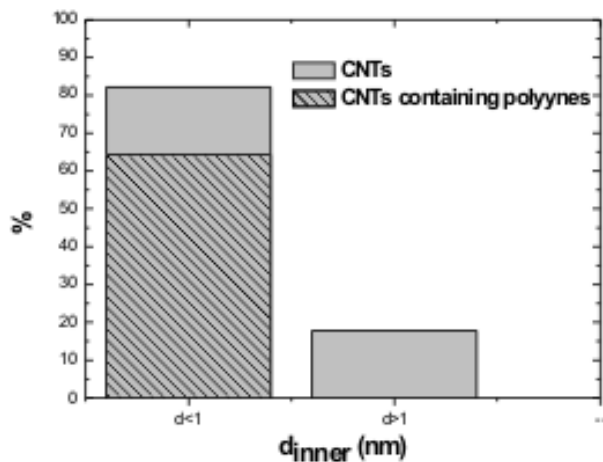
Figure 3.27: Statistical distribution by TEM of the innermost tube diameter size in the produced CNTs. The column corresponding to d < 1 includes simple CNTs (17.9%) and CNTs containing C chains (64.3%). In the latter ones, the outer diameter outer is ranging between 8 and 16 nm.

chain is underestimated, since the chains are shorter than the entire CNT length and hence the TEM observation can have been done in the empty region of the tube.

3.5   Conclusions

The work reported in this Chapter 3 is an attempt (hopefully successful) to shed more light onto the synthesis of carbon nanotubes by arc discharge in liquid nitrogen. Indeed, such synthesis technique is used extensively for CNT mass production, but the structural properties of the produced material are not fully controllable. Therefore, we have tried to investigate the "arcing phenomenon" systematically, correlating the experimental parameters that control arc generation to the structure of the synthesized material.

A macroscopic, morphological analysis of C deposit formed on the cathode during arc discharge has allowed us to observe the presence of two different regions: one mainly consisting of disordered C structures, appearing in the colder regions of the cathode surface (i.e., the radially outer region of the deposit); the other one made of CNTs, forming in the hotter region of the cathode surface and well packed into pillars, whose size and sharpness depend on the voltage applied to start the electric arc. We have identified a parameter (α angle) that allows to visualize the temperature field forming during arc dis- charge for different experimental conditions. The temperature field is related to the inter-electrode distances, in agreement with an existing mathematical model by Bilodeau et al. in the case of arc discharge in gaseous environment. We have shown that the structural quality of CNTs, and the presence of linear C chains depend on and can be controlled by a suitable choice of electrode size and discharge current. In particular, we have shown that the structural order of MWCNTs is higher as the current intensity and electrode diameter are increased. The quality of our deposits is evidenced essentially by two factors: (i) a very low I_D/I_G ratio (for configuration 10-10, at current higher than 50 A, it is about 0.05.); (ii) the observation of active RBMs in the low frequency region of Raman spectra, indicating that nanotubes with very thin (<1 nm) innermost tube diameter are forming. Furthermore, changing the applied voltage and fixing the current at 80A, we do not see any variation of the MWCNTs quality for voltages > 20V, but, we observe differences in the statistical distributions of the innermost and outermost tube diameters . We have produced MWCNTs with very thin innermost tube diameter (<1 nm), in particular, with a diameter of 0.7 nm, that is considered a condition necessary to stabilize the linear carbon chains and, therefore, to form hybrid systems. We have shown that this condition is not sufficient and the choice of both electrode size and discharge current influences the structural order and determines the formation of hybrid systems. In particular, the use of large electrodes (anode 10 mm-cathode 10 mm) does not allow one to obtain linear C chains for any current values explored in this work. This finding can be related to the plasma temperature, that in the case of larger electrodes

is lower than the one achieved for the other electrode configurations (6 mm- 6 mm, 6 mm- 10 mm, 10 mm-6 mm). Finally, we have demonstrated the correlation between one RBM feature suppression and the L-band, never observed in the literature up to now, allowing us to point out the formation of linear C chains in CNTs having a diameter of 0.7 nm, so that the distance between the atoms in the chain and the inner wall is equal to the distance between two graphite planes, as expected.

The results reported in this chapter have been published in the following papers:

- V. Scuderi, S. Scalese, S. Bagiante et al. "Direct observation of the formation of linear C chain/carbon nanotube hybrid systems" CARBON 47 (2009) 2112–2142.

- S. Scalese, V. Scuderi, S. Bagiante, F. Simone, P. Russo, L. D'Urso, G. Compagnini, and V. Privitera "Controlled synthesis of carbon nanotubes and linear C chains by arc discharge in liquid nitrogen" JOURNAL OF APPLIED PHYSICS 107, 014304 (2010)

- S. Bagiante, S. Scalese, V. Scuderi, L. D'Urso, E. Messina, G. Compagnini, and V. Privitera "Role of the growth parameters on the structural order of MWCNTs produced by arc discharge in liquid nitrogen" Phys. Status Solidi B 247, No. 4, 884–887 (2010).

- G. Compagnini, G. Patanè, O. Puglisi, S. Scalese, V. Scuderi, S. Bagiante and V. Privitera " Synthesis of carbon nanowires and nanotubes by plasma ignition in liquid environments" Journal of Optoelectronics and Advanced Materials 12, No. 3, 456-460 (2010).

- S. Scalese, V. Scuderi, S. Bagiante, S. Gibilisco, G. Faraci and Vittorio Privitera " Order and disorder of carbon deposit produced by arc discharge in liquid nitrogen" JOURNAL OF APPLIED PHYSICS 108, 064305 (2010).

- Silvia Scalese, Viviana Scuderi, Salvatore Bagiante, Santo Gibilisco, Giuseppe Faraci, Nicolò Piluso, Francesco La Via, Vittorio Privitera. "Morphology and distribution of carbon nanostructures in a deposit produced by arc discharge in liquid nitrogen" Physica E, in press (2010)

References

[1] M. Ishigami, J. Cuminings, A. Zettl, S. Chen, Chem. Phys. Lett. 319 (2000) 457

[2] S.H. Jung, M.R. Kim, S.H. Jeong, S.U. Kim, O.J. Lee, K.H. Lee, J.H. Suh, C.K. Park, Appl. Phys. A 76 (2003) 285

[3] I. Alexandrou, H. Wang, N. Sano, and G. A. J. Amaratunga, J. Chem. Phys. 120, 1055 (2004).

[4] P. J. F. Harris, Carbon Nanotube Science, Cambridge University Press, Cambridge, 2009.

[5] P. M. Ajayan, Ph. Redlich, and M. Rühle, J. Mater. Res. 12, 244 (1997).

[6] N. S. Koprinarov, M. A. Konstantinova, G. V. Pchelarov, and M. V. Marinov, J. Cryst. Growth 171, 111 (1997).

[7] J. Robertson, Mater. Sci. Eng. R. 37, 129 (2002).

[8] J.-F. Bilodeau, J. Pousse, and A. Gleizes, Plasma Chem. Plasma Process. 18, 285 (1998).

[9] Ferrari A C and Robertson J 2000 Phys. Rev. B 61 14095.

[10] S. Scalese, V. Scuderi, S. Bagiante et al., work in preparation.

[11] G. Compagnini and G. Baratta, Appl. Phys. Lett. 61, 1796 (1992).

[12] X. Zhao et al., Chem. Phys. Lett. 361, 169–1174 (2002).

[13] Kataura H, Kumazawa Y, Maniwa Y, Uemezu I, Suzuki S, Ohtsuka Y and Achiba Y 1999 Synth. Met. 103 2555

[14] S. Scalese, S. Bagiante et al. work in preparetion.

[15] S. Reich, C. Thomsen, and J. Maultzsch, Carbon Nanotubes (Wiley-VCH, Weinheim, 2004), pp. 141–149.

[16] J. M. Benoit et al., Phys. Rev. B 66, 073417–073420 (2002).

[17] D. Kahn and J. P. Lu, Phys. Rev. B 60, 6535–6540 (1999).

[18] A. Hu, Q. B. Lu, W. W. Duley, and M. Rybachuk, J. Chem. Phys. 126, 154705 (2007).

[19] E. G. Gamaly and T. W. Ebbesen, Phys. Rev. B 52, 2083– 2089 (1995).

[20] Bandow S, Takizawa M, Hirahara K, Yudadaka M, Iijima S., Chem Phys Lett 2001;337(1-3):48-54

[21] D. Kienle, J.I. Cerda, A. W. Ghosh, J. Appl. Phys. 100, 043714 (2006)

[22] I. Deretzis, A. La Magna, Nanotechnology 17, 5063 (2006).

[23] Tsuji M, Tsuji T, Kuboyama S, Yoon SH, Korai Y, Tsujimoto T, et al., Chem Phys Lett 2002;355(1–2):101–8.

[24] Cataldo F., Carbon 2004;42(1):129–42.

[25] Nishide D, Wakabayashi T, Sugai T, Kitaura R, Kataura H, Achiba Y, et al., J Phys Chem 2007;111(13):5178–83.

[26] Liu Y, Jones RO, Zhao X, Ando Y., Phys Rev B 2003;68(12):125413-1–7.

[27] Kastner J, Kuzmany H, Kavan L, Dousek FP, Ku¨ rti J., Macromolecules 1995;28(1):344–53.

[28] Ku¨ rti J, Magyar C, Bala´ zs A, Rajczy P., Synth Met 1995;71(1–3):1865–6.

[29] X. Zhao, Y. Ando, Y. Liu, M. Jinno, T. Suzuki, Phys. Rev. Lett. 90 (2003), 187401-1.

[30] Cazzanelli E, Castriota M, Caputi LS, Cupolillo A, Giallombardo C, Papagno L., Phys Rev B 2007;75(1–2):121405-1–4.

[31] M. Jinno, Y. Ando, S. Bandow, J. Fan, M. Yudasaka, and S. Iijima, Chem. Phys. Lett. 418 (2006)109.

[32] Cataldo F., Polyhedron 2004;23:1889–96.

[33] C. Fantini, E. Cruz, A. Jorio, M. Terrones, H. Terrones, G. Van Lier, J-C Charlier, M. S. Dresselhaus, R. Saito, Y. A. Kim, T. Hayashi, H. Muramatsu, M. Endo, M. A. Pimenta, Phys. Rev. B 73, (2006)193408.

[34] A. J. Fetterman, Y. Raitses, and M. Keidar, Carbon 46, 1322 (2008).

Chapter 4

Ultra-clean CNTs for optoelectronic applications

Single-walled carbon nanotubes (SWCNTs) represent attractive building blocks for ultra small electronic devices, for instance as nanoscale interconnects of high current carrying capability [1]. However, the successful fabrication of such devices still requires a deeper understanding of the local electronic properties of SWCNTs and their connection to leads. In this context an increasing number of studies is being directed toward the effect of structural defects and electrode contacts on the charge transport through SWCNTs, both from a theoretical [2, 3] and an experimental [4, 5, 6] point of view. The p-n junction constitutes a fundamental building blocks for modern semiconductor devices. It is the basis for most transistors (field effect and bipolar junction transistors) and optical devices (light emitting diodes and lasers). Therefore, for any new material system, a proper characterization of p-n junctions is crucial for the development of electronic devices. The realization of a p-n junction diode has been demonstrated through chemical doping of an individual nanotube but its electrical properties show leaky behavior due to high doping and abrupt junction formation [7]. An important improvement in this field has been performed by Lee et al. in 2004 [8]. They have demonstrated the electrostatic doping of individual SWNTs to form a p-n junction at room temperature. Electrostatic doping allows the examination of near intrinsic properties of nanotubes without creating dopant states

or changes in the band gap that may results from accompany chemical doping [9]. To obtain molecular-scale information on the electronic structure along electrically contacted SWCNTs, various scanning probe techniques have been applied. These include scanning gate microscopy (SGM) [5, 6], conducting tip atomic force microscopy (CT-AFM) [10], as well as electrostatic AFM (EFM) [4, 11, 12], scanning tunneling microscopy (STM) [12] and scanning photocurrent microscopy (SPCM) [13]. The recent demonstration of optical emission from semiconducting carbon nanotubes with direct band gaps has opened a new field for nano-optics [14]. Over the few years since the first report of light emission, important steps such as single nanotube photoluminescence [15, 16, 17, 18, 19] and electroluminescence [20, 36, 22, 23, 24] have already been taken. Contacted semiconducting carbon nanotubes have enabled photocurrent measurements [13, 25, 26], and superconducting contacts have been used to inject Cooper pairs into carbon nanotubes [27]. Suspended nanotubes have been shown to have higher quantum efficiencies [28] indicating that interactions with substrates strongly affect their optical properties. SPCM offers a good lateral resolution and allows rapid scanning over extended surface regions, which would be highly desirable in order to assess the structural and electronic perfection of larger tube ensembles in an economic time scale. For these reasons SPCM constitutes a powerful tool to probe local variations in the electronic structure along individual, electrically addressable nanotubes. This method is sensitive to the presence of built-in electric fields that separate photogenerated carriers (electrons and holes). Therefore it allows to map the potential landscape along contacted nanotubes, like for example Schottky barriers formed at metallic contacts. This information that until now could be obtained only indirectly from electrical transport studies [29, 30, 31].

In the next chapter we report a detailed step-by-step description of the fabrication process of an optoelectronic device based on ultra clean carbon nanotubes (CNT). Ultra-clean means that nanotubes are grown on the chip in the very last step of the process, and present exceptional electrical, mechanical and optical properties. In the second part of the chapter, we present the preliminary results obtained by electrical and optical characterization (SPCM). Electrical measurements show us that the source-drain current changes when different bias values are applied to to different gates configuration. Optical measurements, realized by means of the SPCM technique, permit to investigate the spatial variations of the potential along the suspended nanotubes for different gates voltages under laser excitation without altering its characteristics. In our case, SPCM allow sus to observe how a precise doping spatial control in the nanotube can be achieved in this kind of device (sec. 4.5 and 4.6).

The measurements were realized at the TU Delft - Technology University of Delft and DIMES-technology center laboratories in the Quantum Transport group, under the supervision of Dr. G.A. Steele and Prof. L.P. Kouwenhoven, (August 2009 -April 2010). The fabrication of a new device was the main purpose of my stage at TU-Delft,

Salvatore Bagiante, PhD Thesis in Material Science, University of Catania, 2010.

and further analyses are currently in progress.

4.1 Electron beam lithography

a) e-beam

resist

Si-p+/SiO$_2$

b) after development

c) metal evaporation

d) lift-off
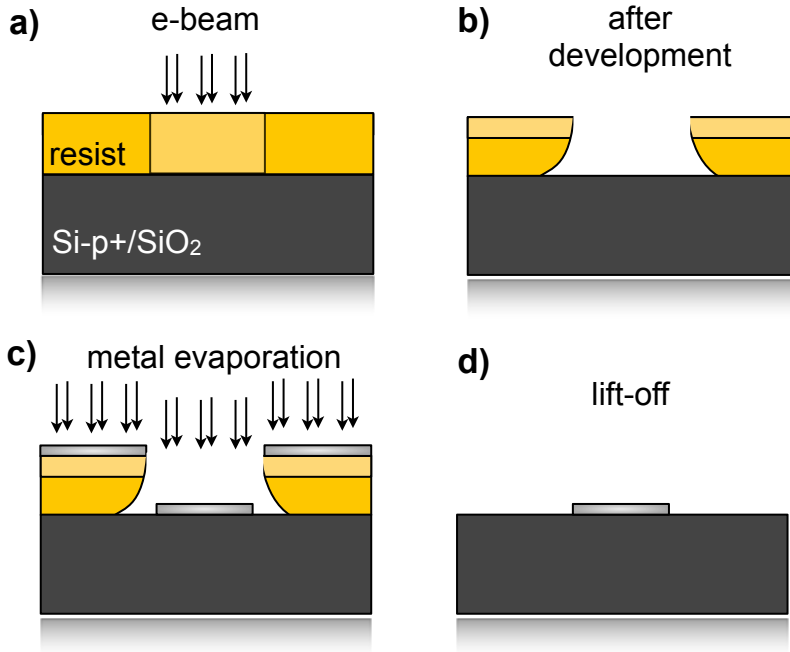
Figure 4.1: Electron beam lithography (a) A double layer of resist is spun on the substrate and the desired pattern is exposed to high energy electron beam; (b) A chemical developer removes the irradiated areas of the resist. Since the bottom layer is more sensitive to e-beam radiation there is a so called undercut; (c) One or more layers of metal (or dielectric) are evaporated on top of the developed resist layer; (d) A chemical solvent (usually acetone) removes the resist with the metal on top of it. Metal remains on the sample only at the predesigned areas. The undercut ensures a proper lift-off.

In order to fabricate a CNT device, a number of different small structures have to be defined on a Si/SiO$_2$ substrate. The method to do this is electron beam (e-beam) lithography. Each e-beam lithography cycle consists of the steps shown in figure 4.1. The smallest structures we can define by this method are around 35 nm large. One can improve this resolution down to ~20nm by optimizing the e-beam focusing, which

is usually done by focusing on on-chip markers close to the exposed areas. The relative alignment accuracy between different e-beam steps is typically better than 50 nm, if we use alignment markers close enough to the exposed areas.

4.2 Catalyst deposition and CVD growth

CNTs are grown by chemical vapor deposition (CVD) [34]. First, spots for the catalyst, from which the CNTs will grow, are defined in a PMMA mask via e-beam lithography. The catalyst consists of 40 mg $Fe(NO_3)^3 \cdot 9H2O$, 4 mg $MoO_2(acac)^2$ and 30 mg Alumina nanoparticles (Degussa Aluminium Oxide C), dissolved in 30 ml methanol. A few droplets of the catalyst are deposited on the substrate with the developed PMMA mask. After baking for 10 min at 150ºC a lift-off in hot acetone is performed, leaving catalyst only at the predefined spots on the substrate. Special care has to be taken not to end up with catalyst all over the sample (the catalyst sticks extremely well to SiO_2) and not only at the pre- defined spots. We usually ensure this by doing a two step lift-off. First, we move the sample quickly through a beaker of warm acetone inside a sonicator. Then the sample is immediately (without letting it become dry) transferred to a second beaker of acetone, where it is left for 5 min. The second step is the CNT growth, as schematized in figure 4.2: the sample is put in a quartz tube inside a furnace at 900ºC under 700 sccm H_2 and 520 sccm CH_4 gas flow for 10 min. Heating up and cooling down is done under Ar flow. Now, from the catalyst spots CNTs have grown in random direction with typical lengths of 1-30 μm. The CVD growth parameters (catalyst composition, temperature and gas flow rates) are optimized to produce a high yield ($> 90\%$) of single-wall CNTs with diameters of 1-5 nm. The peak of the diameter distribution is between 1 and 2 nm [34]. There is no control over the CNT chirality, meaning we probably get a random distribution of chirality (within the given diameter distribution). Indeed, we find that roughly ~1/3 of the CNTs are metallic or have a small bandgap and ~2/3 are semiconducting, as expected. The CVD growth works equally well for growing CNTs on a flat SiO_2 substrate or over predefined metal contacts and trenches.

4.3 Ultra clean carbon nanotube-based device

The common fabrication of a CNT device consists in a CNT deposition on a substrate, followed by all the other fabrication steps, as e-beam lithography, metal deposition and lift-off. There are two main reasons why this "conventional" fabrication method can induce disorder in CNTs: (i) The chemical processing leaves some residue of resist (or chemicals used for development and lift-off) on top of the CNT (ii) the e-beam radiation can induce defects in the CNTs [35]. To prevent fabrication-induced disorder and contamination, the CNT growth can be performed as the very last fabrication
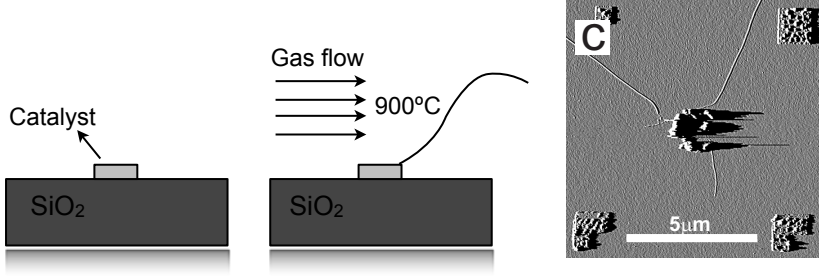
Figure 4.2: CVD growth of CNTs (a) Small islands of catalyst are deposited at predefined positions via e-beam lithography (b) A mixture of growth gases flows over the sample at high temperatures inside a furnace. CNTs grow from the catalyst spots. (c) AFM image of CVD-grown CNTs. From the catalyst island several CNTs have grown in random directions. The typical length is between 1 and 30 μm. The four markers at the corners are for alignment purposes.

step, as described in sections 4.2 and 4.4. The use of ultra-clean carbon nanotubes gives many advantages such as: (i) nanotube not exposed to electron beam, (ii) in the optical measurement the brightness is 10-100 times higher than in a conventional device, (iii) using suspended nanotubes, we remove all possible interactions with the substrate, and (iv)in the electrical measurement the ratio signal/noise ratio is very high. The disadvantages are: (i) during the growth we do not know exactly the position of the CNTs in the device and for this reason only the 10-20% of our devices work; (ii) it necessary to find a metal or alloy, that survive the high temperatures (900ºC) during the CVD-growth of the CNTs.

4.3.1 Issues arising from the metal contacts

As reported in the previous section, one of the main challenges is to find a metal or alloy, such that even narrow (~100nm) gates that are able to survive to the CVD-growth of the CNTs. Another important factor, in order to create a good device, is represented by the Schottky barrier created at the CNT-metal contact. Many studies on conventional CNT-devices (where the deposition of the CNT is the first step of the fabrication) have been performed in order to find the role of metal—nanotube contact in the performance of carbon nanotube [36]. In our case a further complication that is represented by the CVD process as the last step. A good contact material that has been tested in our CVD system is the tungsten-platinum alloy (W/Pt)[37]. W/Pt is a good p-type contact, forming a Schottky barrier that is small for the holes and big for the electrons because its work function is $\Phi \sim 5.6eV$. But, in order to create a device with a good injection of both electrons and holes, we need or of two metals,
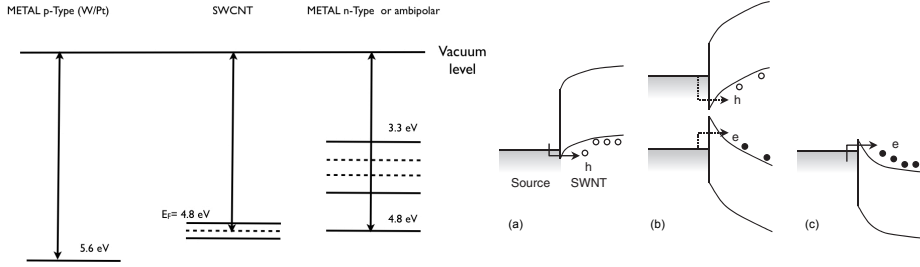
Figure 4.3: On the left alignment of the contact metals work function with the SWCNT Fermi level. On the right schematic band diagrams at the source contacts for the ON state in (a) p-type, (b) ambipolar , and (c) n-type metal [38].

one p-type (figure 4.3a) and the other one n-type (low Schottky barrier for electron, figure 4.3c), or a metal with a work function near to the Fermi level of a SWCNT, that is ~4.8 eV. In this case we will have an ambipolar contact (as reported in figure 4.3b).

In order to find the best candidate for our scope, we have performed many tests on different metals and alloys, as reported in Table 4.1

Elements	Melting point (°C)	Work function (eV)	Thickness (nm)
Co	1499	5	50
Cr	1807	4.5	50
Fe	1583	4.67-4.8	50
Re	3168	4.8	50
Ta	3017	4 – 4.8	50
Zr	1855	4	50
V	1910	4.3	50
Pd	1554	5.22-5.6	50
W	3422	4.35-5.22	50
Alloy			
V/Pt	1800	4.7-4.9	20\5
TiN(sputter)	2930	4.2	70
V/Pt	1800	4.7-4.9	20\5
Cr/Au	900-1000	5.1-5.47	5 \ 45
V/Pt	1800	4.7-4.9	20\5
Silicide			
Pt₂Si	1100	4.9	50\10
CrSi	1600	3.8-4.3	50\10
NiSi	1560	4.6-4.8	50\10
TiSi₂	1540	4.52	50\10

Table 4.1: In this table all metals and alloys with their melting point, work function, and thickness are reported. All films have been deposited on a Si/SiO₂ substrate and tested.

Some metals and alloys, e.g. Co, Fe, CrSi, TiN, have a high melting point, but thin films of these metals/alloys partially melt, create a forest of carbon nanowires or form a carpet of disconnected islands. Typical problems are shown in figure 4.4.
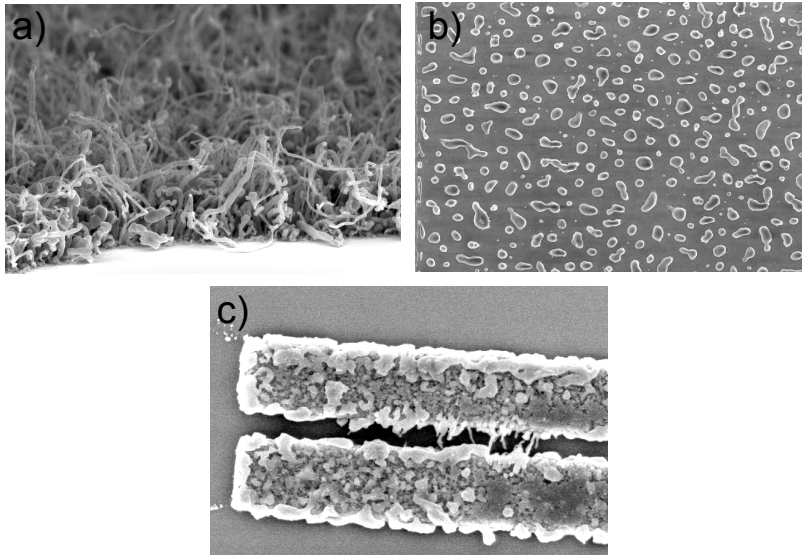
Figure 4.4: Thin metal films after heating up to 900ºC in the CVD oven. SEM images of (a) a 50 nm thick Fe film: after the CVD-growth, carbon nanowires grow; (b) a 50nm thick film of Co after CVD-growth: the thin film transforms into a layer of disconnected islands; (c) a 100 nm thick CrSi film after CVD-growth: the film is composed of big grains disconnected.

Few metals survive the high temperatures and the aggressive environment present in the CVD, but they often show high resistance $> M\Omega$ or inhibit the CNT growth. Among the different materials tested we have found that Rhenium and Nickel silicide (see figure 4.5) present a low resistance (~few ohms) and a work function of ~4.8eV that is perfect to create an ambipolar contact with the nanotube.
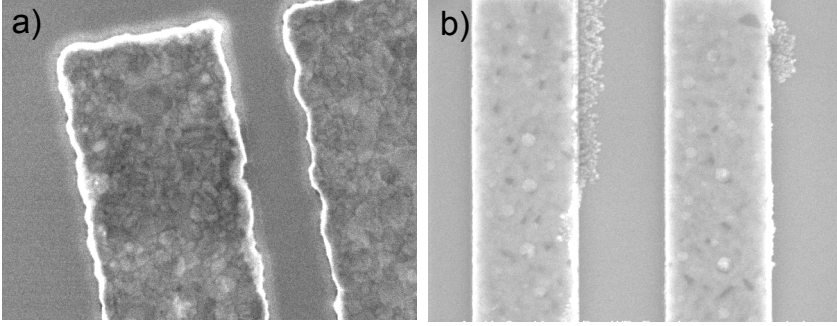
Figure 4.5: (a) Rhenium and (b) NiSi after the CVD-growth. All detail are reported in table 4.1.
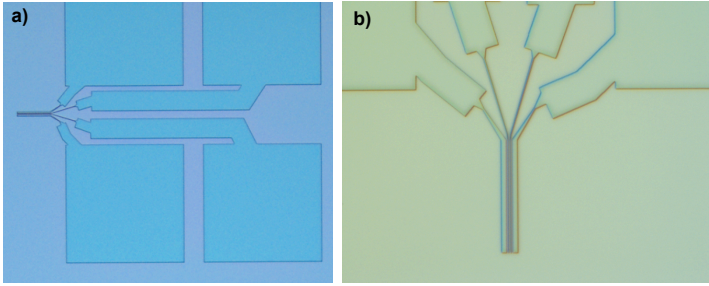
Figure 4.6: (a) optical image of the real device after the lift-off and (b) particular of the gates.

4.4   Device fabrication

For the success of a physics experiment it is of great importance to have a good sample fabrication procedure. This is, perhaps, even more true in nanoscience, where the intrinsically small size of the devices makes them very sensitive to external influences. Although some of these steps are not difficult, many things can go wrong at any of them, and at the end, the fabrication of a good device requires a considerable amount of careful concentration, practice, patience and, why not admit it, good luck. The fabrication process of our device is composed by the following parts: (i) fabrication of gates contacts and markers; (ii) SiO_2 deposition by PECVD; (iii) Al mask deposition and dry etching of SiO_2; (iv) Al wet etch; (v) SiO_2 wet etching and the pads fabrication for the gates; (vi) Catalyst deposition; (vii) nanotube growth. To fabricate a CNT
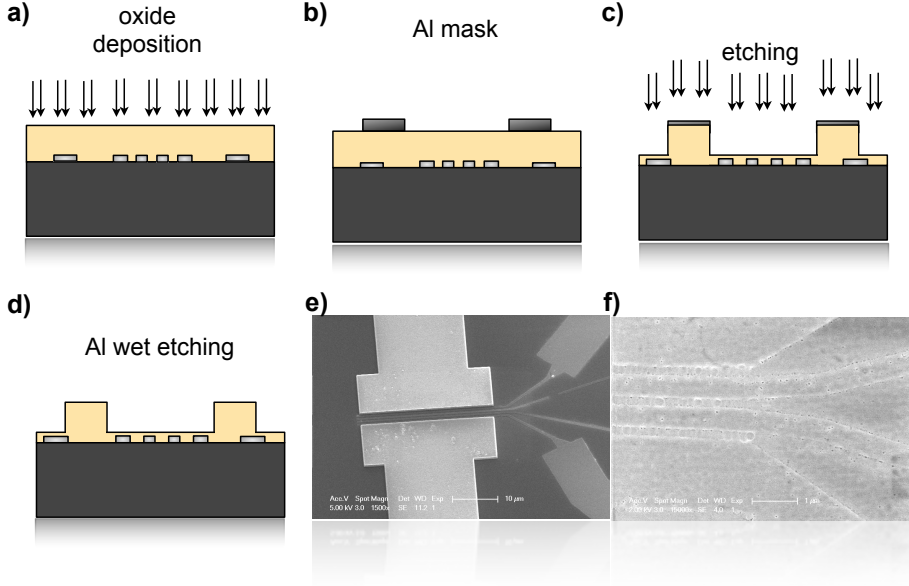
Figure 4.7: (a) PECVD silicon oxide deposition; (b) e-beam lithography and Aluminum deposition; (c) dry etching for remove the SiO2 not covered by Aluminum; (d) Chemical aluminum wet etching; (e) SEM image of the real sample after the wet etching; (f) detail of the gates, where a small layer of SiO2 is suitably left in order to protect the gates.

device, a number of different small structures have to be defined on the substrate. The method to do this is electron beam (e-beam) lithography (see sec. 4.1). In figure 4.6 we report two optical images of our device after the first step of fabrication. In this step we have defined markers, gates and their bond pads. In detail in figure 4.6b the four gates that we use for the electrostatic doping of our ultra clean carbon nanotube are shown.

A thick layer of SiO_2 ~1100nm was deposited on the gates by PECVD at 300^oC and afterwards the desired Aluminum mask pattern is created by e-beam lithography (as reported in figure 4.7 a,b). All SiO_2 surface not covered by aluminum has been dry etched using a C_4F_8 (20sccm), He(100sccm) and CH_4 (10sccm) / O_2 plasma. The O_2 is necessary to prevent the formation of teflon on the sample. This recipe gives an isotropic etching to reproduce exactly on the SiO_2 the patter created by the Al-mask. Thereby, the Al thin layer that remain on the substrate, is removed by a wet etch using a solution of 19 H_3PO_4: 1 HAc : 1 HNO_3: 2 H_2O for t=5min at T=20^oC (figure
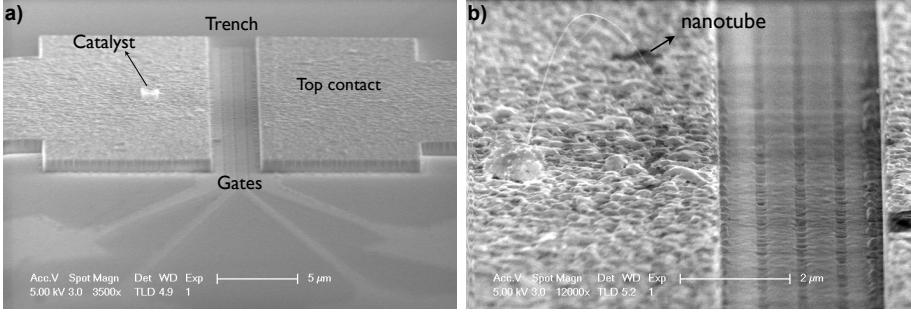
Figure 4.8: SEM image of (a) the final device where it is possible to observe its 3D geometry; (b) detail of the trench after the CVD-growth, where a nanotube that cross the trench is visible.

4.7 c, d, e), with no damage for the SiO$_2$ layer. The thin layer of SiO$_2$ (~80nm) is suitably left in order to avoid that the CNT grown over it short-circuits the gates (figure 4.7 f) .

The structure created by the dry etch (figure 4.7 d), is used for the following creation of the top contacts by means of an e-beam cycle (see figure 4.1). The catalyst for CNT growth is deposited selectively on the top contacts, after defining a pattern area by e-beam lithography. The materials that we use as top contacts can be: W/Pt, Re or NiSi. The SEM image of the device is shown in figure 4.8a. In this picture it is possible to see the four gates, a 3µm trench, the two top contacts and the 3D geometry of our device.

After the CVD-growth we have ultra-clean carbon nanotubes, suspended across the trench (see fig. 4.8b). Using the external gates we can control the injection of carriers modifying the CNT/metal Schottky barrier, while by the internel gates we can control the electrostatic doping of our nanotube.

4.5 Electrical characterization

Typically each substrate contains 720 devices fabricated as described above (sec. 4.4). Due to the fact that the CNT growth is performed as the very last step and the growth direction is random, the yield of working device with only one SWNT crossing the trench is quite low (~20%). Furthermore, as reported in section 4.2, different chiralities are grown, giving rise to semiconducting and metallic nanotubes. In this study where we aim at investigating the optical properties of our devices (photocurrent and later electroluminescence), we have selected only semiconducting SWNTs, which can be easily identified out of transport measurements (described later). All the

Salvatore Bagiante, PhD Thesis in Material Science, University of Catania, 2010.

Figure 4.9: (a) Schematics of the device. (b) SEM image of the device after the bonding the contacts to perform the electrical measurements.

measurements presented here have been performed on devices with contacts made of W/Pt, at room temperature and in air. In order to perform electrical me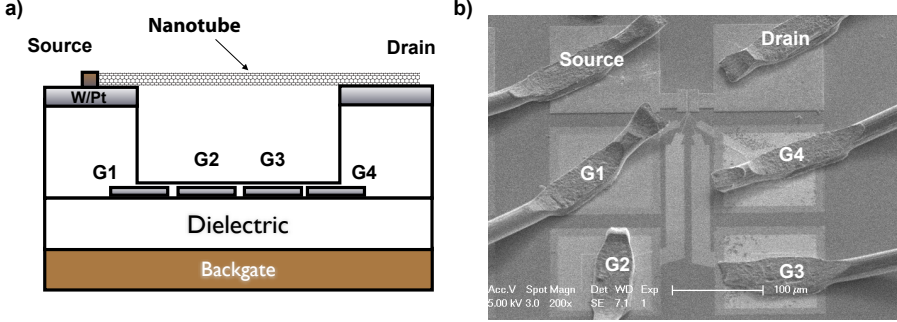asurements, we glued our chips on a chip carrier and wire bonded selected semiconducting devices (probe-station measurements), see Fig. 4.9. We then mounted the chip carrier on the xyz stage of our dedicated setup (described later, Fig. 4.11a) and contacted the devices with voltage sources and current measurement units.

Figure 4.10 shows typical transistor curves of a large band gap semiconducting device. The trench gates and the Si substrate (backgate) are connected (different configurations indicated in inset) to voltage sources that can be swept from -8V to 8V. A constant voltage of VDS=2mV is applied to the drain contact and the current is measured at the source contact. The configuration of the bands is depicted in fig. 4.10 b) and c) for negative and positive gate voltages, respectively. For negative (positive) gate voltage, we expect hole (electron) conduction. The conduction is suppressed when the Fermi level of the contacts is in the gap of the nanotube. In this device we only see hole current for negative bias. Electron current is not present for positive voltage. This unipolarity is observed for many investigated semiconducting nanotubes. We tried to apply up to +90V to the gates of other semiconducting devices and the current remain zero. We found recently that this is due a screening effect attributed to the thin water-oxygen layer adsorbed at the surface of the nanotube and actually the material used for the contacts is not the dominant parameter that determines the nature of the contact-nanotube interface [39].

In order to understand how the electrostatic doping changes in a SWCNT, as the bias is varied in the different gates, various configurations have been tested: (i) only backgate, with the other gates grounded and floating; (ii) only G2 and G3 (internal gates); (iii) only G1 and G4 (external gates); (iv) all gates G1, G2, G3 and G4. As shown in figure 4.10, the current flowing through S and D changes
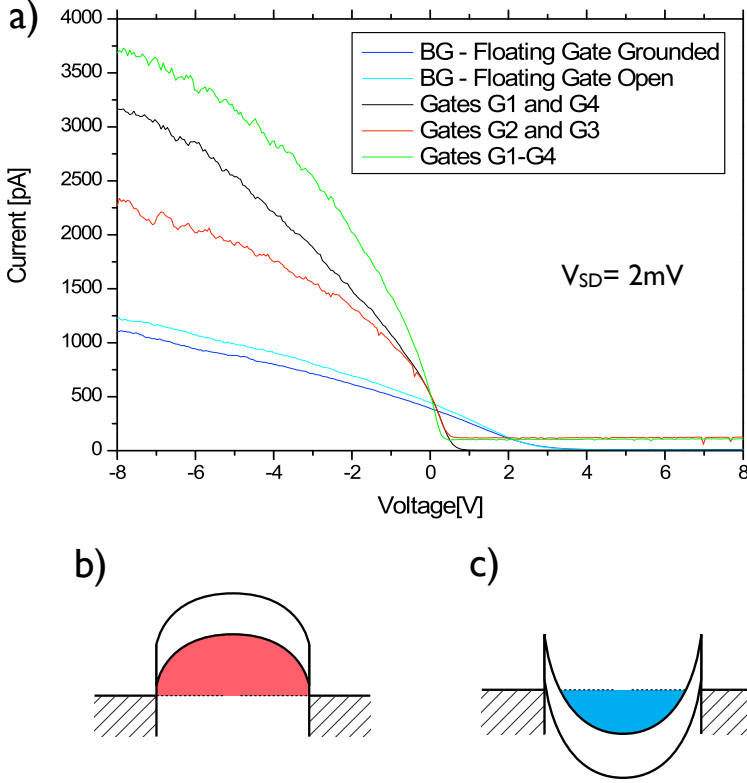
Figure 4.10: (a)Electrical measurements performed applying different bias to the gates BG, G1, G2, G3 and G4 in several configurations: using the Backgate (BG), the external gates G1 and G4, the internal gates G2 and G3 or all gates together. (b) Band diagram scheme in the nanotube for negative a) and positive b) gate bias.
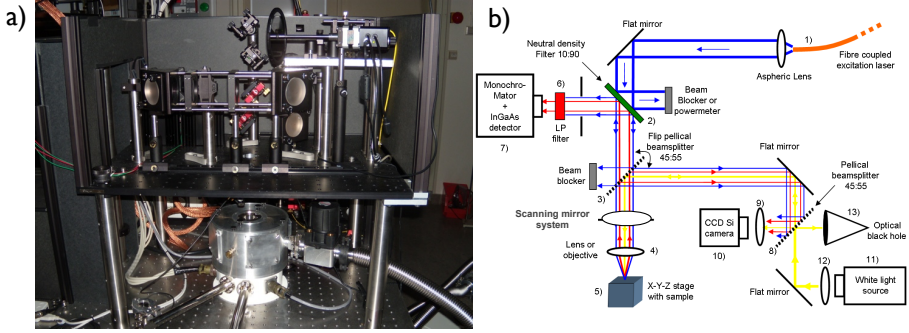
Figure 4.11: a) Photograph of the beam scanner setup; b) Schematic of the SPCM setup.

when the gates configuration is varied. In particular, the current increases from ~1250pA, (R=1.6MΩ) when V=-8V are applied only to the backgate, up to ~3750pA (R=0.53MΩ) when the voltage is applied to all four gates G1-G4. This means that the thickness of the insulator layer (e.g. SiO_2) between gate and nanotube, influence the CNT band bending diagram, reducing the efficiency of the electrostatic doping. In the intermediate configuration applying a -8V voltage to G2 and G3 we find I_{DS}~2250pA (R=0.88MΩ), while with G1 and G4 I_{DS} is ~3250pA (R=0.61MΩ). This difference is due to the gates position in the trench, thereby using the external gates we can better control the Schottky barrier and hence the quantity of the carriers flowing through source and drain contacts.

4.6 Optical measurements: Scanning photocurrent microscopy

The device was characterized by scanning photocurrent microscopy (SPCM). This technique constitutes a very useful tool to study the spatial variations of the potential along suspended nanotubes for different gate voltages under laser excitation. SPCM, compared with other analytical techniques (e.g SEM, AFM), allows the investigation of an individual suspended SWCNT without altering its characteristics. Our SPCM setup uses a diffraction-limited laser beam scanned over the CNT devices by means of galvo mirrors coupled to a telecentric system. Photocurrent images were acquired by recording the drain current (I_{DS}) at zero drain-source bias (V_{DS}) as a function of the laser spot position. A reflection image is recorded simultaneously to determine the absolute position of the photocurrent features. The light excitation is made with a continuous wave green laser (CNI MLL-III-532nm, Output power: 185mW)

attenuated by neutral densities and coupled to a single mode fiber to the setup. A picture and a schematic of our SPCM setup are shown in figure 4.11 a) and b), respectively.

The potential landscape of the nanotube can be tuned by means of electrostatic doping using four gates (G1, G2, G3 and G4), as described in the previous section. For these measurements the laser power exciting the nanotube device was fixed to about 3uW focused a diffraction limited spot of about 800nm[1].
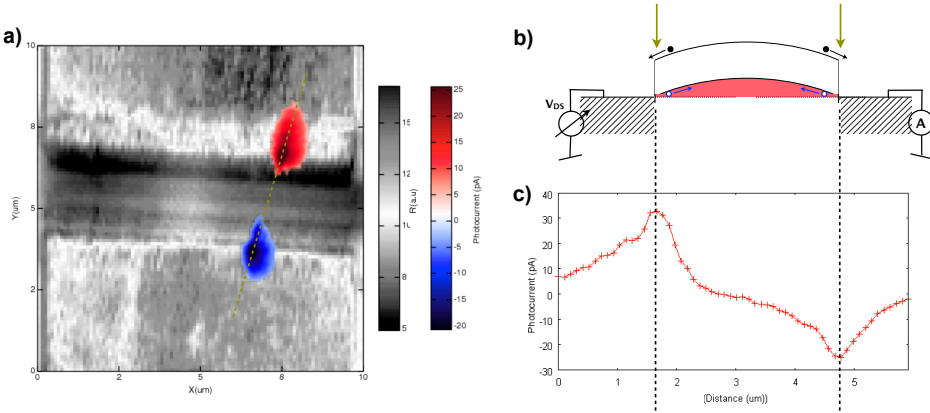
Figure 4.12: A superposition of a reflection image (grey scale) and a photocurrent image (colored scale) for all gates grounded; b) mechanism of the PC generation at the contacts; c) Photocurrent signals recorded along the green dashed line in a).

The source and drain contacts are made of a W/Pt alloy giving rise to p-type contacts to the SWNT suspended between two columns 1um high, across a 3um wide trench.

Figure 4.12a shows a superposition of reflection and photocurrent (PC) images obtained with G1, G2, G3 and G4 grounded. The top contacts, the trench and the buried gates can be visualized in the reflection image. The SWNT clearly shows localized PC spots near both electrode contacts. These localized PC spots are generated by the Schottky barriers due to electronic band bending at the metal/CNT interfaces. Here, the polarity of the PC indicates that the electronic band bends upward toward the middle of the CNT (see fig. 4.12b). Since the zero-bias PC signal originates from local electric fields, the position, intensity, and shape of the PC signals provide detailed information about the local potential in CNT devices. The PC values recorded along the green dashed line in the image of figure 4.12a are reported in figure 4.12c.

---

[1]60/20, 60uW is the reflected power measured with the powermeter, 10/90 beamsplitter. A factor of about 2 is lost in the optics and objective

Here, the position of the positive and negative photocurrent peaks correspond to the trench edges. In figure 4.13 we report the PC and reflection images of a SWCNT obtained by applying a bias of G2=G3=-8V, while G1 and G4 are grounded. In this condition the photocurrent image (see fig. 4.13a) shows a sequence of negative (blue)-positive (red)-negative (blue)-positive (red) PC values, displayed in the photocurrent signal measured along the green dashed line (fig. 4.13c). The origin of this behavior reminiscent of a "camel-back"-like potential shape along the nanotube is not yet understood.
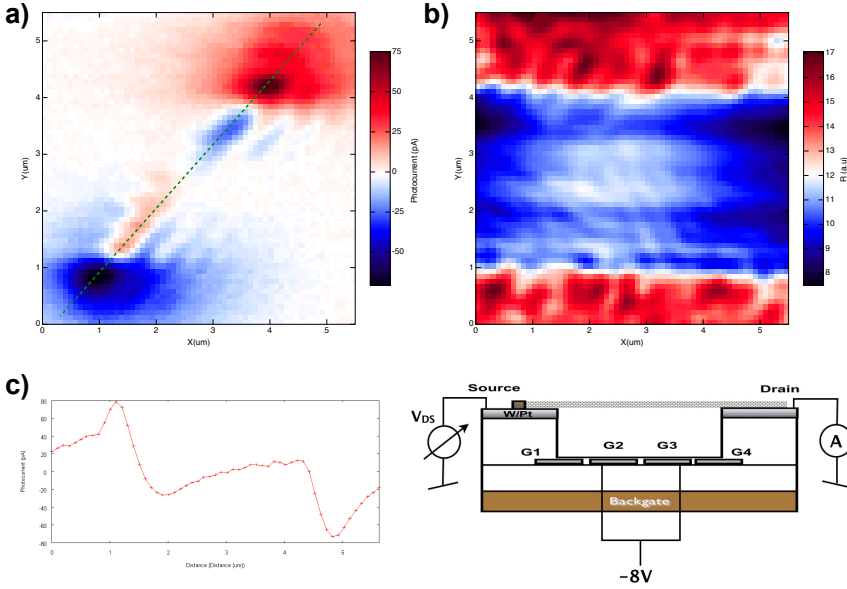
Figure 4.13: a)Photocurrent and b)reflection images of our nanotube fixing G2=G3=-8V and G1,G4 grounded; c) PC signals recorded along the green dashed line in a); d) schematics of the device and the gates bias configuration.

In our device, by changing the gate voltages configuration (with G1=G2=+8V G3=G4=-8V and G1=G2=-8V G3=G4=+8V), we can play with the nanotube energy diagram as reported in figure 4.14c and d, and generate a p-n or n-p junction. In this condition a clear PC spot is localized in the middle of the trench. Note that no PC contribution is given by the Schottky barriers, it is most probably due to the fact that photogenerated holes or electrons at the Schottky barriers cannot reach the opposite contact due to too high barriers. This has to be proved by means of power dependence measurements. This introduces a relevant novelty with respect to the existing works and allows more detailed investigations of the CNT energy band. The two small spots

near to the p-n or n-p junction are probably due to fact that the light reflected by the bottom of the trench is diffracted by the gate patterns (wavelength of the laser close to the pattern size).

Figure 4.14: a) and b) reflection image (grey scale) and photocurrent image(colored scale), superposed, for two different gate bias configurations G1=G2=+8V; G3=G4=-8V and G1=G2=-8V; G3=G4=+8V respectively; c) and d) Energy diagrams and scheme of the device showing the gates bias configuration, corresponding respectively to the n-p and p-n conditions.

We are able to visualize the p-n junction position by analysing the PC signal, and we can have a spatial control of the junction across the trench by changing the voltage applied to the four gates. As reported in figure 4.15, applying the following gate bias: G1=+8V and G2=G3=G4=-8V or G1=G2=G3=-8V and G4=+8V, we are able to move respectively the p-n or n-p junction spot near to the source or near to the drain.

Salvatore Bagiante, PhD Thesis in Material Science, University of Catania, 2010.
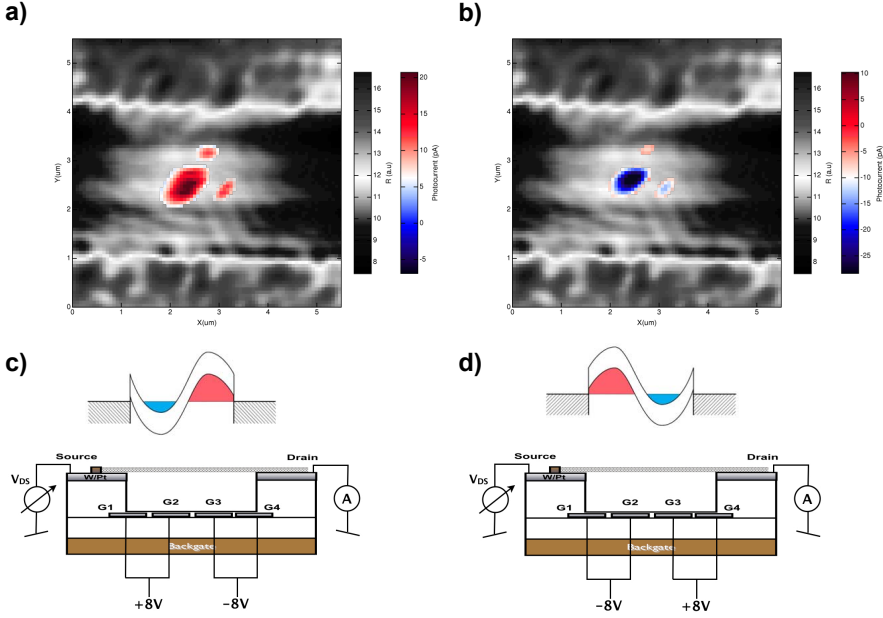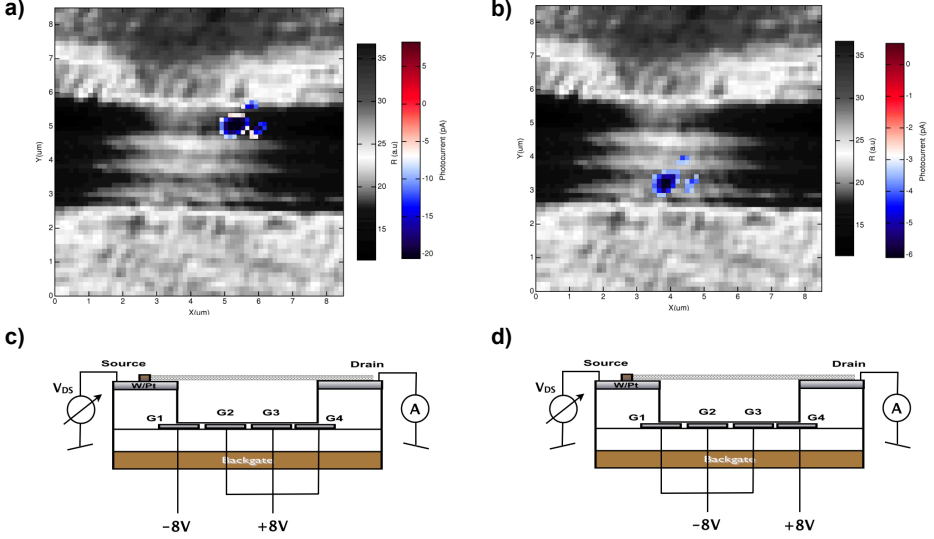

Figure 4.15: a) and b) reflection image (grey scale) and photocurrent image(colored scale), superposed, for two different gate bias configuration G1=-8V; G2=G3=G4=+8V and G1=G2=G3=-8V; G4=+8V respectively. c) and d) schematic of the device and the gates bias configuration.

4.7 Conclusion

In conclusion, we have shown an alternative approach for the fabrication of CNT-based devices: ultra-clean suspended carbon nanotubes can be grown on a device structure, as last step of fabrication. In particular, a new type of device for optoelectronics application has been proposed. Issues related to the process itself have been considered and faced up, such as the choice of the most suitable conductive materials for contacting the CNT. Besides the already tested W/Pt alloy, further conductive materials like Re and NiSi have been found to resist at the CVD process needed for the CNT growth. Their use is under evaluation for the future experiments. We have performed electrical and SPCM measurements on our devices in order to investigate the electron band structure of the suspended carbon nanotube and demonstrated how it is possible to form a p-n junction inside the CNT by electrostatic doping and how the spatial position of the junction can be moved along the CNT with an extremely high precision by varying the electrostatic doping. Further investigations like photocurrent measurements as a function of the gates biasing, laser power, beam position, wavelength and polarization are in progress in order to fully understand the optical

and transport processes involved in such kinds of devices. All these measurements will be performed in vacuum and at low temperature using a cryostat system.

References

[1] Dai H., Wong E. W, Lieber C. M., Science 1996, 272, 523.

[2] Delaney, P.; Choi, H. J.; Ihm, J.; Louie, S. G.; Cohen, M. L. Nature 1998, 391, 466.

[3] Chico, L.; Benedict, L. X.; Louie, S. G.; Cohen, M. L. Phys. ReV. B 1996, 54, 2600.

[4] Bozovic, D.; Bockrath, M.; Hafner, J. H.; Lieber, C. M.; Park, H.; Tinkham, M. Appl. Phys. Lett. 2001, 78, 3693.

[5] Bockrath, M.; Liang, W.; Bozovic, D.; Hafner, J. H.; Lieber, C. M.; Tinkham, M.; Park, H. Science 2001, 291, 283.

[6] Freitag, M.; Johnson, A. T.; Kalinin, S. V.; Bonnell, D. A. Phys. ReV. Lett. 2002, 89, 216801.

[7] C. Zhou, J. Kong, E. Yenilmez, and H. Dai, Science 290, 1552 (2000).

[8] Lee et al. Appl. Phys. Lett., Vol. 85, (2004)

[9] A. Frajian, K. Esfarjani, and Y. Kawazoe, Phys. Rev. Lett. 82, 5084(1999).

[10] Freitag, M.; Radosavljevic, M.; Clauss, W.; Johnson, A. T. Phys. ReV. B 2000, 62, R2307

[11] Bachtold, A.; Fuhrer, M. S.; Plyasunov, S.; Forero, M.; Anderson, E. H.; Zettl, A.; McEuen, P. L. Phys. ReV. Lett. 2000, 84, 6082.

[12] Brian J. LeRoy, Iddo Heller, Vijay K. Pahilwani, Cees Dekker, and Serge G. Lemay, Nano Lett., 2007, 7 (10), pp 2937–2941.

[13] Balasubramanian, K.; Fan, Y.; Burghard, M.; Kern, K.; Friedrich, M.; Wannek, U.; Mews, A. Appl. Phys. Lett. 2004, 84, 2400.

[14] Phaedon Avouris, Marcus Freitag and Vasili Perebeinos, nature photonics, vol. 2, (2008).

[15] J. Lefebvre, Y. Homma, P. Finnie, Phys. Rev. Lett. 90, 217401 (2003).

[16] J. Lefebvre, J. M. Fraser, P. Finnie, Y. Homma, Phys. Rev. B 69, 075403 (2004).

[17] J. Lefebvre, P. Finnie, Y. Homma, Phys. Rev. B 70, 045419 (2004).

[18] J. Lefebvre, D. G. Austing, J. Bond, P. Finnie, Nano Lett 6, 1603 (2006).

[19] J. Lefebvre, P. Finnie, Nano Lett. 8, 1890 (2008).

[20] J. A. Misevich, R. Martel, Ph. Avouris, J. C. Tsang, S. Heinze, J. Tersoff, Science 300, 783 (2003).

[21] J. Chen, V. Perebeinos, M. Freitag, J. Tsang, Q. Fu, J. Liu, P. Avouris, Science 310, 1171 (2005).

[22] M. Freitag, J. Chen, J. Tersoff, J. C. Tsang, Q. Fu, J. Liu, P. Avouris, Phys. Rev. Lett. 93, 076803 (2004).

[23] M. Freitag, J. C. Tsang, J. Kirtley, A. Carlsen, J. Chen, A. Troeman, H. Hilgenkamp, P. Avouris, Nano Lett.6, 1425 (2006).

[24] D. Mann, Y. K. Kato, A. Kinkhabwala, E. Pop, J. Cao, X. Wang, L. Zhang, Q. Wang, J. Guo, H. Dai, Nature Nanotech. 2, 33 (2007).

[25] K. Balasubramanian, M. Burghard, K. Kern, M. Scolari, A. Mews, Nano Lett. 5, 507 (2005).

[26] Y. H. Ahn, A. W. Tsen, Bio Kim, Yung Woo Park and Jiwoong Park, Nano Lett., Vol. 7, No. 11, 2007.

[27] P. Jarillo-Herrero, J. A. van Dam, L. P. Kouwenhoven, Nature 439, 953 (2006).

[28] J. Lefebvre, P. Finie, Phys. Rev. Lett. 98, 167406 (2007).

[29] Bockrath, M.; Cobden, D. H.; McEuen, P. L.; Chopra, N. G.; Zettl, A.; Thess, A.; Smalley, R. E. Science 1997, 275, 1922.

[30] Bezryadin, A.; Verschueren, A. R. M.; Tans, S. J.; Dekker, C. Phys. ReV. Lett. 1998, 80, 4036.

[31] Hunger, Th.; Lengeler, B.; Appenzeller, J. Phys. ReV. B 2004, 69, 195406.

[32] M.J. O'Connel et al science,297,593(2002)

[33] J.A Misewich, science 300,783 (2003)

[34] J. Kong et al., Nature, vol. 395, p. 878, 1998.

[35] B. W. Smith and D. E. Luzzi, J. Appl. Phys., vol. 90, p. 3509, 2001.

[36] Zhihong Chen, Joerg Appenzeller, Joachim Knoch, Yu-ming Lin and Phaedon Avouris, Nano Lett., Vol. 5, No. 7, 2005.

[37] G.A. Steele, G. Gotz & L.P. Kouwenhoven, Nature Nanotechnology, Vol. 4, p. 363 - 367 (2009)

[38] Y. Nosho, Y. Ohno, S. Kishimoto and T. Mizutani, Nanotechnology 17 (2006) 3412–3415.

[39] Carla M. Aguirre, Pierre L. Levesque, Matthieu Paillet, Francis Lapointe, Benoit C. St-Antoine, Patrick Desjardins, and Richard Martel, Adv. Mater. 2009, 21, 3087–3091.

Summary and Outlook

Carbon nanotubes are tiny cylinders made of carbon atoms. Their remarkable electronic and mechanical properties, together with their small size (a few nm in diameter), make them very attractive for scientific research, both from the basic as well as from the technological point of view. In this work the synthesis of CNTs by arc-discharge in liquid nitrogen has been investigated, with the aim of understanding the "arcing phenomenon", through the correlation between the experimental parameters (that control arc generation) and the structure of the synthesized material.

Furthermore, an alternative approach for the fabrication of CNT-based devices for optoelctronics applications, using ultra-clean suspended carbon nanotubes, was studied.

At the present a very important aspect for the CNT production is the ratio between the yied and quality: the aim is to have large amount of CNTs and, at the same time, to reduce the number of purification steps.

We have studied the morfology of our samples in cross section and observed the presence of two different regions: one mainly consisting of disordered C structures, appearing in the radially outer region of the deposit; the other one made of CNTs, forming in the core region of the C deposit and well packed into pillars, whose size and sharpness depend on the voltage starting the electric arc. The formation of different structures has been related to the temperature field during the arc discharge on the cathode surface and in the inter-electrode space.These observations suggest the possibility to improve the CNT yield (i.e. reducing the amount of disordered and amorphous carbon) by using suitable experimental parameters. This could be helpful for reducing the purification steps. Moreover we, have shown the effect of the experimental parameters (current, voltage and rod diameter) on the structural quality of MWCNTs. The quality of our deposits is evidenced essentially by two factors: (i) a very low I_D/I_G ratio (for configuration 10-10, at current higher than 50 A, it is about 0.05.); (ii) the observation of active RBMs in the low frequency region of Raman spectra, indicating that nanotubes with very thin (<1 nm) innermost diameter are formed.

In the same chapter we have finally demonstrated that using this technique, we are
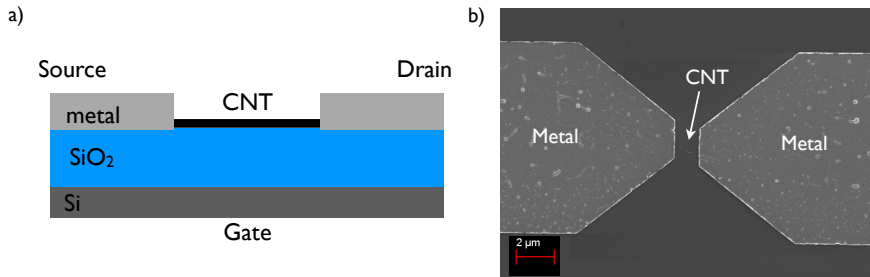
Figure 4.16: a) Scheme of our device; b) SEM image after the fabrication.

able to synthesize also hybrid materials formed by linear carbon chains (LCCs) inside carbon nanotubes. These hybrid systems have been obtained without the presence of any catalytic element. Long linear carbon chains have been synthesized inside MWCNTs, with a number of C atoms between 100 and 200, whereas, as reported in the literature, in the presence of catalytic elements, short carbon chains have been synthesized, containing about 8-18 C atoms, inside DWCNTs. Moreover, we have demonstrated the correlation between one RBM feature suppression and the L-band, characteristic of LCCs, that has never been observed in the literature before. This allowed us to point out the formation of linear C chains in CNTs having a diameter of 0.7 nm, so that the distance between the atoms in the chain and the inner wall was equal to the distance between two graphite planes, as expected.

Future work will be focused to the electrical characterisation of MWCNTs synthesized by arc discharge in liquid nitrogen and their integration into electronic devices. In particular, the realization of a device is required in order to study the electrical characteristics of the MWCNTs. In particular we want to study the hybrid system: LCC@MWCNT. This work is now in progress and in figure 4.16a, we report a scheme of our future device. In figure 4.16b the SEM image of the device structure after the third step of fabrication is shown: (i) fabrication of markers; (ii) nanotube deposition; (iii) nanotube location and electrode fabrication. The last step (iv) sample bonding and room temperature characterization, is now in progress.

The second experimental part of this thesis has been focused on the use of CNTs for optoelectronics applications. The recent demonstration of optical emission from semiconducting carbon nanotubes with direct band gaps has increased the interest in the new field of nano-optics. In the last three years since the first papers on CNTs light emission, important results, such as single nanotube photoluminescence and electroluminescence have been obtained. On this purpose, in chapter 4, with the aim to create an alternative approach for CNT-based device fabrication, ultra-clean carbon suspended nanotube was grown on a device structure, as last step of fabrication. In particular, a new type of device for optoelectronics applications was studied. After

104

reporting the fabrication steps, we have demonstrated how it is possible to control the source-drain current when different bias values are applied, in different gates configuration. In the meantime, using SPCM technique we have investigated the electron band structure of the suspended carbon nanotube. We have demonstrated how it is possible to form a p-n junction inside the CNT by electrostatic doping and how the junction can be moved along the CNT with an extremely high precision, by varying the electrostatic doping. Further investigations like photocurrent measurements as a function of the gates biasing, laser power, beam position, wavelength and polarization are in progress in order to fully understand the optical and transport processes involved in such kinds of devices, that can find application as LEDs (light emitting diode) and phototransistors.

Curriculum Vitae

Salvatore Bagiante

March 24, 1982 Born in Catania, Italy.

1995-2000 Secondary school in Electronics Engineer "I.T.I.S Archimede", Catania (Italy).

2000-2007 Academic degree in Physics, University of Catania (Italy). Dissertation: Synthesis of polycrystalline silicon on plastic substrate. Project: Plast_Ics. Supervisor: Dr. Vittorio Privitera, Prof. ssa Maria Grazia Grimaldi.

2007-2008 Master in : Researcher expert in materials, their characterization and technology of process for the realization of electronics device on plastic substrate. Consorzio Catania Ricerche (CCR). Project: Plast_Ics

2007-2010 PhD in Materials Science at the University of Catania under supervision of Prof. ssa F. Simone and Dr. S. Scalese. Subject: Carbon Nanotubes: Synthesis, Characterization and Integration

List of publications

- V. Privitera, S. Bagiante et al. "Low-Temperature Annealing Combined with Laser Crystallization for Polycrystalline Silicon TFTs on Polymeric Substrate", Journal of The Electrochemical Society, 155 _10_ H764- H770 _2008.

- V. Scuderi, S. Scalese, S. Bagiante et al. "Direct observation of the formation of linear C chain/carbon nanotube hybrid systems" CARBON 47 (2009) 2112–2142.

- S. Scalese, V. Scuderi, S. Bagiante, F. Simone, P. Russo, L. D'Urso, G. Compagnini, and V. Privitera "Controlled synthesis of carbon nanotubes and linear C chains by arc discharge in liquid nitrogen" JOURNAL OF APPLIED PHYSICS 107, 014304 (2010)

- S. Bagiante, S. Scalese, V. Scuderi, L. D'Urso, E. Messina, G. Compagnini, and V. Privitera "Role of the growth parameters on the structural order of MWCNTs produced by arc discharge in liquid nitrogen" Phys. Status Solidi B 247, No. 4, 884–887 (2010).

- G. Compagnini, G. Patanè, O. Puglisi, S. Scalese, V. Scuderi, S. Bagiante and V. Privitera " Synthesis of carbon nanowires and nanotubes by plasma ignition in liquid environments" Journal of Optoelectronics and Advanced Materials 12, No. 3, 456-460 (2010).

- S. Scalese, V. Scuderi, S. Bagiante, S. Gibilisco, G. Faraci and Vittorio Privitera " Order and disorder of carbon deposit produced by arc discharge in liquid nitrogen" JOURNAL OF APPLIED PHYSICS 108, 064305 (2010).

- E. Messina; G. Compagnini; L. D'Urso; O. Puglisi; S. Bagiante; S. Scalese "Size distribution and particle shape in silver colloids prepared by laser ablation in water" Radiation Effects and Defects in Solids: Incorporating Plasma Science and Plasma Technology, Vol.165, Issue 6-10, 579 – 583 (2010).

- Silvia Scalese, Viviana Scuderi, Salvatore Bagiante, Santo Gibilisco, Giuseppe Faraci, Nicolò Piluso, Francesco La Via, Vittorio Privitera. "Morphology and distribution of carbon nanostructures in a deposit produced by arc discharge in liquid nitrogen" Physica E, in press (2010)